

溶劑於高分子發光二極體元件的 三重態能量轉移之影響

碩士研究生：丁浩偉

指導教授：陳方中

國立交通大學光電工程研究所碩士班

中文摘要

我們利用Stern-Volmer的實驗去探討溶劑對三重態能量從磷光分子轉移到共軛高分子的影響。比較不同系統在相同溶劑中的Stern-Volmer淬息常數，我們發現，當磷光分子的三重態能階越高，淬息效率也越高。此外，比較Stern-Volmer的淬息常數與理論的擴散控制速率常數，我們發現並不是所有的放熱性的三重態能量轉移都是擴散控制的。在甲苯中，PFam4-FIrpic和PFam4-Ir(mppy)₃系統的三重態能量轉移是接近擴散控制的。在鄰二氯苯中，PFam4-FIrpic的三重態能量轉移也是接近擴散控制的。然而，對於PFam4-Ir(mppy)₃系統在鄰二氯苯中，和PFam4-Ir(FIPy)₂(acac)系統的在甲苯中，其三重態能量轉移都不是擴散控制的。由於鄰二氯苯對於PFam4而言是劣溶劑，所以導致了PFam4的大小分布在鄰二氯苯中比在甲苯來的廣，這也許是造成相同系統在鄰二氯苯中的淬息效率都比在甲苯中來的小的原因。共溶劑(體積比：甲苯比鄰二氯苯等於一比一)的黏度和溶解參數都介於甲苯與鄰二氯苯之間，因此得到的Stern-Volmer淬息常數也在這三種溶劑之間。在元件效率中，若主動層是由溶在鄰二氯苯溶劑所旋轉塗布上的，元件的效率會比較低，我們推測這可能是因為此時PFam4形成 β 相所導致的。

Solvent Effect on the Triplet Energy Transfer in Polymer Light-Emitting Diodes

Student: Hao-Wei Ting

Advisor: Dr. Fang-Chung Chen

**Institute of Electro-Optical Engineering
National Chiao Tung University**

Abstract

We used the Stern-Volmer experiment to investigate the solvent effect on the triplet energy transfer from the phosphorescent molecule to the conjugated polymer. From the Stern-Volmer quenching constants for the different systems in the same solvent, it shows that the quenching effect is more efficient when the triplet energy of Ir complex becomes much higher than that of the PFam4. Comparing the Stern-Volmer quenching constants with the theoretical diffusion controlled rate constants, we find that not all exothermic triplet energy transfers are diffusion controlled processes. For the PFam4-FIrpic system and the PFam4-Ir(mppy)₃ system in the toluene solutions, the triplet energy transfers are close to diffusion controlled. Similarly, for the PFam4-FIrpic system in the DCB solution, the triplet energy transfer is also close to diffusion controlled. However, for the PFam4-Ir(mppy)₃ system in the DCB solution and the PFam4-Ir(FIPy)₂(acac) system in the toluene solution, the quenching efficiencies are low. Therefore, neither of them is diffusion controlled. The DCB is the poor solvent for the PFam4. So, the distribution of hydrodynamic diameter of PFam4 in the DCB solution is broader than that in the toluene solution. It may cause that, for the same PFam4-Ir complex system, the quenching efficiency in the DCB solution is lower than that in the toluene solution. Because the viscosity (η) and the solubility parameter (δ) of the cosolvent are between that of the

toluene and DCB, the quenching constants in the cosolvent solutions are also between them. The lower efficiency of the device with the emitting layer that was spun cast from the DCB solution may be due to the β -phase conformation of PFam4.



誌 謝

兩年了。從一個當初只是對有機電子有興趣，但是卻了解不多的我，到現在成爲一個對有機電子略有所知，且完成論文的我；一路走來真的必須感謝很多人的幫忙。

首先誠摯地感謝陳方中教授的教導，本論文的實驗方法當初是老師親自帶我操作的，讓我能從旁觀察到很多老師的實驗技巧。而每當實驗遇到問題，透過跟老師的討論，也能順利地解決，且對實驗的下一步提供了新的方向，使我對於高分子發光二極體能有更深入的了解。此外，在生活上，老師也會對我們提供一些他的經驗與看法，讓我們在做人的方法上也能有所收穫。

另外，還必須感謝實驗室的學長姐：文奎、喬舜、祖榮、志平、永昇、立仁、東賢、文生、瑞祥、映頻、惠君、思芳。感謝他們對於實驗方法的傳承，而且每當實驗遇到困難，學長姊們也常常是第一個幫我們想方法的。

我的同屆實驗夥伴們：義凱、上傑、泰元、志力、尹婷、紓婷，感謝大家在這兩年的相互扶持，沒有芥蒂的快樂時光，實驗室的和諧氣氛，總使我在實驗室感到輕鬆自在。祝福大家畢業之後，能順利地完成自己的目標，在各領域上都有傑出的表現。

感謝實驗室的學弟妹：呈祥、昱仁、太獅、曉芬、煒琪、政豪、永軒、信展，感謝你們幫忙處理實驗室的大小事物，讓我們這群碩二能心無旁騖地做實驗。有了你們這些新血的加入，也爲實驗室帶來了不少歡樂的氣氛。

最後我要感謝家人在背後的支持，提供我一個無憂無慮的環境，讓我能順利地完成學業。

Contents

中文摘要.....	i
Abstract.....	ii
誌謝.....	iv
Contents.....	v
List of Table.....	vii
Figure Captions.....	viii
Chapter 1: Introduction.....	1
1-1 Preface.....	1
1-2 Basic operating principle of OLEDs.....	3
1-3 Charge injection.....	4
1-4 Charge transport inside the organic materials.....	8
1-5 Excitons.....	12
1-6 Phosphorescent OLEDs.....	14
1-7 Energy transfer.....	17
Chapter 2: Motivation.....	21
Chapter 3: Experiments.....	23
3-1 Host and dopant materials.....	23
3-2 Stern-Volmer experiment.....	25
3-3 The fabrication process of PLEDs.....	27
3-3-1 ITO substrates cleaning.....	27
3-3-2 Spin-coating of polymer films.....	27

3-3-3 Evaporation of the metal cathodes.....	29
3-4 Analytic Tools.....	30
3-4-1 Atomic Force Microscope (AFM).....	30
3-4-2 UV/Vis spectrometer.....	30
3-4-3 Photoluminescence (PL) and electroluminescence (EL) spectra.....	30
3-4-4 Current, voltage and brightness measurement.....	31
3-4-5 Dynamic light scattering (DLS).....	31
Chapter 4: Results	32
4-1 Stern-Volmer experiment.....	32
4-2 Hydrodynamic radius of PFam4.....	50
4-3 Device performance.....	52
Chapter 5: Discussion	56
5-1 Analysis of Stern-Volmer experiment.....	56
5-2 Analysis of device performance.....	67
Chapter 6: Conclusion	68
Chapter 7: Future Work	70
Reference	71
Appendix	75
Appendix-1 The PFam4-FIrpic system in the toluene solution.....	75
Appendix-2 The PFam4-FIrpic system in the DCB solution.....	78
Appendix-3 The PFam4-FIrpic system in the cosolvent solution.....	81
Appendix-4 The PFam4-Ir(mppy) ₃ system in the toluene solution.....	84
Appendix-5 The PFam4-Ir(mppy) ₃ system in the DCB solution.....	87
Appendix-6 The PFam4-Ir(mppy) ₃ system in the cosolvent solution.....	90
Appendix-7 The PFam4- Ir(FIPy) ₂ (acac) system in the toluene solution.....	93



List of Table

Table 4-1-1	The lifetimes of Ir(mppy) ₃ at various concentrations of PFam4 in toluene.....	37
Table 4-1-2	The lifetimes of Ir(mppy) ₃ at various concentrations of PFam4 in DCB.....	38
Table 4-1-3	The lifetimes of Ir(mppy) ₃ at various concentrations of PFam4 in cosolvent....	39
Table 4-1-4	The lifetimes of FIrpic at various concentrations of PFam4 in toluene.....	41
Table 4-1-5	The lifetimes of FIrpic at various concentrations of PFam4 in DCB.....	42
Table 4-1-6	The lifetimes of FIrpic at various concentrations of PFam4 in cosolvent.....	43
Table 4-1-7	The lifetimes of Ir(FIPy) ₂ (acac) at various concentrations of PFam4 in toluene.....	45
Table 4-1-8	The Stern-Volmer quenching constants of the PFam4-Ir(mppy) ₃ system in different solvents.....	47
Table 4-1-9	The Stern-Volmer quenching constants of the PFam4-FIrpic system in different solvents.....	48
Table 4-1-10	The Stern-Volmer quenching constants of the PFam4-Ir(FIPy) ₂ (acac) system in toluene.....	49

Figure Captions

Figure 1-1	(a) Flexible OLED; (b) SAMSUNG OLED TV.....	1
Figure 1-2	Basic operating principle of OLEDs.....	3
Figure 1-3-1	Schottky thermal emission and Fowler-Nordheim tunneling.....	5
Figure 1-3-2	Space-charge-limited current.....	6
Figure 1-3-3	(a) device structure; (b) band diagram.....	6
Figure 1-3-4	I-V characteristics on a log-log scale for PF2/6am4 at different dopant concentration.....	7
Figure 1-4-1	Electron density projection on the ac plane of the crystal.....	9
Figure 1-4-2	The temperature dependence of electron mobility in the c' direction of naphthalene single crystal.....	10
Figure 1-4-3	(a) Formation of a molecular crystal by a localized charge carrier (b) Process of electronic polarization-formation of induced dipoles μ on neutral molecules of the crystal in the field of a localized positive charge carrier.....	11
Figure 1-5-1	(a) Frenkel exciton; (b) Mott-Wannier exciton.....	12
Figure 1-5-2	Singlet and triplet states of excitons.....	13
Figure 1-7-1	Energy transfer between the host and the dopant molecules.....	18
Figure 1-7-2	Forster energy transfer.....	19
Figure 1-7-3	Dexter energy transfer.....	20
Figure 3-1-1	Chemical structure and spectrum characteristics of PFam4.....	23
Figure 3-1-2	Chemical structure and spectra characteristics of (a)Ir(mppy ₃); (b) FIrpic; (c) Ir(FIPy) ₂ (acac).....	24
Figure 3-3-2-1	The chemical structure of PEDOT:PSS.....	28
Figure 3-3-2-2	The chemical structure of PVK.....	28

Figure 3-3-3	The device structure in this study.....	29
Figure 4-1-1	Normalized absorption spectra of phosphorescent dopants and PFam4 in the toluene solutions.....	32
Figure 4-1-2	Normalized absorption spectra of phosphorescent dopants and PFam4 in the DCB solutions.....	33
Figure 4-1-3	Normalized absorption spectra of phosphorescent dopants and PFam4 in the cosolvent solutions.....	33
Figure 4-1-4	Normalized PL spectra of phosphorescent dopants and PFam4 in toluene solutions.....	34
Figure 4-1-5	Normalized PL spectra of phosphorescent dopants and PFam4 in DCB solutions.....	35
Figure 4-1-6	Normalized PL spectra of phosphorescent dopants and PFam4 in cosolvent solutions.....	35
Figure 4-1-7	A plot of natural logarithm of the photoluminescence intensity of Ir(mppy) ₃ versus time at different PFam4 concentrations in toluene (in monomer unit); [PFam4] = (a) 0; (b)1; (c)2; (d)3; (e)4 mM in monomer unit.....	37
Figure 4-1-8	A plot of natural logarithm of the photoluminescence intensity of Ir(mppy) ₃ versus time at different PFam4 concentrations in DCB (in monomer unit); [PFam4] = (a) 0; (b)1; (c)2; (d)3; (e)4 mM in monomer unit.....	38
Figure 4-1-9	A plot of natural logarithm of the photoluminescence intensity of Ir(mppy) ₃ versus time at different PFam4 concentrations in cosolvent (in monomer unit); [PFam4] = (a) 0; (b)1; (c)2; (d)3; (e)4 mM in monomer unit.....	39
Figure 4-1-10	A plot of natural logarithm of the photoluminescence intensity of FIrpic versus time at different PFam4 concentrations in toluene (in monomer unit); [PFam4] = (a) 0; (b)1; (c)2; (d)3; (e)4 mM in monomer unit.....	41

Figure 4-1-11	A plot of natural logarithm of the photoluminescence intensity of FIrpic versus time at different PFam4 concentrations in DCB (in monomer unit); [PFam4] = (a) 0; (b)1; (c)2; (d)3; (e)4 mM in monomer unit.....	42
Figure 4-1-12	A plot of natural logarithm of the photoluminescence intensity of FIrpic versus time at different PFam4 concentrations in cosolvent (in monomer unit); [PFam4] = (a) 0; (b)1; (c)2; (d)3; (e)4 mM in monomer unit.....	43
Figure 4-1-13	A plot of natural logarithm of the photoluminescence intensity of Ir(FIPy) ₂ (acac) versus time at different PFam4 concentrations in toluene (in monomer unit); [PFam4] = (a) 0; (b)1; (c)2; (d)3; (e)4 mM in monomer unit.....	45
Figure 4-1-14	The Stern-Volmer plot for the PFam4-Ir(mppy) ₃ system in different solvents.....	47
Figure 4-1-15	The Stern-Volmer plot for the PFam4-FIrpic system in different solvents.....	48
Figure 4-1-16	The Stern-Volmer plot for the PFam4-Ir(FIPy) ₂ (acac) system in toluene.....	49
Figure 4-2	(a) The distribution of hydrodynamic diameter of PFam4 in toluene; (b) The distribution of hydrodynamic diameter of PFam4 in DCB.....	51
Figure 4-3-1	J-V plot.....	52
Figure 4-3-2	Luminescence efficiency (cd/A) vs current density.....	53
Figure 4-3-3	AFM morphology of emitting layer (a) PFam4-Ir(mppy) ₃ dissolved in toluene; (b) PFam4-Ir(mppy) ₃ dissolved in DCB.....	54
Figure 4-3-4	Absorption spectra of the pure PFam4 films that were cast from the toluene and DCB, respectively.....	54
Figure 4-3-5	Normalized EL spectra of two types of devices from different solution.....	55
Figure 5-1-1	The triplet energy diagrams.....	57
Figure 5-1-2	Reactants in solution.....	59

Figure 5-1-3	(a) Absorption spectra of PFam4 in toluene, DCB and cosolvent. (b) PL spectra of PFam4 in toluene, DCB and cosolvent.....	63
Figure A-1-1	For the PFam4-FIrpc system in the toluene solution, the photoluminescence decay curve of FIrpc at [PFam4]=0M (a) photoluminescence intensity $I(t)$ versus t ; (b) $\ln I(t)$ versus t	76
Figure A-1-2	For the PFam4-FIrpc system in the toluene solution, the photoluminescence decay curve of FIrpc at [PFam4]=1mM (a) photoluminescence intensity $I(t)$ versus t ;(b) $\ln I(t)$ versus t	76
Figure A-1-3	For the PFam4-FIrpc system in the toluene solution, the photoluminescence decay curve of FIrpc at [PFam4]=2mM (a) photoluminescence intensity $I(t)$ versus t ; (b) $\ln I(t)$ versus t	77
Figure A-1-4	For the PFam4-FIrpc system in the toluene solution, the photoluminescence decay curve of FIrpc at [PFam4]=3mM (a) photoluminescence intensity $I(t)$ versus t ; (b) $\ln I(t)$ versus t	77
Figure A-1-5	For the PFam4-FIrpc system in the toluene solution, the photoluminescence decay curve of FIrpc at [PFam4]=4mM (a) photoluminescence intensity $I(t)$ versus t ; (b) $\ln I(t)$ versus t	78
Figure A-2-1	For the PFam4-FIrpc system in the DCB solution, the photoluminescence decay curve of FIrpc at [PFam4]=0M (a) photoluminescence intensity $I(t)$ versus t ; (b) $\ln I(t)$ versus t	79
Figure A-2-2	For the PFam4-FIrpc system in the DCB solution, the photoluminescence decay curve of FIrpc at [PFam4]=1mM (a) photoluminescence intensity $I(t)$ versus t ; (b) $\ln I(t)$ versus t	79
Figure A-2-3	For the PFam4-FIrpc system in the DCB solution, the photoluminescence decay curve of FIrpc at [PFam4]=2mM (a) photoluminescence intensity $I(t)$ versus t ; (b) $\ln I(t)$ versus t	80

Figure A-2-4	For the PFam4-FIrpc system in the DCB solution, the photoluminescence decay curve of FIrpc at [PFam4]=3mM (a) photoluminescence intensity $I(t)$ versus t ; (b) $\ln I(t)$ versus t	80
Figure A-2-5	For the PFam4-FIrpc system in the DCB solution, the photoluminescence decay curve of FIrpc at [PFam4]=4mM (a) photoluminescence intensity $I(t)$ versus t ; (b) $\ln I(t)$ versus t	81
Figure A-3-1	For the PFam4-FIrpc system in the cosolvent solution, the photoluminescence decay curve of FIrpc at [PFam4]=0M (a) photoluminescence intensity $I(t)$ versus t ; (b) $\ln I(t)$ versus t	82
Figure A-3-2	For the PFam4-FIrpc system in the cosolvent solution, the photoluminescence decay curve of FIrpc at [PFam4]=1mM (a) photoluminescence intensity $I(t)$ versus t ; (b) $\ln I(t)$ versus t	82
Figure A-3-3	For the PFam4-FIrpc system in the cosolvent solution, the photoluminescence decay curve of FIrpc at [PFam4]=2mM (a) photoluminescence intensity $I(t)$ versus t ; (b) $\ln I(t)$ versus t	83
Figure A-3-4	For the PFam4-FIrpc system in the cosolvent solution, the photoluminescence decay curve of FIrpc at [PFam4]=3mM (a) photoluminescence intensity $I(t)$ versus t ; (b) $\ln I(t)$ versus t	83
Figure A-3-5	For the PFam4-FIrpc system in the cosolvent solution, the photoluminescence decay curve of FIrpc at [PFam4]=4mM (a) photoluminescence intensity $I(t)$ versus t ; (b) $\ln I(t)$ versus t	84
Figure A-4-1	For the PFam4-Ir(mppy) ₃ system in the toluene solution, the photoluminescence decay curve of Ir(mppy) ₃ at [PFam4]=0M (a) photoluminescence intensity $I(t)$ versus t ; (b) $\ln I(t)$ versus t	85

Figure A-4-2	For the PFam4-Ir(mppy) ₃ system in the toluene solution, the photoluminescence decay curve of Ir(mppy) ₃ at [PFam4]=1mM (a) photoluminescence intensity I(t) versus t; (b) ln I(t) versus t.....	85
Figure A-4-3	For the PFam4-Ir(mppy) ₃ system in the toluene solution, the photoluminescence decay curve of Ir(mppy) ₃ at [PFam4]=2mM (a) photoluminescence intensity I(t) versus t; (b) ln I(t) versus t.....	86
Figure A-4-4	For the PFam4-Ir(mppy) ₃ system in the toluene solution, the photoluminescence decay curve of Ir(mppy) ₃ at [PFam4]=3mM (a) photoluminescence intensity I(t) versus t; (b) ln I(t) versus t.....	86
Figure A-4-5	For the PFam4-Ir(mppy) ₃ system in the toluene solution, the photoluminescence decay curve of Ir(mppy) ₃ at [PFam4]=4mM (a) photoluminescence intensity I(t) versus t; (b) ln I(t) versus t.....	87
Figure A-5-1	For the PFam4-Ir(mppy) ₃ system in the DCB solution, the photoluminescence decay curve of Ir(mppy) ₃ at [PFam4]=0M (a) photoluminescence intensity I(t) versus t; (b) ln I(t) versus t.....	88
Figure A-5-2	For the PFam4-Ir(mppy) ₃ system in the DCB solution, the photoluminescence decay curve of Ir(mppy) ₃ at [PFam4]=1mM (a) photoluminescence intensity I(t) versus t; (b) ln I(t) versus t.....	88
Figure A-5-3	For the PFam4-Ir(mppy) ₃ system in the DCB solution, the photoluminescence decay curve of Ir(mppy) ₃ at [PFam4]=2mM (a) photoluminescence intensity I(t) versus t; (b) ln I(t) versus t.....	89
Figure A-5-4	For the PFam4-Ir(mppy) ₃ system in the DCB solution, the photoluminescence decay curve of Ir(mppy) ₃ at [PFam4]=3mM (a) photoluminescence intensity I(t) versus t; (b) ln I(t) versus t.....	89

Figure A-5-5	For the PFam4-Ir(mppy) ₃ system in the DCB solution, the photoluminescence decay curve of Ir(mppy) ₃ at [PFam4]=4mM (a) photoluminescence intensity I(t) versus t; (b) ln I(t) versus t.....	90
Figure A-6-1	For the PFam4-Ir(mppy) ₃ system in the cosolvent solution, the photoluminescence decay curve of Ir(mppy) ₃ at [PFam4]=0M (a) photoluminescence intensity I(t) versus t; (b) ln I(t) versus t.....	91
Figure A-6-2	For the PFam4-Ir(mppy) ₃ system in the cosolvent solution, the photoluminescence decay curve of Ir(mppy) ₃ at [PFam4]=1mM (a) photoluminescence intensity I(t) versus t; (b) ln I(t) versus t.....	91
Figure A-6-3	For PFam4-Ir(mppy) ₃ system in the cosolvent solution, the photoluminescence decay curve of Ir(mppy) ₃ at [PFam4]=2mM (a) photoluminescence intensity I(t) versus t; (b) ln I(t) versus t.....	92
Figure A-6-4	For the PFam4-Ir(mppy) ₃ system in the cosolvent solution, the photoluminescence decay curve of Ir(mppy) ₃ at [PFam4]=3mM (a) photoluminescence intensity I(t) versus t; (b) ln I(t) versus t.....	92
Figure A-6-5	For the PFam4-Ir(mppy) ₃ system in the cosolvent solution, the photoluminescence decay curve of Ir(mppy) ₃ at [PFam4]=4mM (a) photoluminescence intensity I(t) versus t; (b) ln I(t) versus t.....	93
Figure A-7-1	For the PFam4-Ir(FIPy) ₂ (acac) system in the toluene solution, the photoluminescence decay curve of Ir(FIPy) ₂ (acac) at [PFam4]=0M (a) photoluminescence intensity I(t) versus t; (b) ln I(t) versus t.....	94
Figure A-7-2	For the PFam4-Ir(FIPy) ₂ (acac) system in the toluene solution, the photoluminescence decay curve of Ir(FIPy) ₂ (acac) at [PFam4]=1mM (a) photoluminescence intensity I(t) versus t; (b) ln I(t) versus t.....	94

Figure A-7-3	For the PFam4-Ir(FIPy) ₂ (acac) system in the toluene solution, the photoluminescence decay curve of Ir(FIPy) ₂ (acac) at [PFam4]=2mM (a) photoluminescence intensity I(t) versus t; (b) ln I(t) versus t.....	95
Figure A-7-4	For the PFam4-Ir(FIPy) ₂ (acac) system in the toluene solution, the photoluminescence decay curve of Ir(FIPy) ₂ (acac) at [PFam4]=3mM (a) photoluminescence intensity I(t) versus t; (b) ln I(t) versus t.....	95
Figure A-7-5	For the PFam4-Ir(FIPy) ₂ (acac) system in the toluene solution, the photoluminescence decay curve of Ir(FIPy) ₂ (acac) at [PFam4]=4mM (a) photoluminescence intensity I(t) versus t; (b) ln I(t) versus t.....	96



Chapter 1 Introduction

1-1 Preface

In 1963, Dr. Pope and coworkers invented the first organic light-emitting diodes (OLED) based on anthracene, but the operating voltage is too high [1]. In 1987, Dr. Tang and Dr. VanSlyke used thermal vapor deposition to make an OLED with thin films, and decreased the operating voltage below 10 V [2]. Since then, the OLED has been extensively studied and developed.

Compared with liquid crystal displays (LCDs) and inorganic light-emitting diodes (LEDs), OLEDs have many benefits. OLEDs emit light by themselves, so they can be thinner than LCDs. OLEDs also have high contrast, fast response, and low fabrication cost due to the easier processes. OLEDs can also be fabricated on plastic substrates to realize flexible displays [figure 1-1(a)(b)].



Figure 1-1(a) Flexible OLED
(www.universaldisplay.com)



1-1(b) SAMSUNG OLED TV
(www.engadget.com/2005/05/20/samsungs-40-inch-oled-tv-pics)

On the other hand, in 1976, Alan Heeger, Alan MacDiarmid, Hideki Shirakawa discovered the conducting polymers [3, 4]. They three were also awarded Nobel Prize in

Chemistry in 2000 for the discovery and development of conductive polymers. In 1990, J. H. Burroughes and his coworkers invented the first polymer light-emitting diode (PLED) [5], and the research in PLEDs has grown tremendously from that time. The fabrication cost of PLEDs is much lower than that of OLEDs based on small organic molecules, because PLEDs can be fabricated by solution process, such as spin-coating and ink-jet printing. It is also easily to make large-area flat-panel displays by solution processes.

Organic materials have great advantages that inorganic materials cannot achieve. We can improve and change the color, electrical, physical and chemical properties by synthesis. Therefore, we can have a variety of organic materials.



1-2 Basic operating principle of OLEDs

In the basic operating principle of OLEDs, electrons are injected from the cathode and holes are injected from the anode. Then, electrons and holes transport inside the organic materials. Finally, electrons and holes combine to form excitons, and excitons will go back to the ground states by emitting light (Figure 1-2).

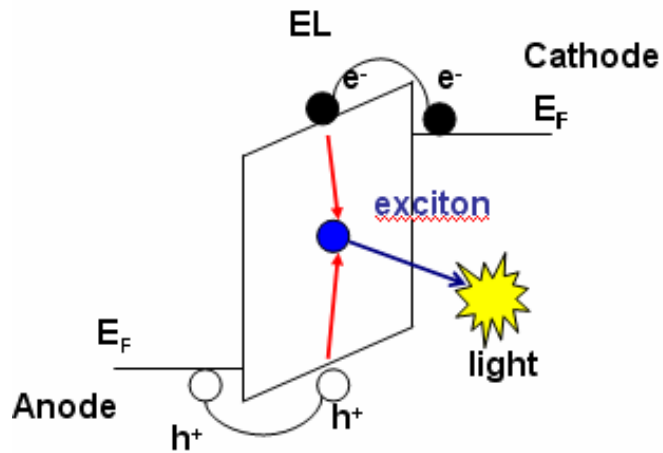


Figure 1-2 Basic operating principle of OLEDs

E_F is the Fermi energy; e^- is electron; h^+ is hole;

EL is the emitting layer

1-3 Charge injection

Charge injection from the electrodes and charge transport inside the organic materials are important issues to achieve high efficiency of OLEDs. They relate to the charge balance and the location of recombination zone. Unbalance electron and hole quantity and the recombination zone near the anode or cathode would decrease the efficiency of OLEDs.

Electrons are injected from the cathode and holes are injected from the anode, respectively. Depending on the barrier height (ϕ_B), there are four charge-injection mechanisms. As $\phi_B < 0.2-0.3$ eV, the charge-injection mechanism is considered as Ohmic contact. Ohmic contact would not significantly perturb the device performance. The current density-voltage (J-V) characteristics for Ohmic contacts is described by [6]

$$J = q\mu_n n_0 \frac{V}{d} \quad (\text{eq. 1-3-1})$$

where q is the charge of the electron, μ_n is the electron mobility and d is the thickness of the active-layer. For much higher barrier height ($\phi_B > 0.2-0.3$ eV), there are two charge-injection mechanisms for the electrode-organic semiconductor interface, Schottky thermal emission and Fowler-Nordheim tunneling injection [7]. As an electron acquires enough energy from the applied voltage, the electron can overcome the barrier height and be injected into the organic layer. The Schottky thermal emission is expressed as [6]

$$J = A^* T^2 \exp\left(\frac{-q\phi_B}{kT}\right) \left[\exp\left(\frac{qV}{kT}\right) - 1\right] \quad (\text{eq. 1-3-2})$$

where A^* is called the effective Richardson constant, T is the absolute temperature, q is the elementary charge, ϕ_B is the barrier height and k is Boltzmann's constant. Another way of charge injection is Fowler-Nordheim tunneling injection; it takes the form [6, 7]

$$J = \left(\frac{q^3 V^2 m_0}{8\pi h \phi_B m^*}\right) \exp\left(-\frac{4\sqrt{2m^* \phi_B^3}}{3\hbar q V}\right) \quad (\text{eq. 1-3-3})$$

where m_0 is the mass of the free electron and m^* is the effective mass (Figure 1-3-1). The tunneling dominates when the width of the barrier is small.

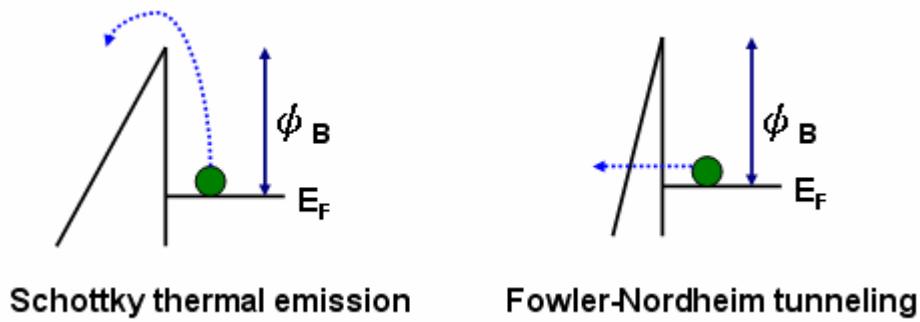


Figure 1-3-1 Schottky thermal emission and Fowler-Nordheim tunneling

The last charge-injection mechanism is space-charge-limited current (SCLC) mechanism [Figure 1-3-2]. Injected charges can accumulate easily to form space charges near the organic/electrode interface because the charge mobility is usually low in organic materials. These accumulated charges would repel further charges from the electrode and induce an internal electric field. Then, the motion of charges is influenced under the applied field and the induced field. The SCLC is described by [6, 7]

$$J = \frac{9\varepsilon\mu V^2}{8L^3} \quad (\text{eq. 1-3-4})$$

where ε is the dielectric constant, L is the film thickness and μ is the mobility.

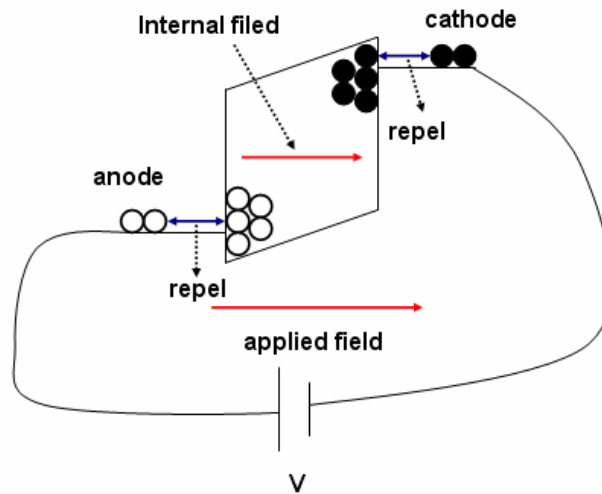


Figure 1-3-2 space-charge-limited current

Generally, there is not one unique mechanism as being responsible for the electrical behavior of OLEDs. We take the host-dopant system as the example, which is researched by H. A. Al Attar and A. P. Monkman [8], where the host is poly[9, 9-bis(2-ethylhexyl)fluorene-2, 7-diy] end-capped with bis(4-methyl phenyl)phenylamine (PF2/6am4) and the dopant is tris(phenylpyridine) iridium(III) ($\text{Ir}(\text{ppy})_3$). The device structure and the band diagram are shown in Figure 1-3-3. The current-voltage (I-V) curve at different dopant concentrations is shown in Figure 1-3-4.

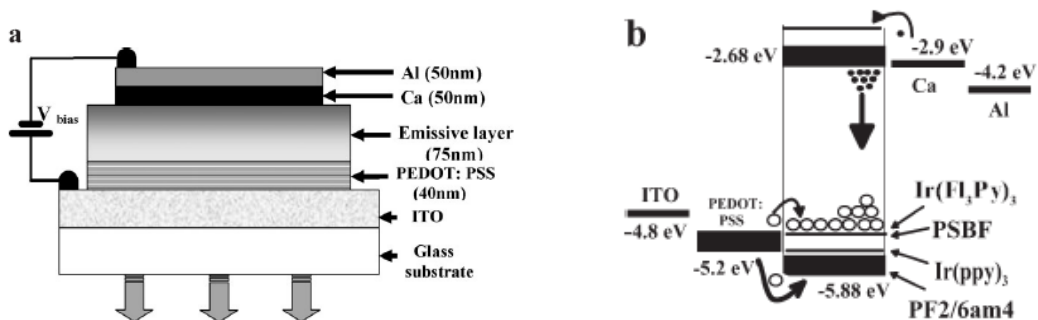


Figure 1-3-3 (a) device structure; (b) band diagram [8]

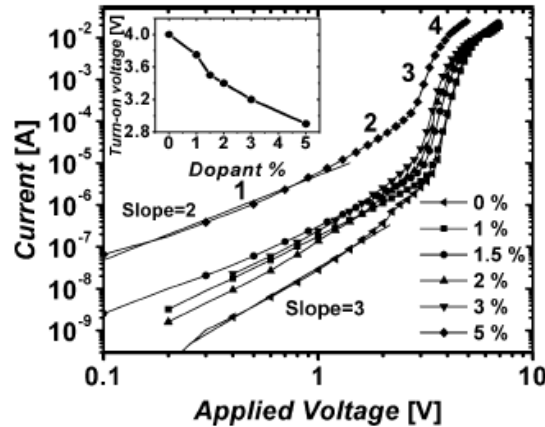
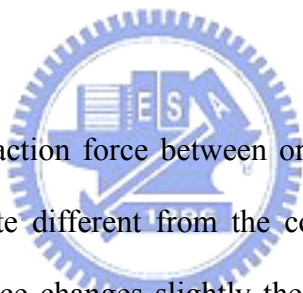


Figure 1-3-4 I-V characteristics on a log-log scale for PF2/6am4 at different dopant concentration [8].

From Figure 1-3-4, there are four different regions that are ascribed to different mechanisms. Because the barrier height on the anode side is 0.6V and that on the cathode side is ohmic contact, the current in regions 1 and 2 is owing to electron injection from the cathode. If the current is obeyed Ohmic's law (eq. 1-3-1), the slope should be one. From Figure 1-3-4, no slope in regions 1 and 2 is one, since there is high density of deep traps in organic semiconductor, in which case the I-V characteristics would show SCLC with a trap-distribution. As doping concentration is 5%, the slope is two. It suggests that the trap sites are all filled by the injected electrons. Any further injected electrons will accumulate in the active layer, and then the behavior of I-V will obey trap-free SCLC mechanism (eq. 1-3-4). Besides, Schottky thermionic emission and tunneling effects may contribute near the end of region 2. In region 3, the device starts to emit light. Region 3 is dominated by hole tunneling (eq. 1-3-3) because injected electrons are trapped near the cathode. The I-V characteristic in region 4 is assign for SCLC with an exponential distribution of trap-level energies [8]. It has also shown that the dopant can decrease the barrier height on the anode side and increase the free-electron density and the electron mobility by reducing the characteristic energy of the electron trap [8].

1-4 Charge transport inside the organic materials

The charge transport inside the organic semiconductor has been a controversial issue. Many scientists have developed a lot of theories to picture the charge transport inside the organic semiconductor. Because the development of inorganic semiconductors, such as Si semiconductor, is earlier and the band theory can give an accurate estimation on the charge motion inside the inorganic semiconductors, scientists first applied the band theory to explain the charge transport inside the organic semiconductors. However, the estimated values from the band theory are inconsistent with the experimental values. Even the bandwidth, which is calculated from the band theory, is quite small. Principally, band theory concepts are not valid for narrow band cases [9].



The intermolecular interaction force between organic molecules is a weak force, Van der Waals force, which is quite different from the covalent force between Si atoms in Si semiconductors. This weak force changes slightly the electronic structure of molecules and molecules retain their individuality in the crystal state. It can be shown that the electron density localizes around the molecule itself from X-ray analysis [Figure 1-4-1], and the optical spectrum of organic crystal is almost the same as an isolated molecule. Nevertheless, there are also some new optical and electronic properties due to collective molecular interaction, such as Davydov splitting. It is therefore necessary to combine molecular and solid-state aspects as treated in the optical and electronic properties of organic crystals [9].

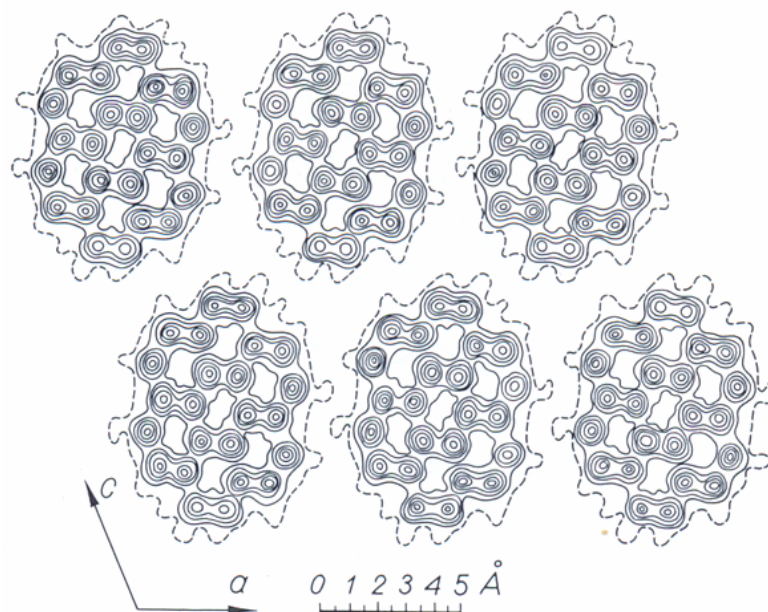


Figure 1-4-1 Electron density projection on the ac plane of the crystal [9]

From the above reasons, the band model maybe is not a practical model for organic semiconductor. In 1966, R. M. Glaeser and R. S. Berry developed a modified hopping model, and the computational values from their model are consistent with the experimental values [9, 10]. According to their model, the mechanism of electron transport in organic semiconductors is tunneling or resonance transfer of an excess charge between neighboring molecules. This process depends on the separation distance between neighboring molecules. If the two neighboring molecules are at the excited vibrational states, the separation distance between them would decrease, and the probability of this process increases. So, this mechanism is a phonon-assisted process. The charge carrier also jumps randomly [9, 10].

However, as temperature below 100K, the charge transport mechanism is dominated by band theory [Figure 1-4-2]. The temperature dependence of mobility is on exponential form. As temperature above 150K, the charge transport mechanism is governed by a hopping model and it is an intermediate region as the temperature is between 100K and 150K [9].

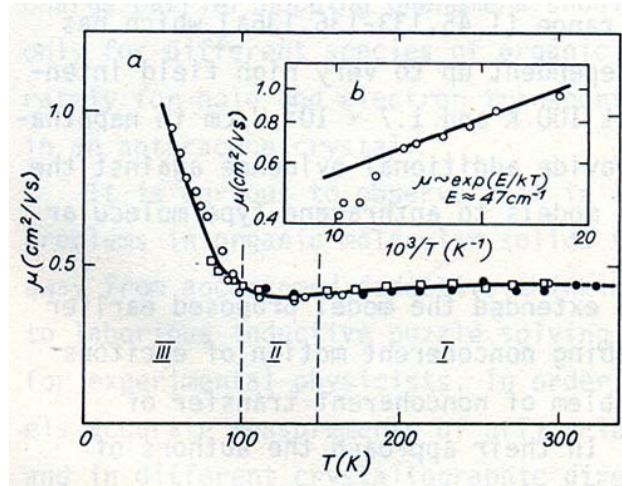


Figure 1-4-2 The temperature dependence of electron mobility in the c' direction of naphthalene single crystal [9]

Most organic semiconductor materials are based on conjugated molecules. The electron cloud of conjugated molecules is quite delocalized and polarizable. The time of a charge carrier localized in a molecule is long, $\tau_h > 10^{-14}$ s. So, if a charge carrier is localized on a definite molecule, its electric field would act on neighboring molecules. Then, the π orbitals of neighboring molecules displace. The neighboring molecules are polarized by the localized charge carrier. Subsequently, the localized charge carrier would move or hop together with the polarization cloud, not a charge carrier alone. Such quantum state formed by the localized charge carrier and polarization cloud of neighboring molecules is called a polaron [Figure 1-4-3] [9, 11].

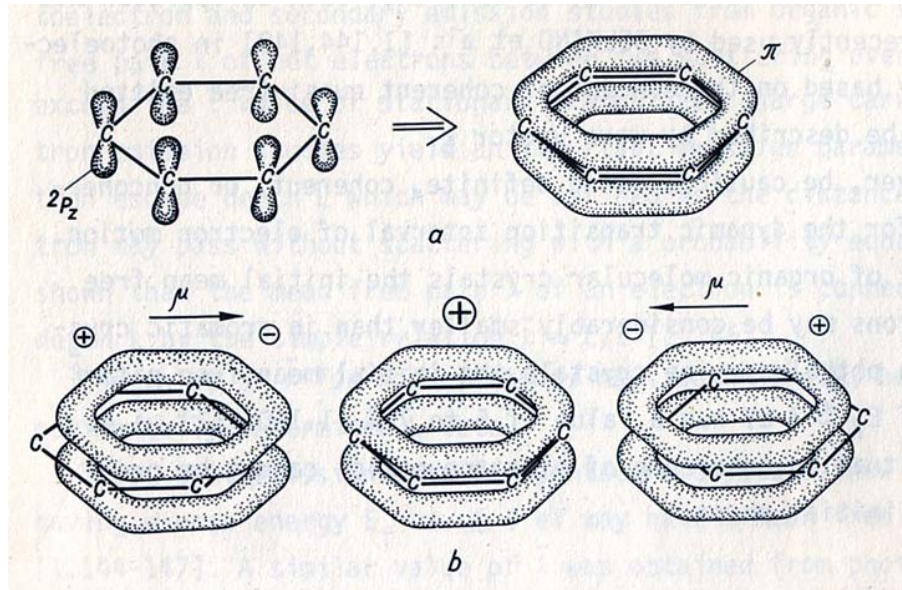
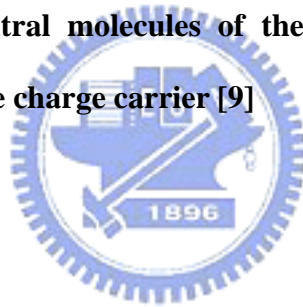


Figure 1-4-3 (a) Formation of a molecular crystal by a localized charge carrier

(b) Process of electronic polarization-formation of induced dipoles μ on neutral molecules of the crystal in the field of a localized positive charge carrier [9]



1-5 Excitons

An electron and a hole may be bound together by their attractive coulomb interaction to form a new quantum state. This bound electron-hole pair is called an exciton. Excitons can move through the crystal and transport their energy to nearby atoms or molecules. Excitons do not transport the charges since excitons are electrically neutral. There are two kinds of excitations: Frenkel excitons and Mott-Wannier excitons [Figure 1-5-1] [11].

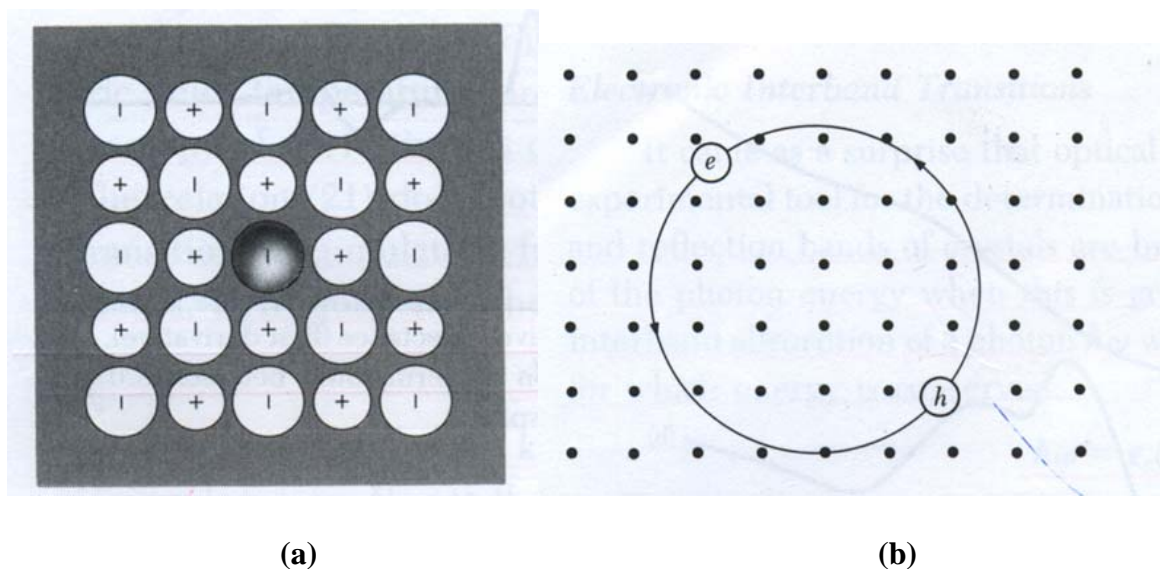


Figure 1-5-1 (a) Frenkel exciton; (b) Mott-Wannier exciton [11]

A Frenkel exciton is a tightly bound exciton and is localized on or near a single atom [Figure 1-5-1 (a)]. A Frenkel exciton is fundamentally an excited atom. In molecular crystal, the covalent binding between atoms, which are in the same molecule, is stronger than the van der Waals binding between different molecules. Therefore, the excitons in molecular crystal are Frenkel excitons [11]. The excitons in OLEDs and PLEDs are also Frenkel excitons [12]. On the other hand, a Mott-Wannier exciton is a weakly bound exciton and the distance between electron-hole pair is comparable with a lattice constants [Figure 1-5-1 (b)] [11].

According to the total spin angular momentum of excitons, there are two types of excitons, singlet excitons and triplet excitons. If the total spin angular momentum (s) is one, the exciton is triplet; if the total spin angular momentum (s) is zero, the exciton is singlet [13][Figure 1-5-2]. From the quantum mechanical spin statistics, there are 25% of excitons are singlets and the other 75% excitons are triplets in OLEDs.

$$\left\{ \begin{array}{l} \uparrow\uparrow \\ \frac{1}{\sqrt{2}}(\uparrow\downarrow + \downarrow\uparrow) \\ \downarrow\downarrow \end{array} \right\} s = 1 \text{ (triplet)} \quad \left\{ \frac{1}{\sqrt{2}}(\uparrow\downarrow - \downarrow\uparrow) \right\} s = 0 \text{ (singlet)}$$

Figure 1-5-2 singlet and triplet states of excitons



1-6 Phosphorescent OLEDs

From the quantum spin statistics, there are 25% of excitons are singlets and the other 75% of excitons are triplets. The triplet excitons cannot emit light for common organic molecules because of the selection rules by quantum mechanics [13]. Therefore, the internal quantum efficiency of OLEDs for usual materials is limited to 25%. However, in 1998, S. R. Forrest's and M. E. Thompson's groups used a phosphorescent dopant to harvest both singlet and triplet excitons and improved the efficiency of OLEDs significantly [14]. In 2001, a green phosphorescent OLED with nearly 100% internal quantum efficiency has also been demonstrated [15].

The phosphorescent dopants are heavy-metal (Pr, Ir, Ru, etc.) complexes. The heavy-metal complex enables to harvest both singlet and triplet excitons because of the heavy-metal effect. The heavy-metal effect is a strong spin-orbital coupling. It can lead to transition between singlet and triplet state and phosphorescence from triplet states.

The spin-orbital coupling constant is described as [16]

$$\zeta_{nl} = \frac{\alpha^2 R Z^4}{n^3 l(l + \frac{1}{2})(l + 1)} \quad (\text{eq. 1-6-1})$$

where α is a constant ($\alpha = \frac{e^2}{4\pi\epsilon_0 \hbar c}$), R is the Rydberg constant, Z is the atomic number, n is the principle quantum number, and l is the angular momentum quantum number. From eq. 1-6-1, we can see that the spin-orbital coupling is proportional to Z^4 . Therefore, spin-orbital coupling effect is much higher in heavy atoms than in light atoms.

In the following context, we will show how the spin-orbital coupling can mix states of

different multiplicity. Consider an operator [16]

$$\Omega = \sum_i R(i) s_z(i) \quad (\text{eq. 1-6-2})$$

where the sum is over all electrons in the molecule, R is an operator that acts on spatial wavefunction, s_z is an operator for z direction of spin wavefunction. The effect of Ω on a singlet state of two electrons, $|0,0\rangle$, can be demonstrated as follows [16]:

$$\begin{aligned} \Omega|0,0\rangle &= \{R(1)s_z(1) + R(2)s_z(2)\}N\varphi(1)\varphi(2)\{\alpha(1)\beta(2) - \beta(1)\alpha(2)\} \\ &= \frac{1}{2}\hbar N(\{R(1)\varphi(1)\}\varphi(2)\{\alpha(1)\beta(2) + \beta(1)\alpha(2)\} \\ &\quad - \varphi(1)\{R(2)\varphi(2)\}\{\alpha(1)\beta(2) + \beta(1)\alpha(2)\}) \\ &= N'\{\varphi'(1)\varphi(2) - \varphi(1)\varphi'(2)\}\{\alpha(1)\beta(2) + \beta(1)\alpha(2)\} \\ &\propto |1,0\rangle \end{aligned}$$

(eq. 1-6-3)

where ϕ is spatial component of the wavefunction, $\phi' = N\phi$, α means $m_s = \frac{1}{2}$ (\uparrow), β means $m_s = -\frac{1}{2}$ (\downarrow), and various constants have been absorbed into the normalization constant N and N'. From the last equation, we can see that the operator Ω transforms a singlet state $|0,0\rangle$ into a triplet state $|1,0\rangle$. It also means that Ω can mix the $M_s=0$ state of triplet with singlet state [16].

The spin-orbital coupling can be expressed as [16]

$$H_{SO} = \sum_i \xi_i / i S_i \quad (\text{eq. 1-6-4})$$

This operator has the form as Ω , and so we should anticipate that the spin-orbital coupling can mix singlet with triplet. For a system with two electrons, it takes the form

$$\begin{aligned}
H_{so} &= \xi_1 l_1 \cdot \mathbf{s}_1 + \xi_2 l_2 \cdot \mathbf{s}_2 \\
&= \frac{1}{2} (\xi_1 l_1 + \xi_2 l_2) \cdot (\mathbf{s}_1 + \mathbf{s}_2) + \frac{1}{2} (\xi_1 l_1 - \xi_2 l_2) \cdot (\mathbf{s}_1 - \mathbf{s}_2)
\end{aligned} \tag{eq. 1-6-5}$$

The operator $\mathbf{s}_1 + \mathbf{s}_2$ cannot mix states of different multiplicity since $\mathbf{s}_1 + \mathbf{s}_2$ commutes with \mathbf{S}^2 , which is the total spin operator. Nevertheless, the operator $\mathbf{s}_1 - \mathbf{s}_2$ does not commute with \mathbf{S}^2 . So, singlet-triplet mixing ascribes to this operator $\mathbf{s}_1 - \mathbf{s}_2$ [16].

$$\langle 1, M_s | H_{so} | 0, 0 \rangle = \frac{1}{2} \langle 1, M_s | (\xi_1 l_1 - \xi_2 l_2) \cdot (\mathbf{s}_1 - \mathbf{s}_2) | 0, 0 \rangle \tag{eq. 1-6-6}$$

Consequently, the remaining orbital operator part of the spin-orbital coupling Hamiltonian is [16]

$$\langle 1, 0 | H_{so} | 0, 0 \rangle = \frac{1}{2} \hbar (\xi_1 l_{1z} - \xi_2 l_{2z}) \tag{eq. 1-6-7}$$

For the z-component of the spin-orbital coupling, its effect is [16]

$$\begin{aligned}
(\mathbf{S}_{1z} - \mathbf{S}_{2z}) | 0, 0 \rangle &= (\mathbf{s}_{1z} - \mathbf{s}_{2z}) \frac{1}{\sqrt{2}} \{ \alpha(1)\beta(2) - \beta(1)\alpha(2) \} \\
&= \hbar \frac{1}{\sqrt{2}} \{ \alpha(1)\beta(2) + \beta(1)\alpha(2) \} \\
&= \hbar | 1, 0 \rangle
\end{aligned} \tag{eq. 1-6-8}$$

From the above proof, we can see that the spin-orbital coupling can mix singlet and triplet states and enable intersystem crossing between different multiplicities. However, this effect (mixing states and intersystem crossing between different multiplicities) is remarkable for heavy atoms. For light atoms, the probability of this effect is limited because spin-orbital coupling is proportional to Z^4 .

1-7 Energy transfer

In phosphorescent OLEDs, all excitons can be harvested on phosphorescent dopants. There are four ways to harvest both singlet and triplet excitons at the triplet state of phosphorescent dopant, theoretically. As an electron or a hole is trapped at the phosphorescent dopant, the dopant will recombine with the opposite carrier and eventually an exciton will be formed at the dopant. First, if an exciton is at the triplet state of the dopant, it will decay to the ground state by emitting light. Second, if an exciton is at the singlet state of the dopant, the exciton will transfer to the triplet state by intersystem crossing, which is realized and fast for the phosphorescent dopant due to the strong spin-orbital coupling. The trapping charge at the dopant site to form exciton contributes to the electroluminescence much [17, 18]. Third, as an exciton is formed at the singlet state of the host, the exciton will transfer to the singlet state of the dopant through Forster energy transfer, or to the triplet state of the dopant through Dexter energy transfer. Finally, if an exciton is formed at the triplet state of the host, it will transfer to the triplet state of the dopant by Dexter energy transfer. These mechanisms are shown in Figure 1-7-1.

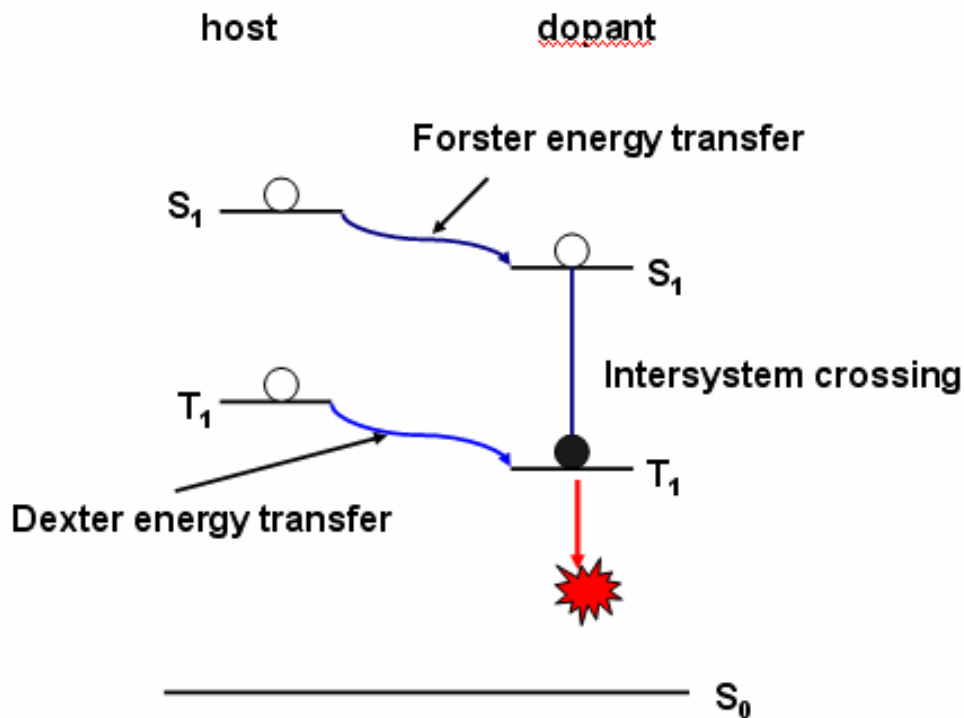


Figure 1-7-1 Energy transfer between the host and dopant molecules. S_1 is the singlet state, T_1 is the triplet state, S_0 is the ground state

There are two kinds of energy transfer mechanisms: Forster energy transfer and Dexter energy transfer [19, 20]. Forster energy transfer involves a dipole-dipole interaction between the energy donor and the energy acceptor. An excited molecule can be supposed as an electric dipole moment. The electric field generated by the excited molecule causes electrostatic forces, Coulombic force, to exert on the nearby molecules. Then, a resonance coupling may occur. The electrons of a nearby molecule at the ground state may oscillate in the same frequency as the excited molecule. Finally, energy transfer happens. Energy donor becomes a non-excited molecule and energy acceptor becomes an excited molecule [Figure 1-7-2]. The rate of the Forster energy transfer is described as:

$$k_{D^* \rightarrow A}(\text{Forster}) = \frac{9000 \ln 10 k^2}{128 \pi^6 N_A n^4 T_D R^6} \int_0^{\infty} f_D(\nu) \epsilon_A(\nu) \frac{d\nu}{\nu^4} \quad (\text{eq. 1-7-1})$$

where κ is an orientation factor ($\kappa^2 = \frac{2}{3}$ for random donor-acceptor orientation), N_A is Avogadro's number, τ_D is the lifetime of the donor, f_D is the emission spectrum of the donor, ϵ_A is the molar decadic extinction coefficient of the acceptor, and ν is the wavenumber. We define Forster radius, R_0 , as the distance between the donor and acceptor at which the probability of the energy transfer equals to that of the unimolecular decay process of the donor.

$$R_0^6 = \frac{9000 \ln 10 \kappa^2}{128 \pi^6 n^4 N_A} \int_0^\infty f_D(\nu) \epsilon_A(\nu) \frac{d\nu}{\nu^4} \quad (\text{eq. 1-7-2})$$

Forster energy transfer can be quite strong over large distance because it is via Coulombic force. There is one restriction on Forster energy transfer: Forster energy transfer requires that both donor and acceptor are singlet states. The donor and acceptor must respectively obey selection rules before and after energy transfer process because the Forster energy transfer is a long distance interaction [19, 20, 21].

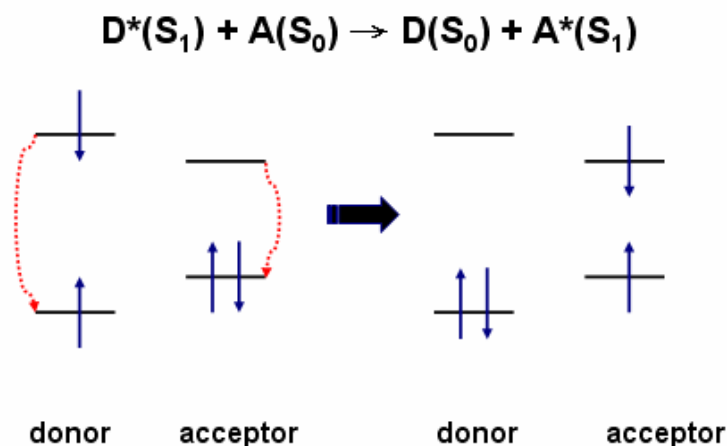


Figure 1-7-2 Forster energy transfer

D is the donor, A is the acceptor

Dexter energy transfer is via direct electron exchange between the donor and acceptor. Dexter energy transfer can occur between singlet states or triplet states or between singlet and triplet states since Dexter energy transfer needs the ΔS (S is the total spin angular momentum, $\Delta S = S_{\text{after energy transfer}} - S_{\text{before energy transfer}}$) of donor-acceptor system to be zero. Dexter energy transfer requires orbital overlap between the donor and the acceptor, so Dexter energy transfer happens at short distance between the donor and acceptor. The probability of Dexter energy transfer is written in the form

$$P_{D^* \rightarrow A}(\text{Dexter}) = \left(\frac{2\pi}{\hbar}\right) Z^2 \int_0^\infty f_D(\nu) \epsilon_A(\nu) d\nu \quad Z^2 \propto e^{-2r/L} \quad (\text{eq. 1-7-3})$$

where Z^2 is a quantity that cannot be directly related to optical experiments, r is the distance between the donor and acceptor and L is an effective average Bohr radius for the donor and acceptor. In the equation of the probability of the Dexter energy transfer, the emission and absorption spectra are normalized [Figure 1-7-3] [19, 20, 22].

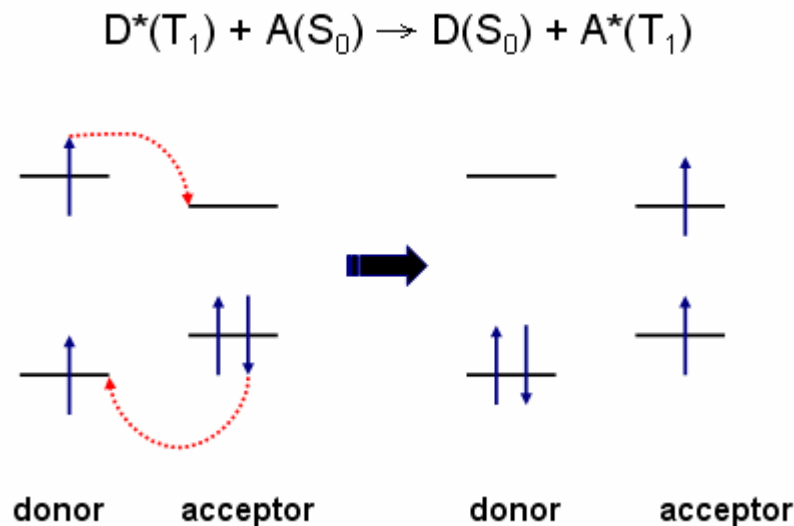


Figure 1-7-3 Dexter energy transfer

Chapter 2 Motivation

According to quantum mechanical spin statistics, there are 25% of excitons are singlets and the other 75% of excitons are triplets. In 1998, Thompson's and Forrest's group added a phosphorescent dopant to harvest both singlet and triplet excitons [14]. In 2001, a green OLED based on small molecules with an internal quantum efficiency of nearly 100% has been demonstrated [15]. On the other hand, PLEDs based on conjugated polymers alone as an emitting layer had high efficiency [23-25]. However, while phosphorescent PLEDs based on conjugated polymers with phosphorescent dopants showed higher efficiencies, the efficiencies were still lower than OLEDs based on small molecules with phosphorescent dopants. [26, 27]

In phosphorescent PLEDs, energy transfer plays an important role in determining the efficiency of the devices. For example, phosphorescent OLEDs with exothermic energy transfer from the host to the dopant is more efficient than that with endothermic energy transfer from host to dopant [28]. Chen *et al.* showed that a "backward triplet energy transfer" may occur as the triplet energy of the dopant is higher than that of the host polymer, and it would decrease the efficiency of phosphorescent PLEDs [29, 30].

In 2003, M. Sudhakar used the Stern-Volmer experiment to investigate the triplet exciton confinement in the dopant site [31], and he expected that the triplet energy transfer from the dopant to the host was through Dexter mechanism, and exothermic energy transfer was diffusion controlled. The Stern-Volmer experiments are usually performed in solutions, and therefore we expect the type of solvent may influence the energy transfer processes.

Since the major fabrication processes of PLEDs are solution processes, we also

speculate that the solvent may also be an important factor in the performance of PLEDs.

Several papers have mentioned that the solvent effect on the conformation of conjugated polymer and the performance of PLEDs with the emitting layer containing single kind of conjugated polymer [32-36]. However, fewer researches focus on the solvent effect on the conjugated polymer-phosphorescent dopant system in solution and on the performance of phosphorescent PLEDs is few.

In this work, we will use the Stern-Volmer experiment to research in the solvent effect on the triplet exciton confinement in the dopant site as the triplet energy of the dopant is higher than that of the host polymer and the solvent effect on the performance of phosphorescent PLEDs.



Chapter 3 Experiments

3-1 Host and dopant materials

The host material is poly(9, 9-dioctylfluorenyl-2, 7-diyl) end capped with N, N-Bis(4-methyl-phenyl)-4-aniline (PFam4). The dopants are Iridium (III) tris(2-(4-totyl)pyridinato-N,C²) (Ir(mppy)₃), Iridium (III) bis(2-(4,6-difluorephenyl)pyridinato-N,C²) (FIrpic) and Bis(2-(9,9-dihexylfluorenyl)-1-pyridine)(acetylacetonate)iridium(III) (Ir(FIPy)₂(acac)) [Figure 3-1-1 and 3-1-2]. These materials were purchased from American Dye Source. The molecular weight (Mw) of PFam4 is 100000, which corresponds to 256 monomers. We use PFam4 as the host polymer because polyfluorene has high photoluminescent efficiency and high conductivity [37, 38].

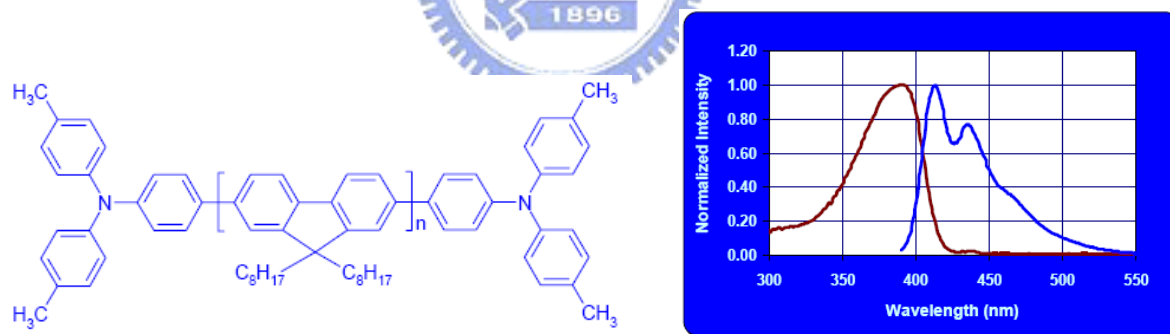
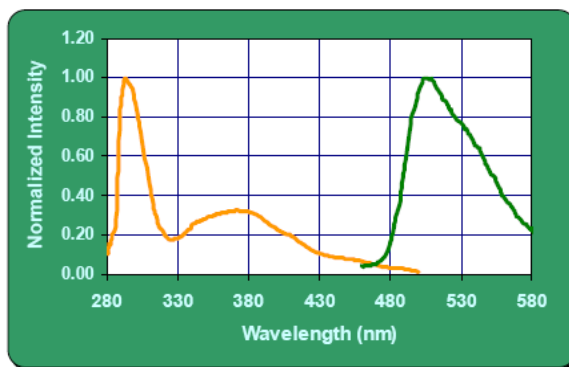
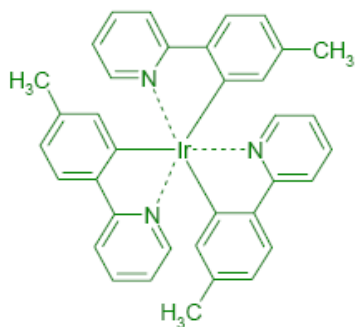
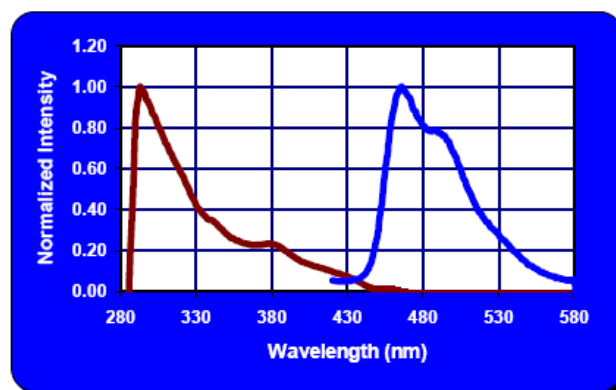
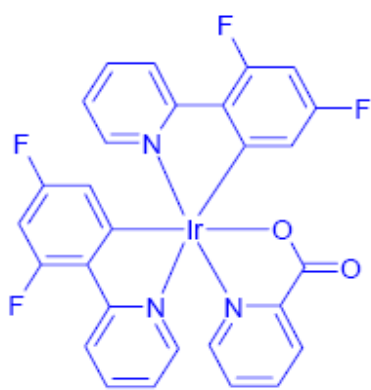


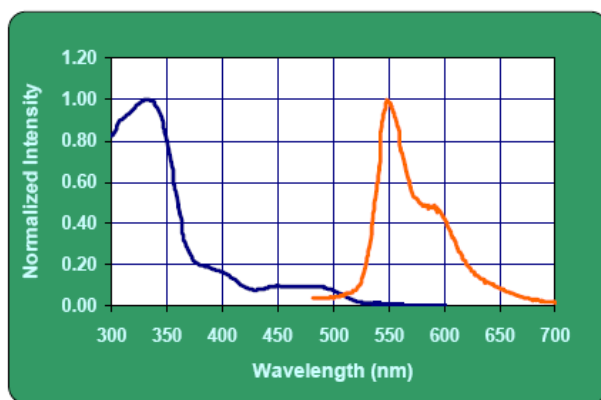
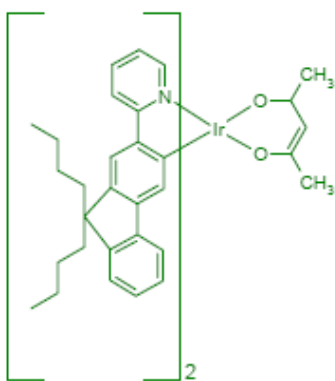
Figure 3-1-1 Chemical structure and spectrum characteristics of PFam4



(a)



(b)



(c)

Figure 3-1-2 Chemical structure and spectra characteristics of
(a) Ir(mppy)₃; (b) Ir(pic)F₂; (c) Ir(FIPy)₂(acac)

3-2 Stern-Volmer experiment

All solutions were prepared in a N₂ filled glovebox. The O₂ level in the glovebox was kept about 1 ppm. Toluene and 1, 2-dichlorobenzene (DCB) were used as the solvents. PFam4 was dissolved in toluene at 75-80°C and dissolved in DCB at 90°C. Both solutions were heated and stirred for one hour. We also dissolved PFam4 in the cosolvent, which was prepared by mixing toluene with DCB by 1:1 v/v (v is volume). PFam4 was dissolved in the cosolvent at 85°C and stirred for one hour. All Ir complexes were dissolved in toluene, DCB and cosolvent respectively, and all solutions were heated at 40°C and stirred at least four hours. Finally, we mixed the host polymer with different dopants at various concentrations. The concentrations of dopants were all the same, 5x10⁻⁵ M, and there were four different concentrations of PFam4 for each Stern-Volmer experiment, 1mM, 2mM, 3mM and 4mM in monomer unit.

In order to investigate the triplet energy transfers from the phosphorescent molecules to the conjugated polymers (PFam4), the dopants were selectively excited. An N₂ dye-laser was used as the pulsed light source. The dopants were selectively excited at 445nm, where PFam4 has negligible absorption. A high speed Si photodiode (Thorlabs, DET 110) was used as the photo-detector. A digital oscilloscope (Tektronix, TDS 3034B) was connected to the photodiode to record the emission decay curves of the dopants. From the slope of a plot of ln I(t) (intensity) versus time, we can determine the lifetime. All measurements were carried out at 25°C.

The lifetimes of phosphorescent dopants at various concentrations of PFam4 were, then, analyzed by the Stern-Volmer equation:

$$\frac{\tau_0}{\tau} = 1 + k_q \tau_0 [\text{PFam4}] \quad (\text{eq. 3-1})$$

where τ_0 is the phosphorescent lifetime of the excited molecule without PFam4, τ is the lifetime with addition of PFam4, [PFam4] is the concentration of PFam4, and k_q is called the Stern-Volmer quenching constant. Stern-Volmer experiment is a good tool to investigate the quenching effect or quenching efficiency.

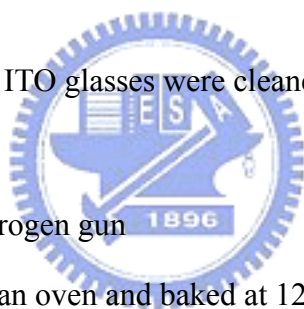


3-3 The fabrication process of PLEDs

3-3-1 ITO substrates cleaning

The steps of ITO substrates cleaning are:

1. In order to remove greasiness, ITO glasses were cleaned with detergent solution for 30 mins in a sonicator.
2. In order to remove the detergent, ITO glasses were cleaned in DI water for 30 mins in a sonicator for twice times.
3. In order to remove water, ITO glasses were cleaned in acetone for 30 mins in a sonicator.
4. In order to remove acetone, ITO glasses were cleaned in isopropanol for 30 mins in a sonicator.
5. Drying ITO glasses by a nitrogen gun
6. ITO glasses were placed in an oven and baked at 120°C for at least 12 hours.



3-3-2 Spin-coating of polymer films

First, ITO glass was exposed to UV-Ozone for 15 mins to make ITO glass be hydrophilic. Poly(3,4-ethylenedioxythiophene):poly(styrene sulfonate) (PEDOT:PSS) [Figure 3-3-2-1] film was spun-cast from an aqueous solution at a spinning speed of 4000 rpm for one minute and baked at 120°C for one hour. The thickness of the PEDOT:PSS film was about 70nm. The PEDOT:PSS film can modify the surface of ITO and also serves as a hole transport layer. After baking, the substrate was transferred into a glove box filled of N₂ gas to

avoid O₂ and water.

Poly(vinylcarbazole) (PVK) [Figure 3-3-2-2] was spun cast on the top of the PEDOT:PSS layer at a spinning speed of 5000 rpm for 40 secs. The PVK solution was prepared at a concentration of 1.0 wt% in DCB. Then, the substrate was baked at 80°C for 30 mins to remove the solvent. The thickness of PVK film was about 20nm. The PVK film serves as a hole transport layer.

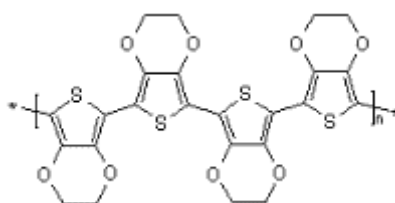


Figure 3-3-2-1 The chemical structure of PEDOT:PSS

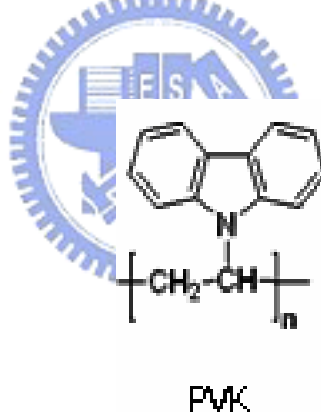


Figure 3-3-2-2 The chemical structure of PVK

PFam4 with 3.0wt% doped Ir(mppy)₃, which dissolved in two different kinds of solvents, toluene and DCB, were used as the light-emitting material. Both solutions were at the same concentration of 1.8wt%. The light-emitting films from two different kinds of solvents were spun-cast on the top of the PVK layer at a spinning speed of 1000 rpm for 40 secs. The substrates, then, baked at 80°C for 30 mins to remove the solvent. The thickness of the light emitting layers prepared from toluene and DCB solutions were 118.26nm and 81.52nm respectively.

3-3-3 Evaporation of the metal cathodes

First, 500 Å of Ca was thermally evaporated onto the light-emitting layer. Finally, 1000Å of Al was thermally evaporated onto the Ca layer. The pressure of the chamber was at 6×10^{-6} Torr. The detailed design is illustrated in [Figure 3-3-3].

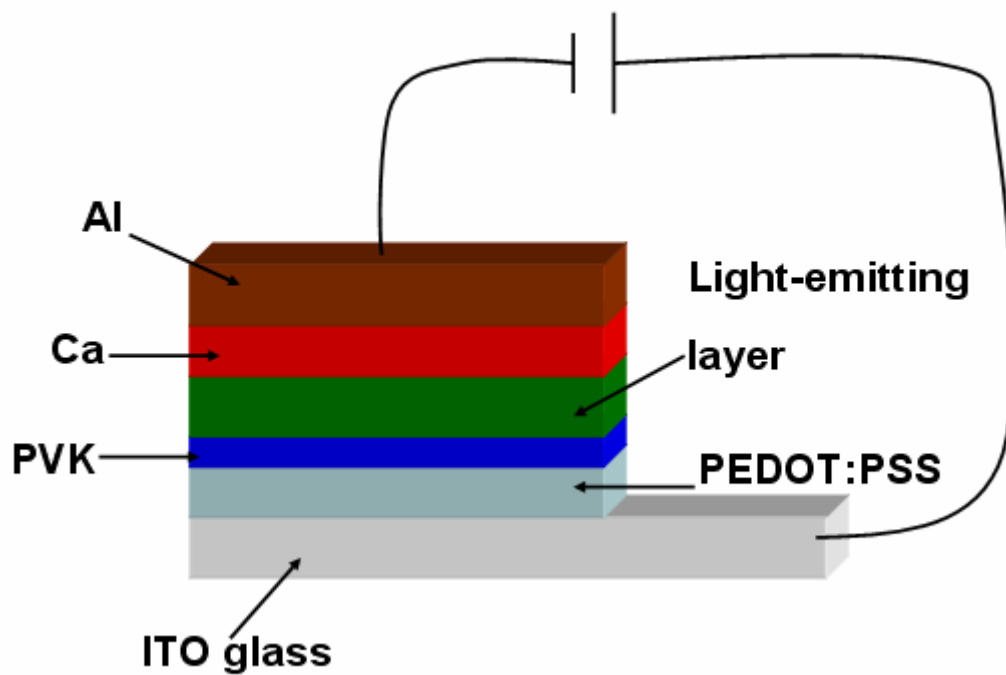


Figure 3-3-3 The device structure in this study

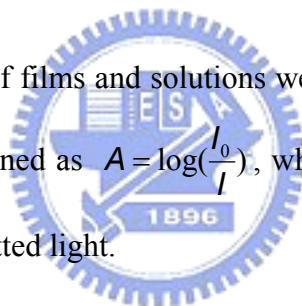
3-4 Analytic Tools

3-4-1 Atomic Force Microscope (AFM)

AFM was purchased from DI instrument. We used the tapping-mode AFM to get the information about the surface morphology of the emitting layer. We also used AFM to measure the thickness of the film.

3-4-2 UV/Vis spectrometer

The UV-Vis absorption of films and solutions were measured on Perkin Elmer Lambda 650. The absorption, A , is defined as $A = \log\left(\frac{I_0}{I}\right)$, where I_0 is the intensity of incident light and I is the intensity of transmitted light.



3-4-3 Photoluminescence (PL) and electroluminescence (EL) spectra

The PL spectra of films and solutions were measured on Edinburgh Instruments. The EL spectra of devices were measured on PR650.

3-4-4 Current, voltage and brightness measurement

The current-voltage characteristics were obtained from Keithley 2400. As device was working, light from the device was measured on a silicon photodiode and the photocurrent produced by the photodiode was measured on Keithley 2000. Finally, the brightness measurement was calibrated by PR-650.

3-4-5 Dynamic light scattering (DLS)

There are many models to describe the polymer conformation in solution. We take the PFam4 polymer as a sphere in solution. We used the dynamic light scattering (Brookhaven, 90Plus) to measure the hydrodynamic radius of PFam4 in the solution. The concentration of PFam4 was prepared at 4mM in monomer unit in toluene and DCB respectively. The laser light at 658nm was used as the light source. A detector measured the time-dependent fluctuation in the scattering light at 90° angle. All measurements were performed at 25°C. The refractive index (n) of toluene and DCB at 25°C are 1.494 and 1.549 respectively [39]. The viscosity (η) of toluene at 25°C is 0.553cp and that of DCB at 25°C is 1.324cp [39].

Chapter 4 Results

4-1 Stern-Volmer experiment

In order to investigate the triplet energy transfers from the phosphorescent molecules to the conjugated polymers, the dopants were selectively excited. Figure 4-1-1, Figure 4-1-2 and Figure 4-1-3 show the absorption spectra of solutions in toluene, DCB and cosolvent, respectively. From Figure 4-1-1, Figure 4-1-2 and Figure 4-1-3, it shows that PFam4 has negligible absorption at 445nm in toluene, DCB and cosolvent. Thus, as we excited the PFam4-Ir complex solutions at 445nm by dye laser, it would only excite the Ir complex. The absorption at 445nm has been assigned as triplet metal to ligand charge transfer transitions ($^3\text{MLCT}$) for Ir complex [40, 41].

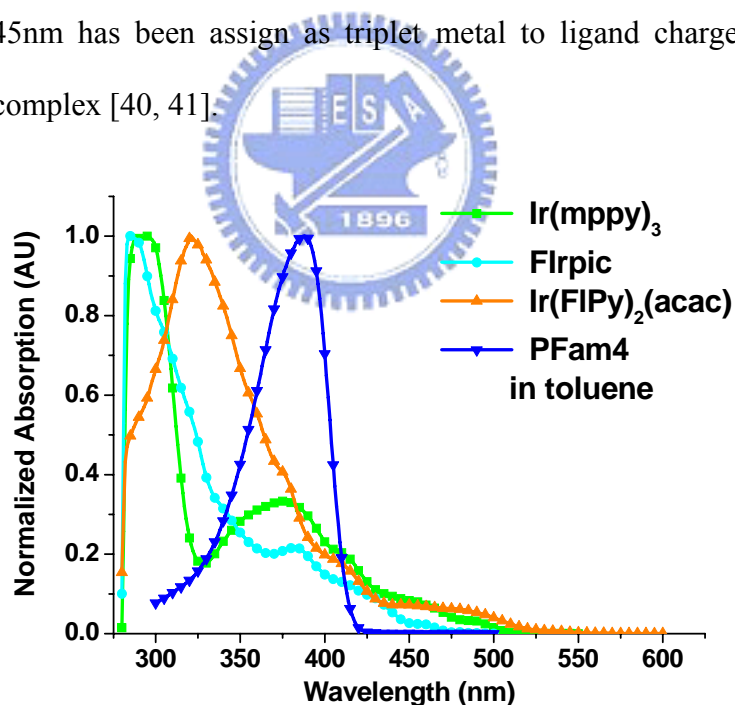


Figure 4-1-1 Normalized absorption spectra of phosphorescent dopants and PFam4 in the toluene solutions. All Ir complexes were at the same concentration, 5×10^{-5} M, while PFam4 was at 5×10^{-5} M in monomer unit

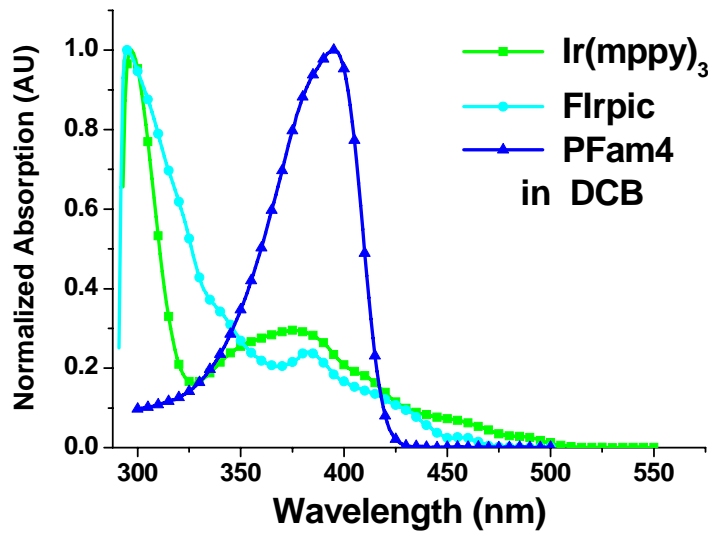


Figure 4-1-2 Normalized absorption spectra of phosphorescent dopants and PFam4 in the DCB solutions. All Ir complexes were at the same concentration, 5×10^{-5} M, while PFam4 was at 5×10^{-5} M in monomer unit

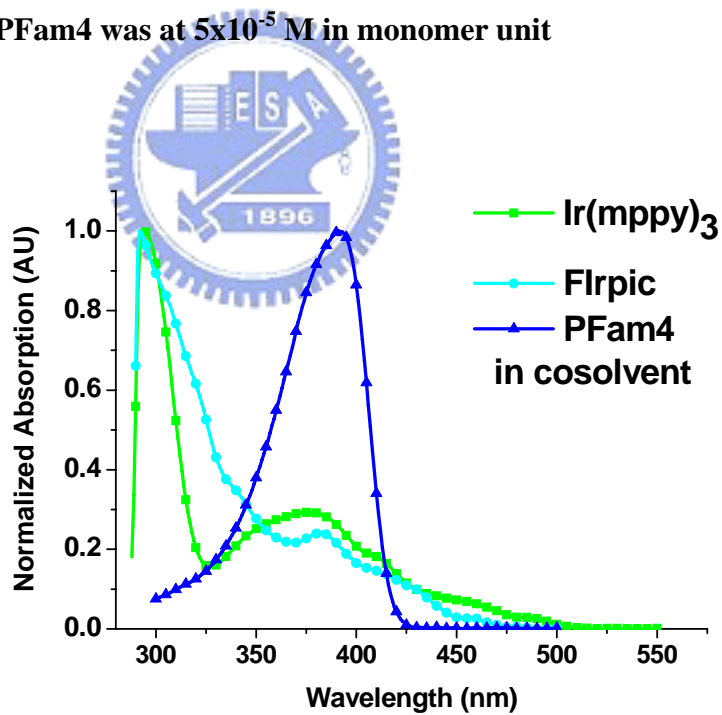


Figure 4-1-3 Normalized absorption spectra of phosphorescent dopants and PFam4 in the cosolvent solutions. All Ir complexes were at the same concentration, 5×10^{-5} M, while PFam4 was at 5×10^{-5} M in monomer unit

Figure 4-1-4, Figure 4-1-5 and Figure 4-1-6 show the photoluminescence (PL) spectra of solutions in toluene, DCB and cosolvent, respectively. The PL spectra of phosphorescent dopants were excited at 445nm, which is the same wavelength as the laser light used in lifetime measurement. The PL spectra of PFam4 in toluene, DCB and cosolvent were excited at 388nm, 395nm and 391nm respectively, where PFam4 has maximum absorption in toluene, DCB and cosolvent, respectively.

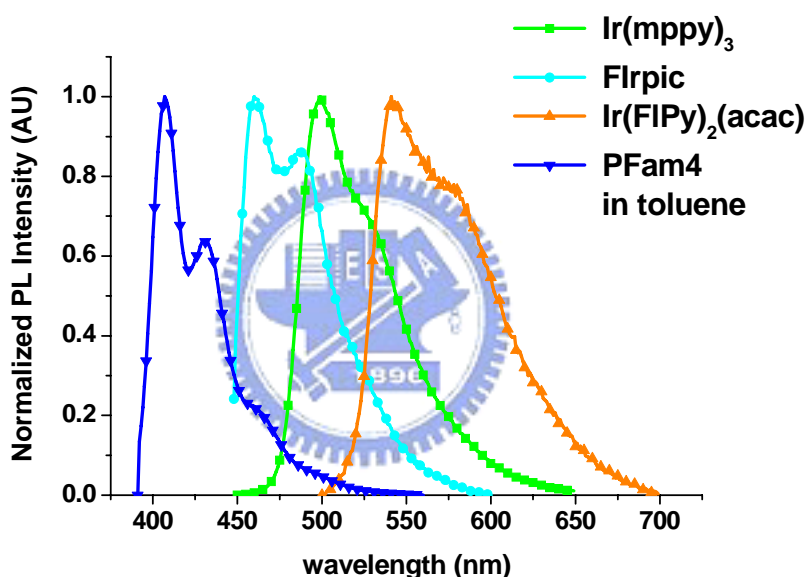


Figure 4-1-4 Normalized PL spectra of phosphorescent dopants and PFam4 in toluene solutions. Phosphorescent dopants were excited at 445nm and PFam4 was excited at 388nm

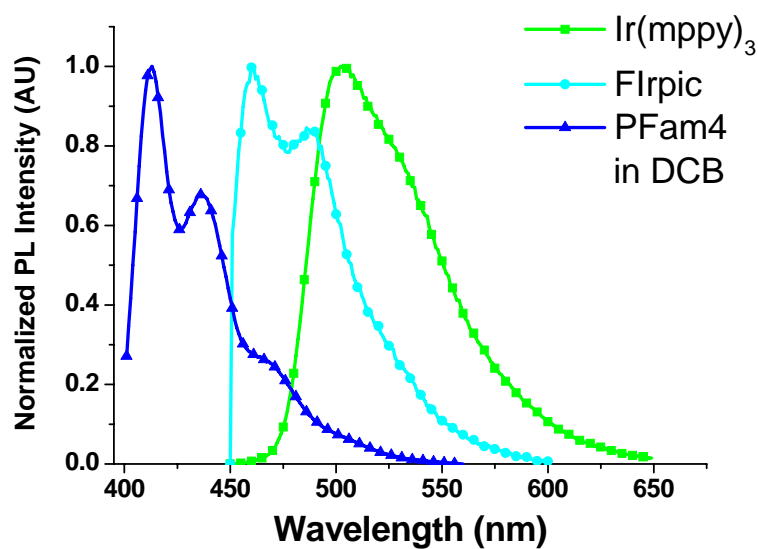


Figure 4-1-5 Normalized PL spectra of phosphorescent dopants and PFam4 in DCB solutions. Phosphorescent dopants were excited at 445nm and PFam4 was excited at 395nm

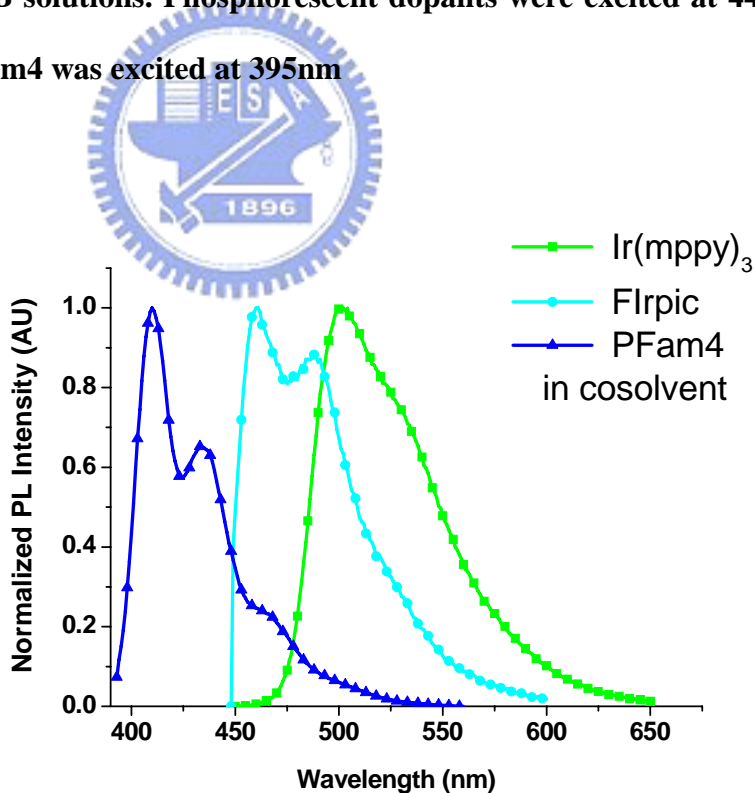


Figure 4-1-6 Normalized PL spectra of phosphorescent dopants and PFam4 in cosolvent solutions. Phosphorescent dopants were excited at 445nm and PFam4 was excited at 391nm

All emission curves depending on time of dopants could be fitted to a single exponential equation well to get the lifetimes of dopants at various PFam4 concentrations. The lifetime of dopant in a single exponential decay way can be expressed as

$$I(t) = I_0 e^{-t/\tau} \quad (\text{eq. 4-1-1})$$

where $I(t)$ is the time-dependent intensity, I_0 is the intensity at time zero, t is time and τ is the lifetime. We determined the lifetime from the slope of a plot of $\ln I(t)$ versus time. Figure 4-1-7, Figure 4-1-8 and Figure 4-1-9 show the natural logarithm of photoluminescence intensity of $\text{Ir}(\text{mppy})_3$, $\ln I(t)$, depending on time at various PFam4 concentrations in toluene, DCB and cosolvent (1:1 v/v for toluene and DCB), respectively. The lifetimes of $\text{Ir}(\text{mppy})_3$ calculated from the slopes for the systems in toluene, DCB, and cosolvent are summarized in Table 4-1-1, Table 4-1-2 and Table 4-1-3, respectively.



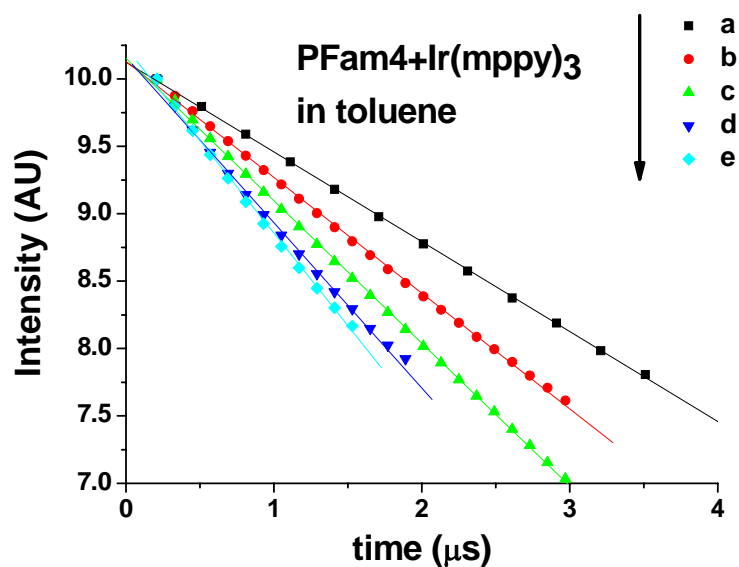


Figure 4-1-7 A plot of natural logarithm of the photoluminescence intensity of Ir(mppy)_3 ($\ln I(t)$) versus time at different PFam4 concentrations in toluene (in monomer unit); $[\text{PFam4}] = (\text{a}) 0; (\text{b}) 1; (\text{c}) 2; (\text{d}) 3; (\text{e}) 4 \text{ mM}$ in monomer unit.

[PFam4] mM (monomer unit)	The lifetime of Ir(mppy)_3 at various concentrations of PFam4 in toluene (μs)
0	1.5
1	1.16
2	0.95
3	0.82
4	0.73

Table 4-1-1 The lifetimes of Ir(mppy)_3 at various concentrations of PFam4 in toluene (in monomer unit).

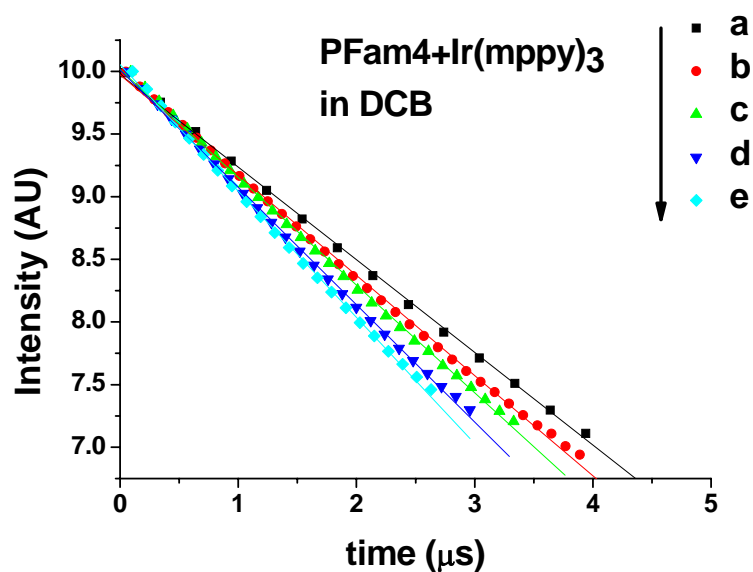


Figure 4-1-8 A plot of natural logarithm of the photoluminescence intensity of Ir(mppy)₃ (ln I(t)) versus time at different PFam4 concentrations in DCB (in monomer unit); [PFam4] = (a) 0; (b) 1; (c) 2; (d) 3; (e) 4 mM in monomer unit.

[PFam4] mM (monomer unit)	The lifetime of Ir(mppy) ₃ at various concentrations of PFam4 in DCB (μs)
0	1.35
1	1.25
2	1.16
3	1.07
4	1

Table 4-1-2 The lifetimes of Ir(mppy)₃ at various concentrations of PFam4 in DCB (in monomer unit).

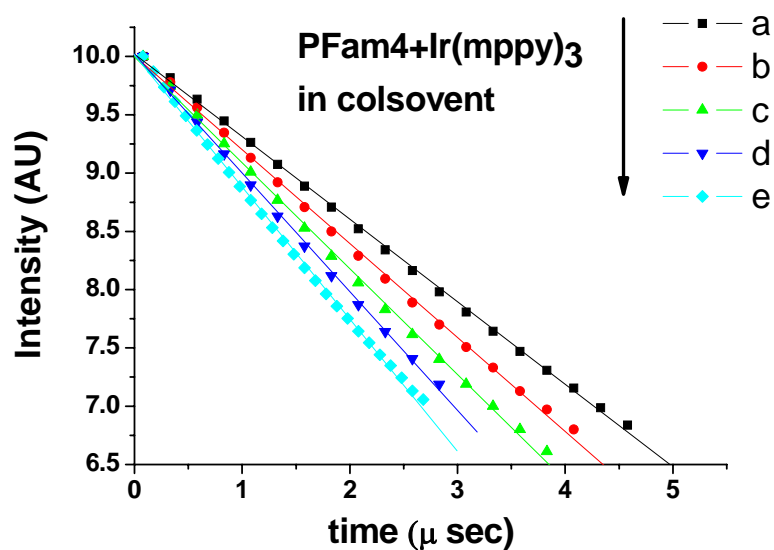


Figure 4-1-9 A plot of natural logarithm of the photoluminescence intensity of Ir(mppy)_3 ($\ln I(t)$) versus time at different PFam4 concentrations in cosolvent (in monomer unit); $[\text{PFam4}] =$ (a) 0; (b) 1; (c) 2; (d) 3; (e) 4 mM in monomer unit.

[PFam4] mM (monomer unit)	The lifetime of Ir(mppy)_3 at various concentrations of PFam4 in cosolvent (μs)
0	1.41
1	1.24
2	1.1
3	0.98
4	0.88

Table 4-1-3 The lifetimes of Ir(mppy)_3 at various concentrations of PFam4 in cosolvent (in monomer unit).

Figure 4-1-10, Figure 4-1-11 and Figure 4-1-12 show the natural logarithm of photoluminescence intensity of FIrpic, $\ln I(t)$, depending on time at various PFam4 concentrations in toluene, DCB and cosolvent (1:1 v/v for toluene and DCB), respectively. The lifetimes of FIrpic calculated from the slopes for the systems in toluene, DCB, and cosolvent are summarized in Table 4-1-4, Table 4-1-5 and Table 4-1-6, respectively.



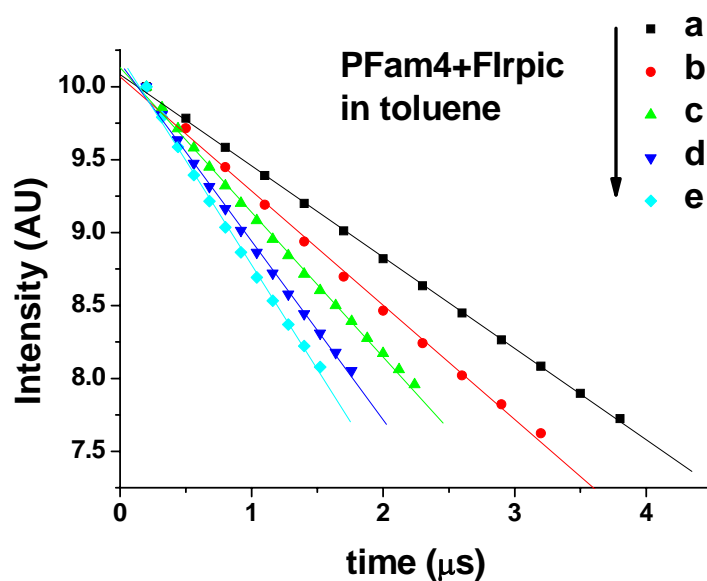


Figure 4-1-10 A plot of natural logarithm of the photoluminescence intensity of FIrpic ($\ln I(t)$) versus time at different PFam4 concentrations in toluene (in monomer unit); [PFam4] = (a) 0; (b)1; (c)2; (d)3; (e)4 mM in monomer unit.

[PFam4] mM (monomer unit)	The lifetime of FIrpic at various concentrations of PFam4 in toluene (μs)
0	1.6
1	1.28
2	1.01
3	0.82
4	0.7

Table 4-1-4 The lifetimes of FIrpic at various concentrations of PFam4 in toluene (in monomer unit).

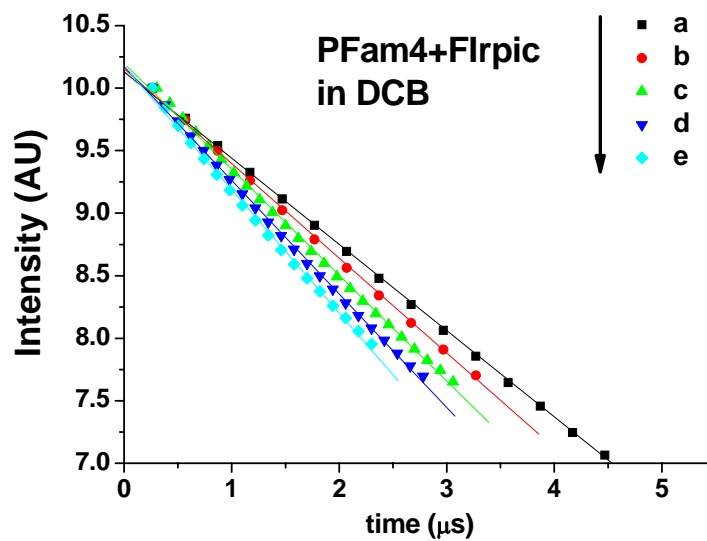


Figure 4-1-11 A plot of natural logarithm of the photoluminescence intensity of Flrpic ($\ln I(t)$) versus time at different PFam4 concentrations in DCB (in monomer unit); [PFam4] = (a) 0; (b)1; (c)2; (d)3; (e)4 mM in monomer unit.

[PFam4] mM (monomer unit)	The lifetime of Flrpic at various concentrations of PFam4 in DCB (μs)
0	1.45
1	1.32
2	1.18
3	1.1
4	1.01

Table 4-1-5 The lifetimes of Flrpic at various concentrations of PFam4 in DCB (in monomer unit).

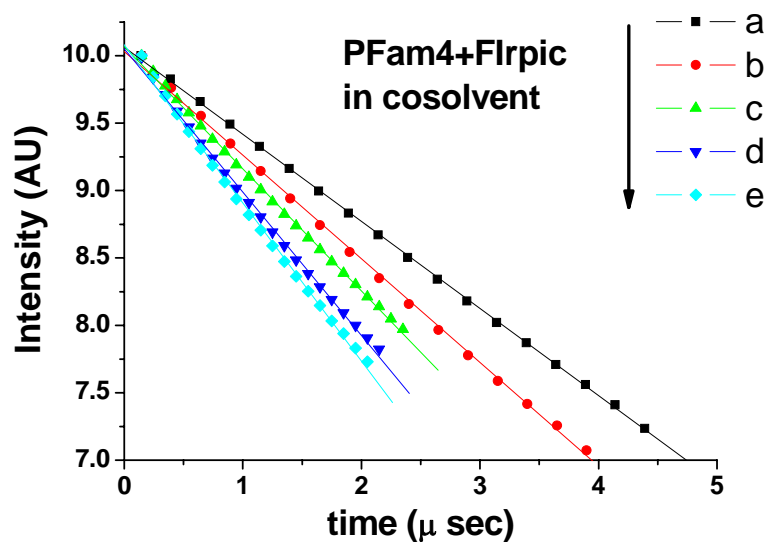


Figure 4-1-12 A plot of natural logarithm of the photoluminescence intensity of Flrpic ($\ln I(t)$) versus time at different PFam4 concentrations in cosolvent (in monomer unit); [PFam4] = (a) 0; (b)1; (c)2; (d)3; (e)4 mM in monomer unit.

[PFam4] mM (monomer unit)	The lifetime of Flrpic at various concentrations of PFam4 in cosolvent (μs)
0	1.55
1	1.3
2	1.1
3	0.94
4	0.85

Table 4-1-6 The lifetimes of Flrpic at various concentrations of PFam4 in cosolvent (in monomer unit).

Figure 4-1-13 shows the natural logarithm of photoluminescence intensity of $\text{Ir}(\text{FIPy})_2(\text{acac})$, $\ln I(t)$, depending on time at various PFam4 concentrations in toluene, and the lifetimes of $\text{Ir}(\text{FIPy})_2(\text{acac})$ calculated from the slopes are summarized in Table 4-1-7.



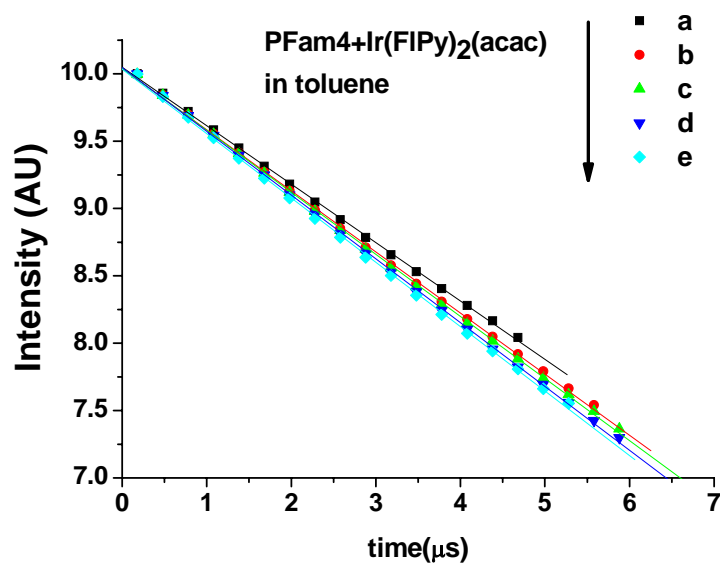


Figure 4-1-13 A plot of natural logarithm of the photoluminescence intensity of Ir(FIPy)₂(acac) (ln I(t)) versus time at different PFam4 concentrations in toluene (in monomer unit); [PFam4] = (a) 0; (b)1; (c)2; (d)3; (e)4 mM in monomer unit.

[PFam4] mM (monomer unit)	The lifetime of Ir(FIPy) ₂ (acac) at various concentrations of PFam4 in toluene (μ s)
0	2.3
1	2.2
2	2.17
3	2.11
4	2.09

Table 4-1-7 The lifetimes of Ir(FIPy)₂(acac) at various concentrations of PFam4 in toluene (in monomer unit).

The lifetimes of phosphorescent dopants at various concentrations of PFam4 were, then, analyzed by Stern-Volmer equation [19]:

$$\frac{\tau_0}{\tau} = 1 + k_q \tau_0 [\text{PFam4}] \quad (\text{eq. 4-1-1})$$

where τ_0 is the phosphorescent lifetime of the excited molecule without PFam4, τ is the lifetime with addition of PFam4, $[\text{PFam4}]$ is the concentration of PFam4, and k_q is called the Stern-Volmer quenching constant. Stern-Volmer experiment is a good tool to investigate the quenching effect or quenching efficiency of the quencher, PFam4. Figure 4-1-14, Figure 4-1-15 and Figure 4-1-16 show the Stern-Volmer plots for PFam4-Ir(mppy)₃, PFam4-FIrpic and PFam4-Ir(FIPy)₂(acac) systems respectively. The Stern-Volmer quenching constants calculated from the slopes are summarized in Table 4-1-8, Table 4-1-9 and Table 4-1-10 for PFam4-Ir(mppy)₃, PFam4-FIrpic and PFam4-Ir(FIPy)₂(acac) systems respectively.



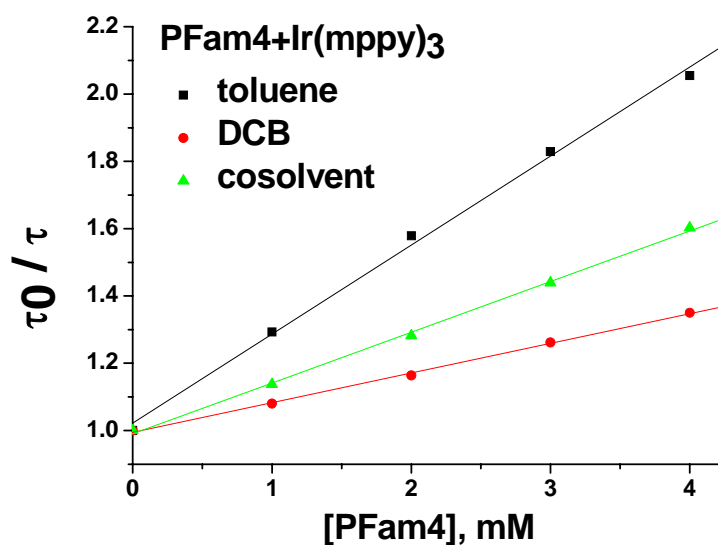


Figure 4-1-14 The Stern-Volmer plot for the PFam4-Ir(mppy)₃ system in different solvents.

	Stern-Volmer quenching constant of PFam4 - Ir(mppy) ₃ system		
quenching constant k_q	toluene	DCB	cosolvent
k_q in monomer unit	$1.76 \times 10^8 \text{ (Ms)}^{-1}$	$6.53 \times 10^7 \text{ (Ms)}^{-1}$	$1.07 \times 10^8 \text{ (Ms)}^{-1}$
k_q in polymer unit	$4.52 \times 10^{10} \text{ (Ms)}^{-1}$	$1.67 \times 10^{10} \text{ (Ms)}^{-1}$	$2.73 \times 10^{10} \text{ (Ms)}^{-1}$

Table 4-1-8 The Stern-Volmer quenching constants of the PFam4-Ir(mppy)₃ system in different solvents.

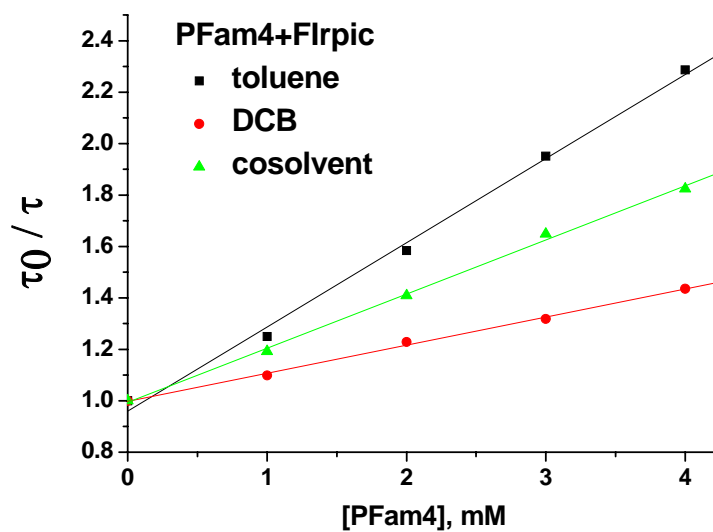


Figure 4-1-15 The Stern-Volmer plot for the PFam4-FIrpc system in different solvents.

	Stern-Volmer quenching constant of PFam4 – FIrpc system		
quenching constant k_q	toluene	DCB	cosolvent
k_q in monomer unit	$2.05 \times 10^8 \text{ (Ms)}^{-1}$	$7.52 \times 10^7 \text{ (Ms)}^{-1}$	$1.36 \times 10^8 \text{ (Ms)}^{-1}$
k_q in polymer unit	$5.24 \times 10^{10} \text{ (Ms)}^{-1}$	$1.93 \times 10^{10} \text{ (Ms)}^{-1}$	$3.47 \times 10^{10} \text{ (Ms)}^{-1}$

Table 4-1-9 The Stern-Volmer quenching constants of the PFam4-FIrpc system in different solvents.

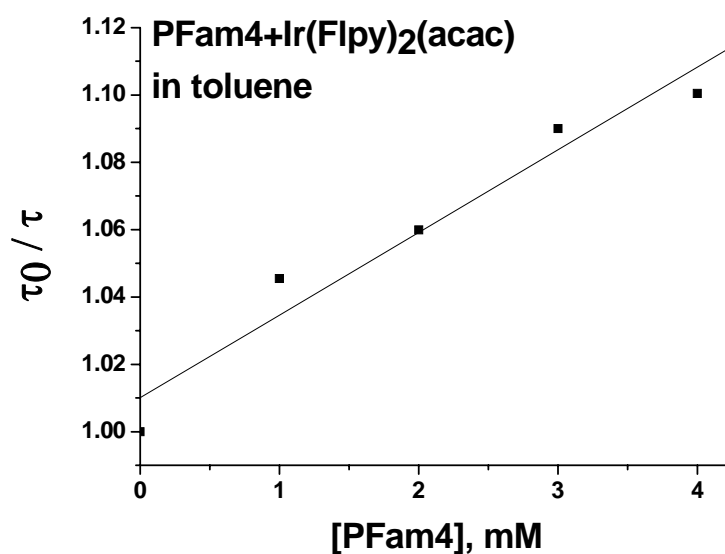


Figure 4-1-16 The Stern-Volmer plot for the PFam4-Ir(FIPy)₂(acac) system in toluene.

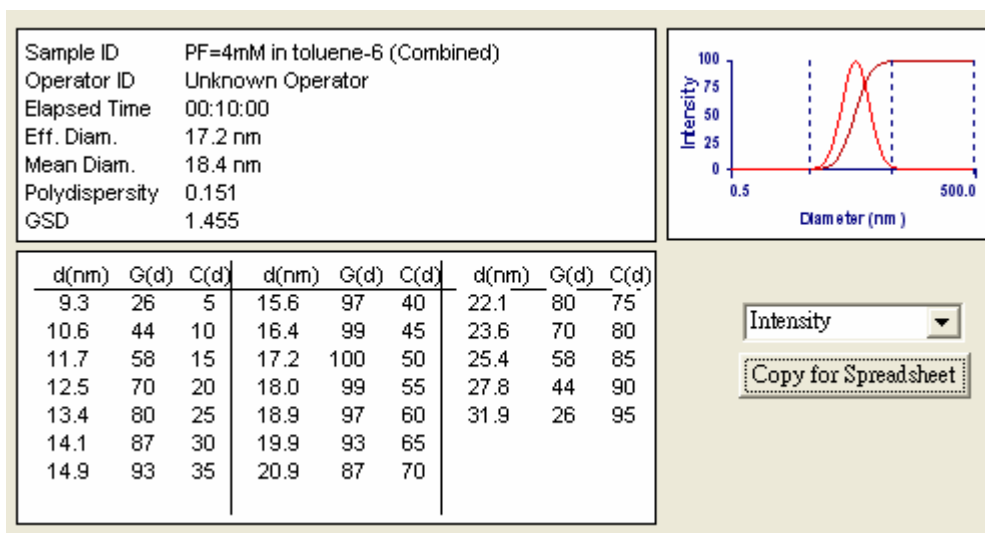
	Stern-Volmer quenching constant of PFam4 –Ir(FIPy) ₂ (acac) system	
quenching constant k_q	Toluene	
k_q in monomer unit	$1.07 \times 10^7 \text{ (Ms)}^{-1}$	
k_q in polymer unit	$2.73 \times 10^9 \text{ (Ms)}^{-1}$	

Table 4-1-10 The Stern-Volmer quenching constants of the PFam4-Ir(FIPy)₂(acac) system in toluene.

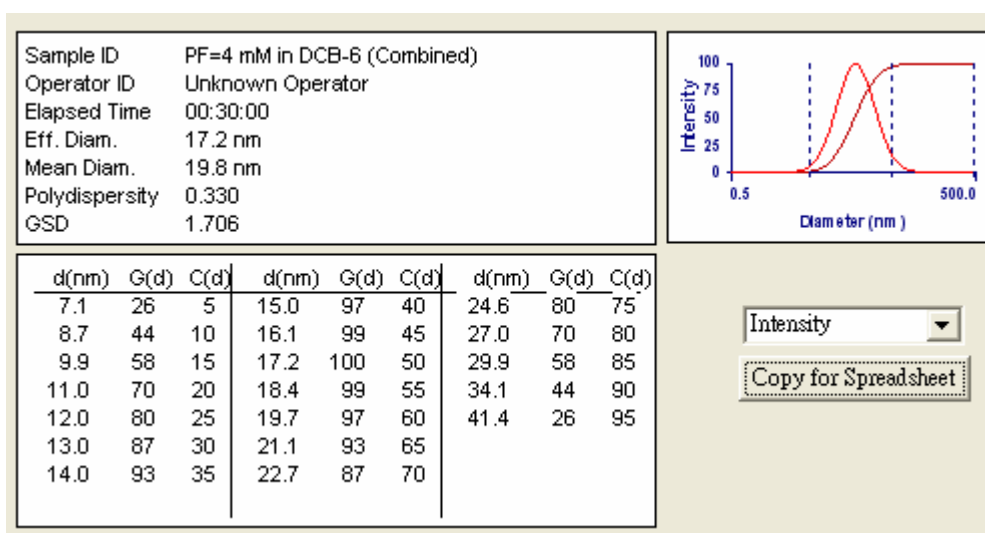
4-2 Hydrodynamic radius of PFam4

The hydrodynamic radii of PFam4 in toluene and DCB were measured on dynamic light scattering (DLS). The concentrations of PFam4 in toluene and DCB were both at 4mM in monomer unit. Figure 4-2 shows the distributions of the hydrodynamic diameters in toluene and DCB. The mean hydrodynamic radii for PFam4 in toluene and in DCB are 9.2nm and 9.9nm, respectively. The polydispersity of PFam4 in the toluene solution is 0.151 and that in the DCB solution is 0.330. The hydrodynamic radius of PFam4 in toluene that we measured is close to that of PF2/6 with similar molecular weight in toluene, which is published before [42].





(a)



(b)

Figure 4-2 (a) The distribution of hydrodynamic diameter of PFam4 in toluene

(b) The distribution of hydrodynamic diameter of PFam4 in DCB

(The size of the PFam4 shown in the figure is hydrodynamic diameter. The hydrodynamic radius is one-half of the hydrodynamic diameter.)

4-3 Device performance

The structure of the devices are ITO/PEDOT:PSS/PVK/PFam4-Ir(mppy)₃/Ca/Al. The thickness of PEDOT:PSS and PVK films are about 70nm and 20nm, respectively. We fabricated two different kinds of devices: one emitting layer of the device is spun cast from the toluene solution, and the other is spun cast from the DCB solution. The concentration of these two kinds of solutions are at 1.8wt% and PFam4 were doped with 3 wt% Ir(mppy)₃. The thickness of the emitting layers, that PFam4-Ir(mppy)₃ dissolved in toluene and DCB, are 118.26nm and 81.52nm, respectively. The current density (J) versus voltage (V) of the devices is shown in Figure 4-3-1. The luminescence efficiency versus current density of the devices is shown in Figure 4-3-2.

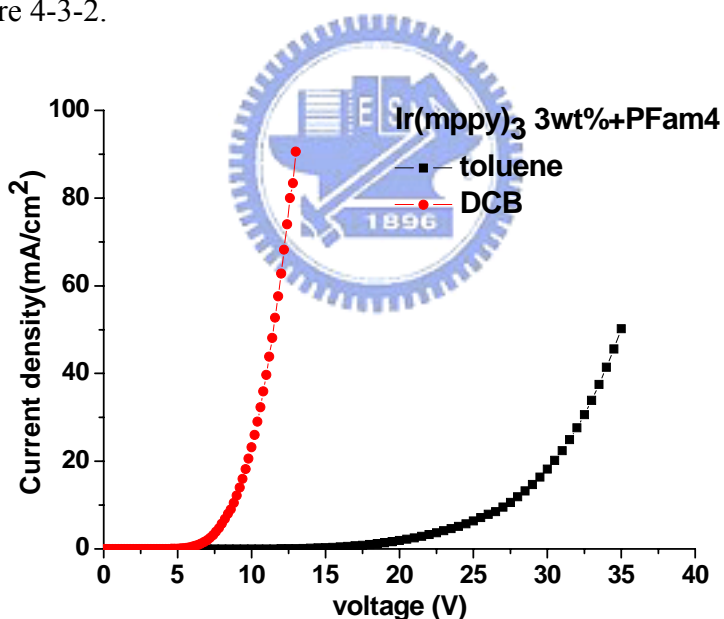


Figure 4-3-1 J-V plot

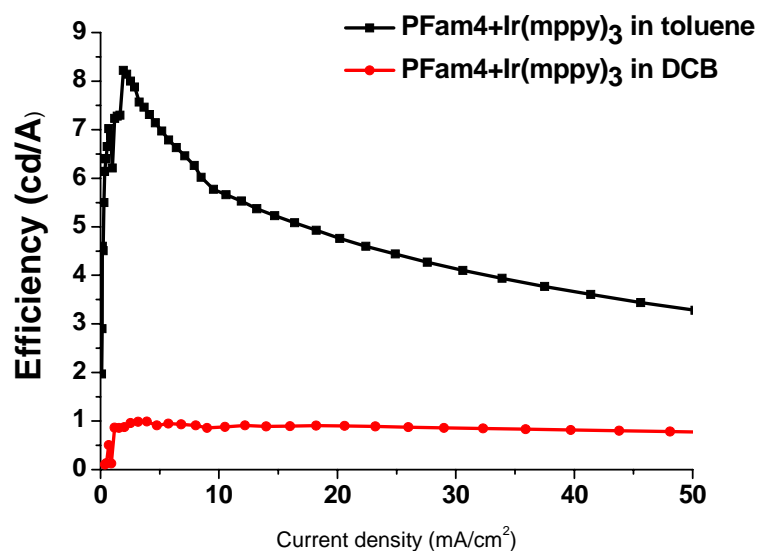


Figure 4-3-2 Luminescence efficiency (cd/A) vs current density

Figure 4-3-3 shows the AFM morphology of emitting layers, which are spun cast from the toluene solution and DCB solution. The roughness of the emitting layer which was spun cast from the toluene solution is 2.063nm and that which was spun cast from the DCB solution is 11.344nm. The absorption spectra of the neat PFam4 films without doped Ir(mppy)₃, which were spun cast from the toluene and DCB respectively, are shown in Figure 4-3-4. The EL spectra of these two types of devices are shown in Figure 4-3-5.

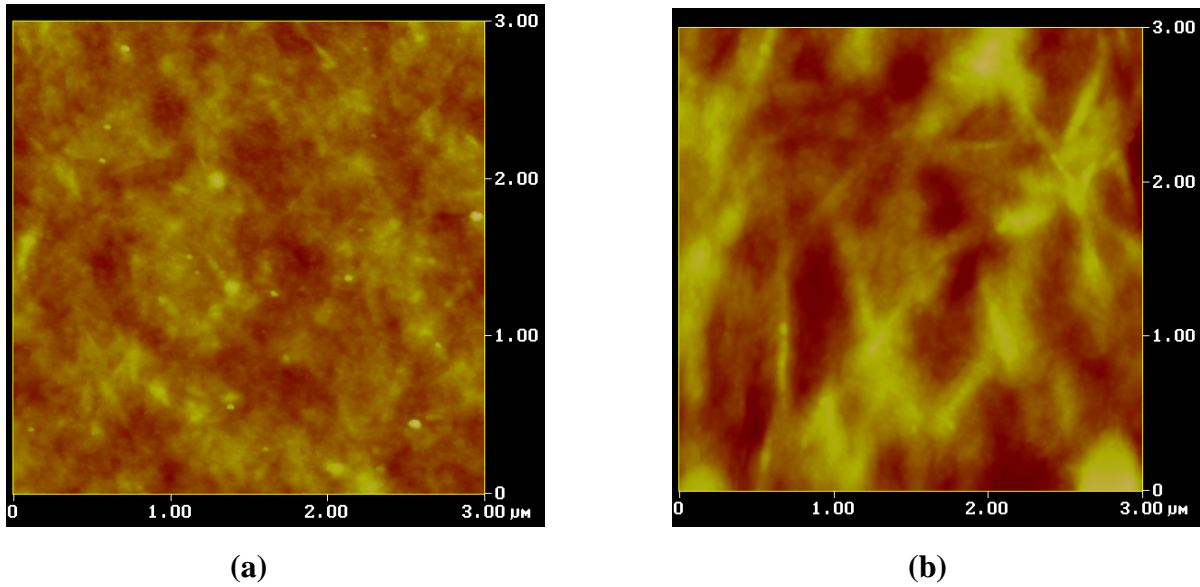


Figure 4-3-3 AFM morphology of the emitting layer (a) PFam4-Ir(mppy)₃ dissolved in toluene; (b) PFam4-Ir(mppy)₃ dissolved in DCB

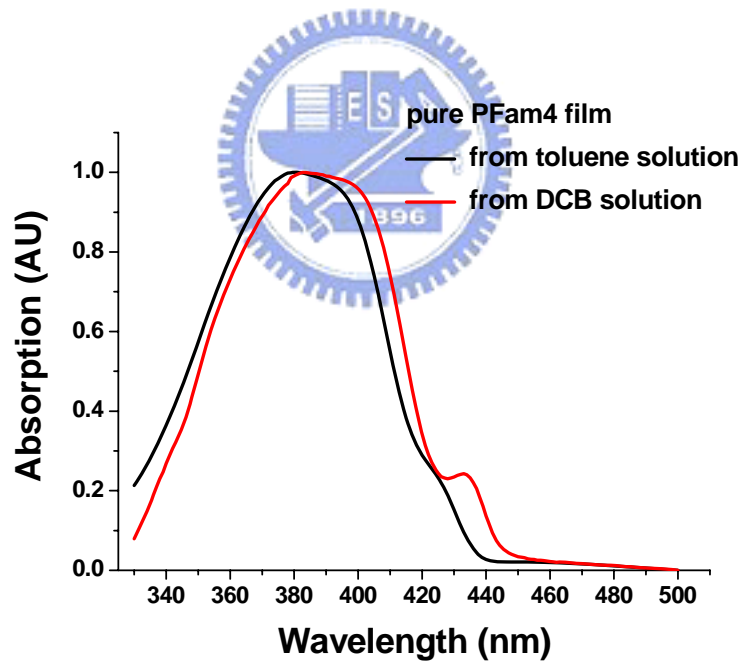


Figure 4-3-4 Absorption spectra of the pure PFam4 films that were spun cast from the toluene and DCB, respectively

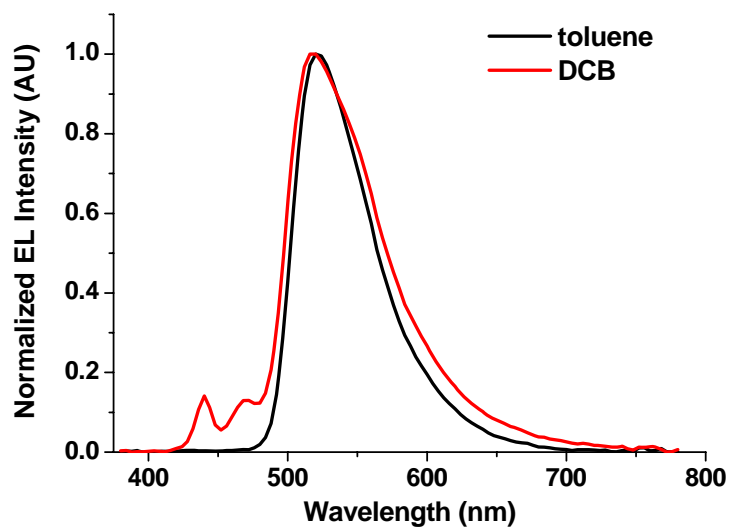


Figure 4-3-5 Normalized EL spectra of two types of devices from different solutions



Chapter 5 Discussion

5-1 Analysis of Stern-Volmer experiment

The lifetimes of Ir(mppy)₃, FIrpic and Ir(FIPy)₂(acac) in the dilute toluene solutions are 1.5, 1.6, and 2.3 μ sec respectively, which are nearly to Ir complexes with similar structures that were published earlier [40, 41, 43-46]. The lifetimes of Ir(mppy)₃ and FIrpic in the dilute DCB solutions are shorter than that in the dilute toluene solutions because the larger refractive index (n) of DCB causes a faster radiative decay (n_(DCB)=1.549 and n_(toluene)=1.494) [39, 47]. From the Strickler-Berg equation, the radiative decay rate (k_r) or the lifetime (τ₀) can be expressed as [48]

$$k_r = \frac{1}{\tau_0} = 2.88 \times 10^{-9} n^2 \langle \tilde{\nu}_f^{-3} \rangle_{av}^{-1} \frac{g_l}{g_u} \int \epsilon d \ln \tilde{\nu}, \quad \langle \tilde{\nu}_f^{-3} \rangle_{av}^{-1} = \frac{\int I(\tilde{\nu}) d\tilde{\nu}}{\int \tilde{\nu}^{-3} I(\tilde{\nu}) d\tilde{\nu}} \quad (\text{eq. 5-1-1})$$

where n is the refractive index of the solvent, ε is the molar extinction coefficient, I is the luminescence intensity, $\tilde{\nu}$ is the wavenumber, g_l and g_u are the degeneracies of the lower and upper states, respectively. For allowed transitions, the oscillator strength is almost invariant with the environment. Therefore, the lifetime is inverse proportional to the square of the refractive index, τ₀ ∝ n⁻² [47, 49]. The solvent refractive index would influence the radiative decay rate and the absorption rate, but the reason is still unclear [49, 50]. From the refractive

indexes of toluene and DCB, $\frac{n_{(DCB)}^2}{n_{(toluene)}^2}$ yields 1.07. The lifetime of Ir(mppy)₃ in toluene is

1.5 μ s and that in DCB is 1.35 μ s. Then, $\frac{\tau_{0(toluene)}}{\tau_{0(DCB)}}$ of Ir(mppy)₃ equals 1.11. By the same

way, the lifetime of FIrpic in toluene is $1.6 \mu\text{s}$ and that in DCB is $1.45 \mu\text{s}$. So, $\frac{\tau_{0(\text{toluene})}}{\tau_{0(\text{DCB})}}$ of FIrpic equals 1.1. Evidently, the relation between the lifetime of $\text{Ir}(\text{mppy})_3$ or FIrpic and the solvent refractive index is consistent with $\tau_0 \propto n^{-2}$. On the other hand, because the refractive index of the cosolvent should be between that of toluene and DCB, the lifetimes of the Ir complexes in the cosolvent solutions are also between that in the toluene and DCB solutions. $\text{Ir}(\text{FIpy})_2(\text{acac})$ has more ligand centered (LC) $^3\pi - \pi$ character, longer lifetime and phosphorescence spectrum shifts to longer wavelength from the incorporation of 9,9-dihexylfluorene into the ligand site to increase π -conjugated length [45]. The triplet energies of FIrpic is 2.65eV [28]. The triplet energy of PFam4 is 2.15eV, which is deduced from phosphorescence spectrum at low temperature [51]. We calculated the triplet energies of $\text{Ir}(\text{mppy})_3$ and $\text{Ir}(\text{FIpy})_2(\text{acac})$ from their highest peaks of phosphorescence spectra. Thus, the triplet energies of $\text{Ir}(\text{mppy})_3$ and $\text{Ir}(\text{FIpy})_2(\text{acac})$ are 2.49 and 2.29, respectively [Figure 4-1-4]. The triplet energy diagrams of these compounds are illustrated in Figure 5-1-1.

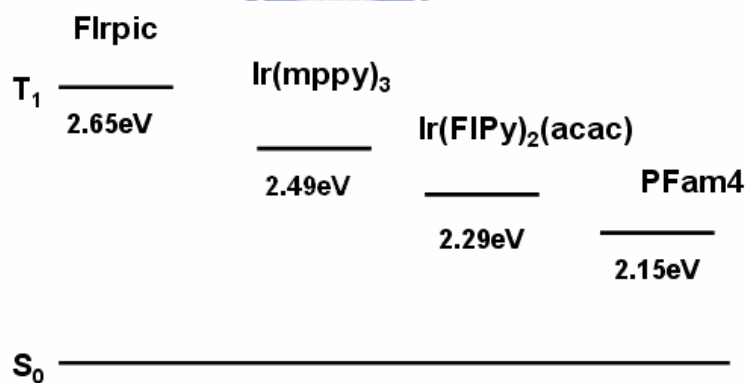
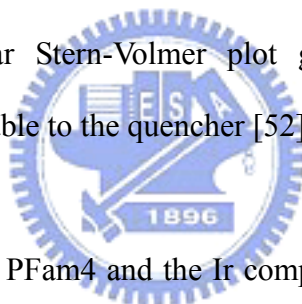


Figure 5-1-1 The triplet energy diagrams

In our experiments, the triplet energy donor is Ir complex and the triplet energy acceptor is PFam4. Since the triplet absorption of PFam4 is negligible, the triplet energy transfer between Ir complex and PFam4 is only dominated by Dexter energy transfer. Forster

energy transfer is efficient if the spectra overlap is significant. However, spectra overlap is not crucial for Dexter energy transfer [47]; Dexter energy transfer can exchange energy by directly exchange electrons.

The triplet energies of all three Ir complexes are higher than that of PFam4, so the triplet energy transfers from all Ir complexes to the PFam4 polymers are thermodynamically favored. From the Stern-Volmer quenching constants in the same solvent, we can see that the quenching effect is more efficient when the triplet energy of Ir complex becomes much higher. For the PFam4-Ir(FIPy)₂(acac) system, the energy transfer is still an exothermic energy transfer, but the quenching constant is lower than that of PFam4-Ir(mppy)₃ by about one order. From Figure 4-1-14 to 4-1-16, the Stern- Volmer plots of all systems in toluene, DCB and cosolvent are linear. A linear Stern-Volmer plot generally suggests a single kind of fluorophores, all equally reachable to the quencher [52].



For energy transfer, the PFam4 and the Ir complex in solution need to diffuse toward each other to certain distance to exchange energy between each other [Figure 5-1-2]. The maximum distance that an Ir complex can diffuse during the lifetime is given by

$$x = \sqrt{2Dt} \quad (\text{eq. 5-1-2})$$

where D is the diffusion coefficient and t is time [19, 52 and 53]. Diffusion coefficients can be obtained from the Stokes-Einstein equation,

$$D = \frac{kT}{6\pi\eta R} \quad (\text{eq. 5-1-3})$$

where k is the Boltzman constant, η is the solvent viscosity, T is the temperature and R is the molecular radius[52, 53]. We may assume that the radii of all Ir complexes are about 5Å [47]. Then, the diffusion coefficients of all dopants in toluene (η (toluene)=0.553cp) at 25°C are $7.9 \times 10^{-10} \text{ m}^2/\text{s}$. Therefore, during the lifetime, the maximum distances that the dopants can

diffuse in the toluene solutions are 48.7nm, 50.3nm, 60.3nm for Ir(mppy)₃, FIrpic and Ir(FIPy)₂(acac), respectively. Similarly, the diffusion coefficients of all dopants in DCB (η (DCB)=1.324 cp) at 25°C are 3.3×10^{-10} m²/s, and during the lifetime, the maximum distances that the dopants can diffuse in the DCB solutions are 29.8nm and 30.9nm for Ir(mppy)₃ and FIrpic, respectively. These distances are very long to enhance the probability that, during the lifetime, the distance between the PFam4 and the Ir dopant is within the reaction distance.

There is one theoretical diffusion controlled rate constant for reactants in solution, k_{dif} . The equation of the theoretical diffusion controlled rate constant is called Smoluchowski equation and is expressed as [52, 53],

$$k_{dif} = 4\pi R^* (D_{PFam4} + D_{Ir}) N_A (1000 \text{ L/m}^3) \quad (\text{eq. 5-1-4})$$

where R^* is the reaction distance from each other, D is the diffusion coefficient and N_A is Avogadro's number.

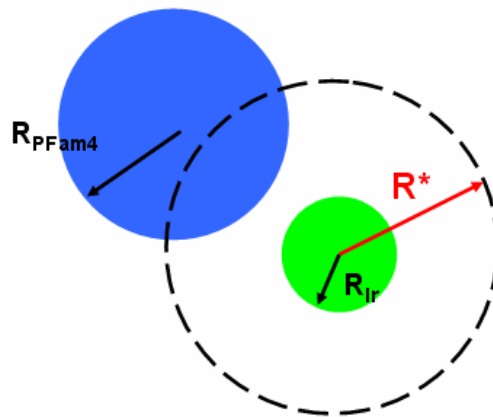


Figure 5-1-2 reactants in solution

The mean hydrodynamic radius of PFam4 in toluene at 4mM in monomer unit is 9.2nm and the diffusion coefficient of PFam4 in toluene is 4.3×10^{-11} m²/s. So far, the only unknown parameter in Smoluchowski equation (eq. 5-1-2) is R^* , which is the reaction distance between

the Ir dopant and the PFam4. The reaction distance R^* is generally assumed to be the sum of the molecular radii of the donor and the quencher, by $R_{PFam4} + R_{Ir}$ [52, 53]. Then, the calculated result of k_{dif} in the toluene solution is $6.11 \times 10^{10} \text{ (Ms)}^{-1}$. By comparing k_q with k_{dif} , we can get the quenching efficiency ($\frac{k_q}{k_{dif}}$) and see whether the quenching process is diffusion controlled or not [52]. For example, if quenching efficiency is 60%, then 60% of the collisional encounters are effective in quenching. For the PFam4-FIrpic system in the toluene solution ($k_q=5.24 \times 10^{10} \text{ (Ms)}^{-1}$), the quenching efficiency is 86%. Similarly, for the PFam4-Ir(mppy)₃ system in the toluene solution ($k_q=4.52 \times 10^{10} \text{ (Ms)}^{-1}$), the quenching efficiency is 74%. Therefore, the triplet energy transfers for the PFam4-FIrpic and PFam4-Ir(mppy)₃ systems in the toluene solutions are close to diffusion controlled. By the same way, the diffusion coefficient of PFam4 in DCB is $1.7 \times 10^{-11} \text{ m}^2/\text{s}$, and the k_{dif} for PFam4-Ir dopant system in DCB yields $2.73 \times 10^{10} \text{ (Ms)}^{-1}$. Then, the quenching efficiencies for the PFam4-FIrpic ($k_q=1.93 \times 10^{10} \text{ (Ms)}^{-1}$) system and the PFam4-Ir(mppy)₃ ($k_q=1.67 \times 10^{10} \text{ (Ms)}^{-1}$) system in the DCB solutions are 71% and 61%, respectively. Apparently, the triplet energy transfer for the PFam4-FIrpic system in the DCB solution is also close to diffusion controlled, but for the PFam4-Ir(mppy)₃ system in the DCB solution, the triplet energy transfer may not be diffusion controlled.

Looking back to the PFam4-Ir(FIPy)₂(acac) system in the toluene solution [Table 4-1-7, Table 4-1-10 and Figure 4-1-16], the lifetime of Ir(FIPy)₂(acac) changes little as adding PFam4 in the solution. So, the Stern-Volmer quenching constant is quite small, $2.73 \times 10^9 \text{ (Ms)}^{-1}$ in polymer unit, which is much smaller than the k_{dif} and is lower than that of PFam4-Ir(mppy)₃ ($4.52 \times 10^{10} \text{ (Ms)}^{-1}$) by about one order. Even though the triplet energy of Ir(FIPy)₂(acac) is slightly larger than that of PFam4 by 0.14eV, the triplet energy transfer from Ir(FIPy)₂(acac) to PFam4 is still exothermic energy transfer. Because of incorporation of

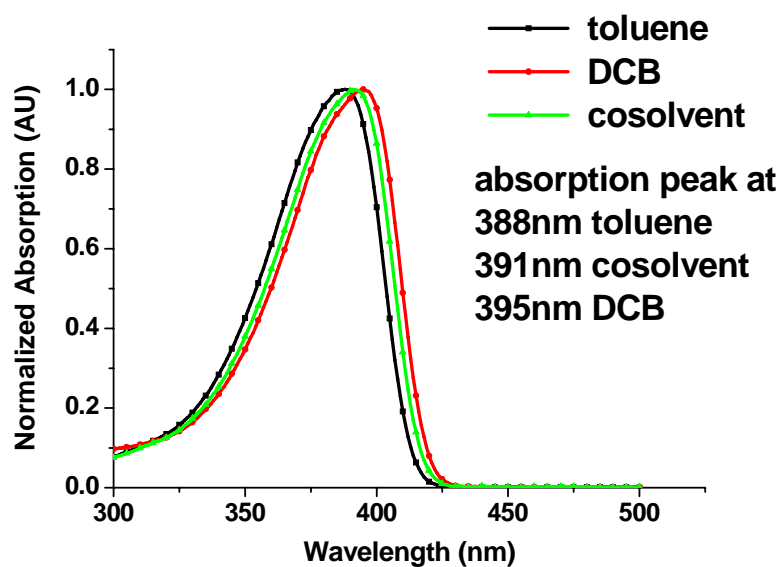
9,9-dihexylfluorene into the ligand site of Ir(FIPy)₂(acac), the Ir(FIPy)₂(acac) has more LC ³ π - π character, and the Ir(FIPy)₂(acac) ligand has closer excitonic wave function with PFam4 [54]. It can enhance Dexter energy transfer between them. The closer wave function and small energy difference (0.14eV) may result in an oscillating triplet energy transfer between Ir(FIPy)₂(acac) and PFam4. The quenching efficiency for the PFam4- Ir(FIPy)₂(acac) system in the toluene solution is only 4.5%. Obviously, the triplet energy transfer for PFam4- Ir(FIPy)₂(acac) system in the toluene solution is not diffusion controlled.

We carried out the Stern-Volmer experiments in three different solvents, toluene, DCB and cosolvent. The PFam4 may have different conformations in these solutions. It has been shown that poly[9,9-dioctylfluorene-2,7-diyl] (PFO) takes a rodlike conformation in good solvent (δ of THF=9.1 (cal/cm³)^{1/2} and δ of chloroform=9.3 (cal/cm³)^{1/2}, δ is solubility parameter) and moderately good solvent (δ of toluene=8.9 (cal/cm³)^{1/2}) [32-35, 39]. However, PFO may behave β -phase, like a sheetlike structure, in poor solvents, such as methylcyclohexane (MCH) and dichloroethane (DCE) (δ of MCH=7.82 (cal/cm³)^{1/2} and δ of DCE=9.8 (cal/cm³)^{1/2}). The β -phase conformation of PFO always accompanies a resolved absorption band around 420-450nm. In order to make PFO in poor solvent to show additional resolved absorption band at longer wavelength, it needs to leave the solution for quite long time or cool the solution to much lower temperature, 0°C for MCH as an example.

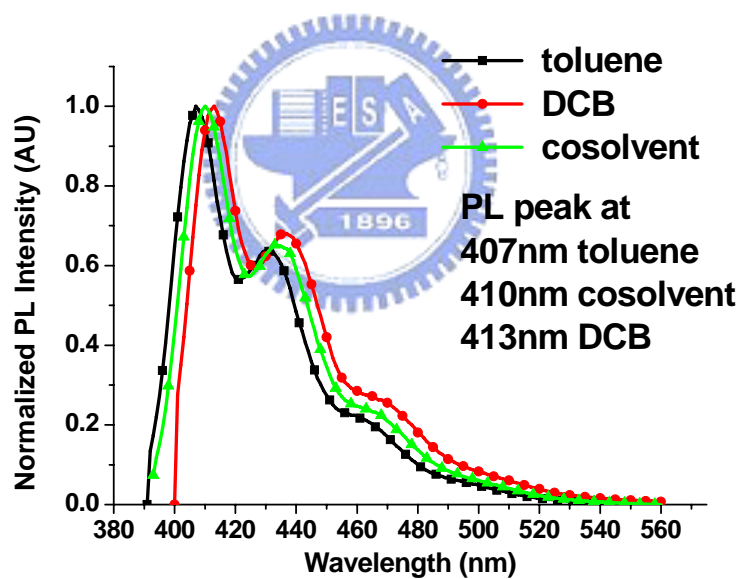
The δ of DCB is 10.05 (cal/cm³)^{1/2} [39], which is poorer than DCE for PFO. We may expect the appearance of β -phase conformation of PFam4 in DCB and cosolvent. However, from Figure 5-1-3 (a), PFam4 in DCB and cosolvent do not show any additional resolved absorption band around 420-450nm. On the other hand, the absorption and PL spectra of PFam4 in the DCB and cosolvent solutions are redshift relative to that in the toluene solution [Figure 5-1-3]. The redshift in absorption and PL spectra in the DCB and cosolvent

solutions are due to the greater polarity of DCB; the dielectric constant (ϵ) of DCB is 9.93 and the dipole moment (μ) of DCB is 2.14D; the ϵ of toluene is 2.38 and the μ of toluene is 0.31D [39,55]. The highest peak of absorption spectrum of PFam4 in toluene, cosolvent and DCB are at 388nm, 391nm and 395nm, respectively. The highest peak of PL spectrum of PFam4 in toluene, cosolvent and DCB are at 407nm, 410nm and 413nm, respectively.





(a)



(b)

Figure 5-1-3 (a) Absorption spectra of PFam4 in toluene, DCB and cosolvent. All concentrations are at 5×10^{-5} M; (b) PL spectra of PFam4 in toluene, DCB and cosolvent. All concentrations are at 5×10^{-5} M

For the PFam4-FIrpic and PFam4-Ir(mppy)₃ systems, the quenching efficiency in the DCB solution is lower than that in the toluene solution. From the Stokes-Einstein and Smoluchowski equations (eq. 5-1-3 and 5-1-4), there are two factors that would influence the quenching process: the solvent viscosity and the hydrodynamic radius of PFam4. However, the mean hydrodynamic radius of PFam4 in the toluene solution is almost the same as that in the DCB solution. Thus, it seems that the lower quenching efficiency in the DCB solution is largely caused by the solvent viscosity. Nevertheless, the solvent viscosity would only affect the diffusion speeds or the diffusion coefficients of the host polymers and the phosphorescent dopants. The solvent viscosity would not affect the quenching efficiency. We think that the lower quenching efficiency in the DCB solution is largely caused by the broader distribution of hydrodynamic diameter of PFam4 in the DCB solutions. The distribution of hydrodynamic diameter of PFam4 in the DCB solution is much broader than that in the toluene solution (Figure 4-2). The polydispersity of PFam4 in the toluene solution is 0.151 and that in the DCB solution is 0.330. We think that the broader distribution of hydrodynamic diameter of PFam4 in the DCB solution may result from the poor solvent characteristic. In the poor solvent, DCB, PFam4 may not stretch well and form a smaller coil or entangle with other PFam4 polymers to form a bigger coil. Therefore, it results in a broader distribution of hydrodynamic diameter of PFam4 in the DCB solution. That would decrease the collision probability between the PFam4 polymers and the Ir complexes, and then it leads to a smaller Stern-Volmer quenching constant in the DCB solution. Because the quenching efficiency is defined as $\frac{k_q}{k_{dif}}$, a smaller Stern-Volmer quenching constant would decrease the quenching efficiency. That is why the quenching efficiency in the DCB solution is lower than that in the toluene solution for the same PFam4-Ir complex system.

The influence of the PFam4 conformation on the quenching process can also be

proved by comparing the theoretical diffusion controlled rate constant, k_{dif} , and the measured Stern-Volmer quenching constant, k_q . From the calculated k_{dif} , the $\frac{k_{dif}(toluene)}{k_{dif}(DCB)}$ yields 2.24.

However, the $\frac{k_q(toluene)}{k_q(DCB)}$ for the PFam4-FIrpc system is 2.72 and that for the

PFam4-Ir(mppy)₃ system is 2.71. The $\frac{k_q(toluene)}{k_q(DCB)}$ values are larger than the

$\frac{k_{dif}(toluene)}{k_{dif}(DCB)}$ value for both the PFam4-FIrpc and PFam4-Ir(mppy)₃ systems because the

Stern-Volmer quenching constants in the DCB solutions are smaller. If the quenching efficiency in the DCB solution were the same as that in the toluene solution, the Stern-Volmer quenching constant in the DCB solution for the PFam4-FIrpc system would be 2.34×10^{10}

(Ms)⁻¹ ($\frac{k_q(toluene) = 5.24 \times 10^{10}}{2.24} = 2.34 \times 10^{10}$ (Ms)⁻¹), and that for the PFam4-Ir(mppy)₃

system would be 2.02×10^{10} (Ms)⁻¹ ($\frac{k_q(toluene) = 4.52 \times 10^{10}}{2.24} = 2.02 \times 10^{10}$ (Ms)⁻¹).

Nevertheless, the measured Stern-Volmer quenching constant in the DCB solution for the PFam4-FIrpc system is 1.93×10^{10} (Ms)⁻¹, and that for the PFam4-Ir(mppy)₃ system is 1.67×10^{10} (Ms)⁻¹. We think that the smaller Stern-Volmer quenching constant in the DCB

solution that we measured is evidence that the broader distribution of hydrodynamic diameter of PFam4 in the DCB solution would lead to smaller Stern-Volmer quenching constants. A

smaller Stern-Volmer quenching constant in DCB would decrease the quenching efficiency in the DCB solution and lead to larger value of $\frac{k_q(toluene)}{k_q(DCB)}$.

On the other hand, from the same host-dopant system in different solvents, the rank of the quenching constant is $k_q(toluene) > k_q(cosolvent) > k_q(DCB)$. Because the η and the δ of the cosolvent are between that of the toluene and DCB, the quenching constants in the

cosolvent solutions are also between them.



5-2 Analysis of device performance

The fabrication conditions of these two types of device are the same, but the thickness of the emitting layer which was spun cast from DCB solution is thinner than the other. It may be due to that the hole-transport layer, PVK, was partly dissolved in DCB solvent as spin coating the emitting layer onto it. From Figure 4-3-1, the turn on voltage of the device, which the emitting layer was spun cast from the DCB solution, is lower than the other. That may be due to the film which was spun cast from the DCB solution is thinner than the other. On the other hand, the PFam4 film, which was spun cast from the DCB solution, has β -phase conformation. The β -phase conformation can be seen from Figure 4-3-4. The absorption spectrum of neat PFam4 film that was spun cast from DCB solution has additional absorption peak at 433nm, which is close to the previous published paper that had additional absorption peak at 436~438nm, that were assigned for β -phase conformation [32-35]. The β -phase conformation is a sheetlike conformation; The PFam4 polymers aggregate to form a sheetlike conformation. So, as the exciton is formed at PFam4, the exciton may diffuse easily within the sheetlike conformation of PFam4 polymers and may directly emit light at PFam4 polymers. It is why the residual PFam4 emission can be seen in the device with the emitting layer that was spun cast from the DCB solution (poor solvent for PFam4), but not seen in the device with the emitting layer that was spun cast from the toluene solution (good solvent for PFam4), from Figure 4-3-5. From Figure 4-3-3, the surface of the emitting layer that was spun cast from the toluene solution is smooth, but that which that was spun cast from the DCB solution is rough.

Chapter 6 Conclusion

Since the triplet absorption of PFam4 is negligible, the triplet energy transfer from the Ir complex to the PFam4 is dominated by Dexter energy transfer. From the Stern-Volmer quenching constants for different systems in the same solvent, we can see that the quenching effect is more efficient when the triplet energy of Ir complex becomes much higher than that of PFam4. Compared the k_q , Stern-Volmer quenching constants, with the k_{dif} from Smoluchowski equation, we conclude that the triplet energy transfers for both the PFam4-FIrpic system and PFam4-Ir(mppy)₃ system in the toluene solutions are close to diffusion controlled. For the PFam4-FIrpic system in the DCB solution, the triplet energy transfer is also close to diffusion controlled. However, the triplet energy transfer for neither the PFam4-Ir(mppy)₃ system in the DCB solution nor the PFam4-Ir(FIPy)₂(acac) system in the toluene solution is diffusion controlled. An oscillating energy transfer between Ir(FIPy)₂(acac) and PFam4 may occur.

The absorption and PL spectra of PFam4 in the DCB and cosolvent solutions are redshift relative to that in the toluene solution because of the greater polarity of DCB. From the absorption spectrum, it is shown that no β -phase conformation of PFam4 in the DCB and cosolvent solutions. Although the mean hydrodynamic radius of PFam4 in the toluene solution is almost the same as that in the DCB solution, the distribution of hydrodynamic diameter of PFam4 in the DCB solution is much broader than that in the toluene solution. The broader distribution of hydrodynamic diameter of PFam4 in the DCB solution is resulted from the poor solvent characteristic. In the poor solvent, DCB, PFam4 may not stretch well and form a smaller coil or entangle with other PFam4 polymers to form a bigger coil. It would decrease the collision probability between PFam4 and Ir complexes in the DCB solution and

lead to a smaller Stern-Volmer quenching constant in the DCB solution. Therefore, for the same PFam4-Ir complex system, the quenching efficiency in the DCB solution is lower than that in the toluene solution. The effect of the PFam4 conformation on the quenching process is also described by comparing $\frac{k_q(\text{toluene})}{k_q(\text{DCB})}$ with $\frac{k_{dif}(\text{toluene})}{k_{dif}(\text{DCB})}$. The $\frac{k_q(\text{toluene})}{k_q(\text{DCB})}$ for the PFam4-FIrpc and the PFam4-Ir(mppy)₃ systems are larger than $\frac{k_{dif}(\text{toluene})}{k_{dif}(\text{DCB})}$. Because the η and the δ of the cosolvent are between that of the toluene and DCB, the quenching constants in the cosolvent solutions are also between them. The lower efficiency of the device with the emitting layer that was spun cast from the DCB solution was due to the β -phase conformation of PFam4.



Chapter 7 Future Work

From the Stokes-Einstein equation and the Smoluchowski equation (eq. 5-1-3 and 5-1-4), we realized that the quenching process is influenced by the temperature. The temperature would affect the diffusion coefficients of the molecules in the solution because the solvent viscosity is a function of the temperature. The temperature would also vary the conformation of the molecules in the solution. Therefore, a further study on the relation between the Stern-Volmer quenching constant and the temperature is needed.



Reference

- 1 M. Pope, H. P. Kallmann, P. Magnante et al., "Electroluminescence in Organic Crystals," *J. Chem. Phys.* **38** (8), 2042-2043 (1963).
- 2 C. W. Tang, S. A. VanSlyke et al., "Organic electroluminescent diodes," *Appl. Phys. Lett.* **51**(12), 913-915 (1987).
- 3 H. Shirakawa, E. J. Louis, A. G. MacDiarmid, C. K. Chiang, A. J. Heeger et al., "Synthesis of electrically conducting organic polymers: halogen derivatives of polyacetylene, $(\text{CH})_x$," *Chem. Commun.* **16**, 578-580 (1977).
- 4 C. K. Chiang, C. R. Fincher, Jr., Y. W. Park, A. J. Heeger, H. Shirakawa, E. J. Louis, S. C. Gau, A. G. MacDiarmid et al., "Electrical Conductivity in Doped Polyacetylene," *Phys. Rev. Lett.* **39** (17), 1098-1101 (1977).
- 5 J. H. Burroughes, D. D. C. Bradley, A. R. Brown, R. N. Marks, K. Mackay, R. H. Friend, P. L. Burnst, A. B. Holms et al., "Light-emitting diodes based on conjugated polymers," *Nature* **347** (6293), 539-541 (1990).
- 6 S. M. Sze, *Physics of Semiconductor Devices*, 2nd ed., New York, Wiley.
- 7 J. Shinar, *Organic Light Emitting Devices, A Survey*, Springer-Verlag, New York, 2004.
- 8 H. A. Al Attar, A. P. Monkman et al., "Dopant effect on the charge injection, transport, and device efficiency of an electrophosphorescent polymer light-emitting device," *Adv. Funct. Mater.* **16** (17), 2231-2242 (2006).
- 9 E. A. Silinsh, *Organic Molecules Crystals*, Springer-Verlag Berlin Heidelberg New York, Germany, 1978.
- 10 K. H. Probst, N. Karl, "Energy-levels of electron and hole traps in band-gap doped anthracene-crystals," *Phys. Status Solidi (a)* **27** (2), 499-508 (1975).
- 11 C. Kittel, *Introduction to Solid State Physics* 7th ed., Wiley, 1996.
- 12 S. K. Saha, Y. K. Su, F. S. Suang, "Temperature dependence of electroluminescence in tris-(8-hydroxy) quinoline aluminum (Alq_3) light emitting diode," *IEEE Journal of Quantum, Electronics* **37** (6), 807-812 (2001).
- 13 D. J. Griffiths, *Introduction to quantum mechanics*, 2nd ed., Pearson Prentice Hall, 2005.
- 14 M. A. Baldo, D. F. O'Brien, Y. You, A. Shoustikov, S. Sibley, M. E. Thompson, S. R. Forrest et al., "Highly efficient phosphorescent emission from organic electroluminescent devices," *Nature* **395** (6698), 151-154 (1998).
- 15 C. Adachi, M. A. Baldo, M. E. Thompson, S. R. Forrest et al., "Nearly 100% internal phosphorescence efficiency in an organic light-emitting device," *J. Appl. Phys.* **90** (10), 5048-5051 (2001).
- 16 P. W. Atkins and R. S. Friedman, *Molecular quantum mechanics*, 3rd ed., Oxford, 1997.
- 17 P. A. Lane, L. C. Palilis, D. F. O'Brien, C. Giebeler, A. J. Cadby, D. G. Libzey, A. J. Campbell, W. Blau, D.D.C. Bradley et al., "Origin of electrophosphorescence from a

- doped polymer light emitting diode,” *Phys. Rev. B* **63** (23), 235206 (2001)
- 18 X. Gong, J. C. Ostrowski, D. Moses, G. C. Bazan, A. J. Heeger et al., “Electrophosphorescence from a polymer guest-host system with an iridium complex as guest: Forster energy transfer and charge trapping,” *Adv. Funct. Mater.* **13**(6), 439-444 (2003)
 - 19 N. J. Turro, *Modern molecular photochemistry*, University Science Books, 1991.
 - 20 A. A. Shoustikov, Y. You, M. E. Thompson et al., “ Electroluminescence Color Tuning by Dye Doping in Organic Light-Emitting Diodes,” *IEEE J. Selected Topics in Quantum Electronics* (**4**), 3-13 (1998).
 - 21 T. Forster et al., “Transfer Mechanisms of Electronic Excitation,” *Disc. Faraday Soc.* **27** (7), 7-17 (1959)
 - 22 D. L. Dexter et al.,” A theory of sensitized luminescence in solids,” *J. Chem. Phys.* **21** (5), 836-850 (1953)
 - 23 T. F. Guo, S.C. Chang, Y. Yang, R. C. Kwong, M. E. Thompson et al., “Highly efficient electrophosphorescent polymer light-emitting devices “ *Organic Electronics* **1** (1), 15-20 (2000).
 - 24 S. R. Tseng, S. Y. Li, H. F. Meng, Y. H. Yu, C. M. Yang, H. H. Liao, S. F. Horng, C. S. Hsu et al., “ High-efficiency blue multilayer polymer light-emitting diode based on poly(9,9-dioctylfluorene)“ *J. Appl. Phys.* **101**, 84510-84513 (2007).
 - 25 T. F. Guo, F. S. Yang, Z. J. Tsai, T. C. Wen, S. N. Hseih, Y. S. Fu, C. T. Chung et al,”Organic oxide/Al composite cathode in efficient polymer light-emitting diodes” *Appl. Phys. Lett.* **88**, 113501-113503 (2006).
 - 26 F. C. Chen, Y. Yang, M. E. Thompson, J. Kido et al.”High-performance polymer light-emitting diodes doped with a red phosphorescent iridium complex” *Appl. Phys. Lett.* **80** (12), 2308-2310 (2002)
 - 27 R. W. T. Higgins, A. P. Monkman, H. –G. Nothofer, U. Scherf et al. “Energy transfer to porphyrin derivative dopants in polymer light-emitting diodes” *J. Appl. Phys.* **91** (1), 99-105 (2002).
 - 28 R. J. Homes, S. R. Forrest, Y. –J. Tung, R. C. Kwong, J. J. Brown, S. Garon, M. E. Thompson et al.” Blue organic electrophosphorescence using exothermic host–guest energy transfer,” *Appl. Phys. Lett.* **82** (15), 2422-2424 (2003).
 - 29 F. C. Chen, G. He, Y. Yang et al., “Triplet exciton confinement in phosphorescent polymer light-emitting diodes, “ *Appl. Phys. Lett.* **82** (7), 1006-1008 (2003)
 - 30 F. C. Chen, S. C. Chang, G. He, S. Pyo, Y. Yang, M. Kurotaki, J. Kido et al., “Energy transfer and triplet exciton confinement in polymeric electrophosphorescent devices, “ *J. Polym. Sci., Part B: Polym. Phys* **41** (21), 2681-2690 (2003)
 - 31 M. Sudhakar, P. I. Djurovich, T. E. Hogen-Esch, M. E. Thompson et al.“ Phosphorescence quenching by conjugated polymers“ *J. Am. Chem. Soc.* **125** (26), 7796-7797 (2003)
 - 32 M. Grell, D. D. C. Bradley, X. Long, T. Chamberlain, M. Inbasekaran, E. P. Woo, M.

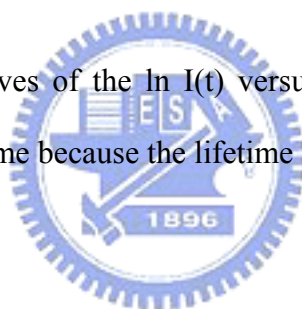
- Soliman et al.” Chain geometry, solution aggregation and enhanced dichroism in the liquidcrystalline conjugated polymer poly(9,9-dioctylfluorene),” *Acta Polym.* **49** (8), 439-444 (1998).
- 33 M. Grell, D. D. C. Bradley, G. Ungar, J. Hill, K. S. Whitehead et al. “Interplay of physical structure and photophysics for a liquid crystalline polyfluorene,” *Macromolecules* **32** (18), 5810-5817 (1999)
- 34 M. Knaapila, V. M. Garamus, F. B. Dias, L. Almasy, F. Galbrecht, A. Charas, J. Morgado, H. D. Burrows, U. Scherf, A. P. Monkman et al. “Influence of solvent quality on the self-organization of archetypical hairy rods-branched and linear side chain polyfluorenes: rodlike chains versus “beta-sheets” in solution,” *Macromolecules* **39** (19), 6505-6512 (2006)
- 35 F. B. Dias, J. Morgado, A. L. Macanita, F. P. da Costa, H. D. Burrows, A. P. Monkman et al.” Kinetics and thermodynamics of poly(9,9-dioctylfluorene) β -phase formation in dilute solution,” *Macromolecules* **39** (17), 5854-5864 (2006).
- 36 M. J. Banach, R. H. Friend, H. Sirringhaus et al., “Influence of the casting solvent on the thermotropic alignment of thin liquid crystalline polyfluorene copolymer films, ,, *Macromolecules* **37** (16), 6079-6085 (2004).
- 37 S. Janietz, D. D. C. Bradley, M. Grell, C. Giebeler, M. Inbasekaran, E. P. Woo et al., “Electrochemical determination of the ionization potential and electron affinity of poly(9,9-dioctylfluorene),” *Appl. Phys. Lett.* **73** (17), 2453-2455 (1998).
- 38 M. Redecker, D. D. C. Bradley, M. Inbasekaran, E. P. Woo et al., “Nondispersive hole transport in an electroluminescent polyfluorene,” *Appl. Phys. Lett.* **73** (11), 1565-1567 (1998).
- 39 J. A. Riddick, W. B. Bunger, T. K. Sakano, *Organic Solvents*, 4th ed., John Wiley & Son, 1986
- 40 S. Lamansky, P. Djurovich, D. Murphy, F. Abdel-Razzq, H. E. Lee, C. Adachi, P. E. Burrows, S. R. Forrest, M. E. Thompson et al.” Highly phosphorescent bis-cyclometalated Iridium complexes: synthesis, photophysical characterization, and use in organic light emitting diodes,” *J. Am. Chem. Soc.* **123** (18), 4304-4312 (2001).
- 41 S. Lamansky, P. Djurovich, D. Murphy, F. Abdel-Razzq, R. Kwong, I. Tsyba, M. Bortz, B. Mui, R. Bau, M. E. Thompson et al.”Synthesis and characterization of phosphorescent cyclometalated Iridium complexes,” *Inorg. Chem.* **40** (7), 1704-1711 (2001).
- 42 G. Fytas, H. G. Nothofer, U. Scherf, D. Vlassopoulos, G. Meier et al.“ Structure and dynamics of nondilute polyfluorene solutions,” *Macromolecules* **35** (2), 481-488 (2002).
- 43 S. M. King, H. A. Al-Attar, R. J. Evans, A. Congreve, A. Beeby, A. P. Monkman et al. “The use of substituted Iridium complexes in doped polymer electrophosphorescent devices: the influence of triplet transfer and other factors on enhancing device performance,” *Adv. Funct. Mater.* **16** (13), 1043-1050 (2006)
- 44 A. Tsuboyama, H. Iwawaki, M. Furugori, T. Mukaide, J. Kamatani, S. Igawa, T.

- Moriyama, S. Miura, T. Takiguchi, S. Okada, M. Hoshino, K. Ueno et al." Homoleptic cyclometalated iridium complexes with highly efficient red phosphorescence and application to organic light-emitting diode, "J. Am. Chem. Soc. **125** (42), 12971-12979 (2003).
- 45 M. Tavasli, S. Bettington, M. R. Bryce, H. A. Al Attar, F. B. Dias, S. King, A. P. Monkman et al."Oligo(fluorenyl) pyridine ligands and their tris-cyclometalated iridium(III) complexes: synthesis, photophysical properties and electrophosphorescent devices,"J. Mater. Chem **15** (46), 4963-4970 (2005).
- 46 T. Tsuboi, H. Murayama, S. J. Yeh, C. T. Chen et al. "Energy transfer between fluorescent CBP host and blue phosphorescent FIrpic and FIrN4 guests," Optical Materials **29** (11), 1299-1304 (2007).
- 47 D. Wasserberg, S. C. J. Meskers, R. A. J. Jassen et al."Phosphorescent resonant energy transfer between iridium complexes," J. Phys. Chem. A **111** (8), 1381-1388 (2007)
- 48 S. J. Strickler, R. A. Berg et al., "Relationship between absorption intensity and fluorescence lifetime of molecules," J. Chem. Phys. **37** (4), 814-822 (1962).
- 49 J. Mohanty, W. M. Nau et al."Refractive index effects on the oscillator strength and radiative decay rate of 2,3-diazabicyclo[2.2.2]oct-2-ene," Photochem. Photobiol. Sci., **3**, 1026-1031 (2004)
- 50 D. Toptygin et al. "Effects of the solvent refractive index and its dispersion on the radiative decay rate and extinction coefficient of a fluorescent solute," J. Fluorescence **13** (3), 201-219 (2003).
- 51 C. Rothe, A. P. Monkman et al. "Dynamics and trap-depth distribution of triplet excited states in thin films of the light-emitting polymer poly(9,9-di(ethylhexyl)fluorene), " Phys. Rev. B **65**, 73201-73204 (2002)
- 52 J. R. Lakowicz, Principles of Fluorescence Spectroscopy, 2nd ed., Kluwer Academic/Plenum Publisger, New York, 1999.
- 53 J. S. Winn, Physical Chemistry, Harper Collins, New York, 1995
- 54 H. A. Al Attar, A. P. Monkman, M. Tavasli, S. Bettington, M. R. Bryce et al. " White polymer light-emitting diode based on a fluorene polymer/ Ir complex blend system, "Appl. Phys. Lett. **86** (12), 121101-121103 (2005).
- 55 G. G. Guilbault, Practical Fluorescence, 2nd ed., M. Dekker, 1990.

Appendix

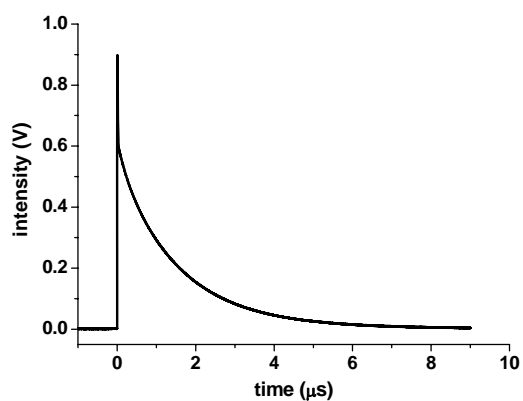
In this section, we will demonstrate the measurement method of the lifetimes of Ir dopants at different concentrations of PFam4 from raw data, which composes of two steps. First, we plot a figure of natural logarithm of photoluminescence intensity of the Ir dopant, $\ln I(t)$, versus time (t). Second, the lifetime is determined from the slope of the middle section of the curve which forms a straight line. The early stage and final stage of the recording time are excluded from the lifetime calculation. The intensity of the early stage belongs to that of the laser light, and the laser pulse duration is much shorter than the phosphorescence lifetime of the Ir dopant. On the other hand, the final part of the curve is significantly influenced by noise and is fluctuated.

In this section, the curves of the $\ln I(t)$ versus time are offset upward. It does not influence the result of the lifetime because the lifetime is determined from the slope.

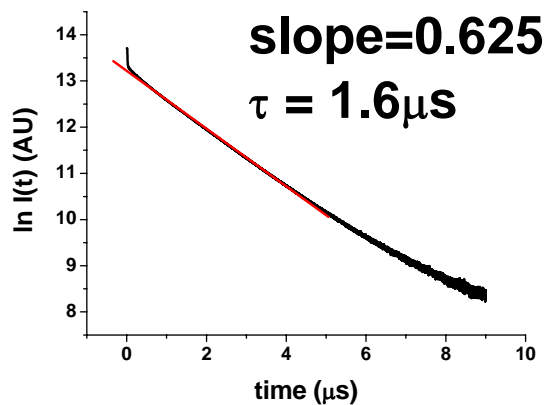


Appendix-1 The PFam4-FIrpic system in the toluene solution

Figure A-1-1, A-1-2, A-1-3, A-1-4 and A-1-5 show the processes to get the lifetimes of FIrpic at $[PFam4]=0$ M, 1mM, 2mM, 3mM and 4mM (in monomer unit) in the toluene solution, respectively.

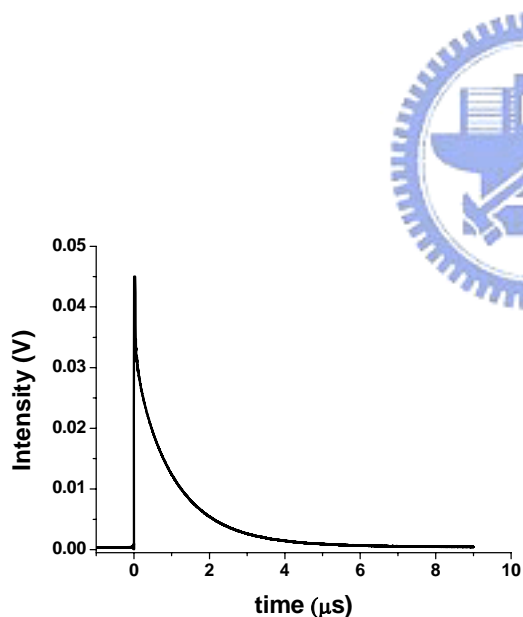


(a)

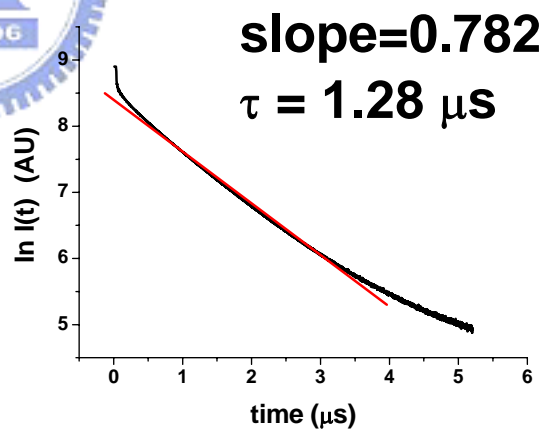


(b)

Figure A-1-1 For the PFam4-FIrpic system in the toluene solution, the photoluminescence decay curve of FIrpic at [PFam4]=0M (a) photoluminescence intensity $I(t)$ versus t ; (b) $\ln I(t)$ versus t

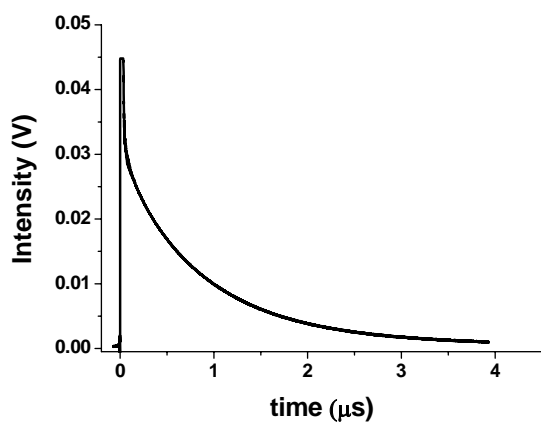


(a)

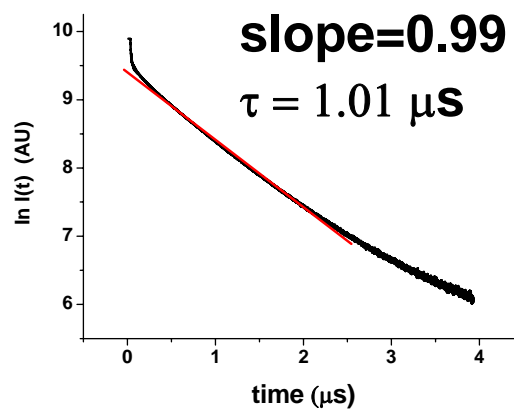


(b)

Figure A-1-2 For the PFam4-FIrpic system in the toluene solution, the photoluminescence decay curve of FIrpic at [PFam4]=1mM (a) photoluminescence intensity $I(t)$ versus t ; (b) $\ln I(t)$ versus t

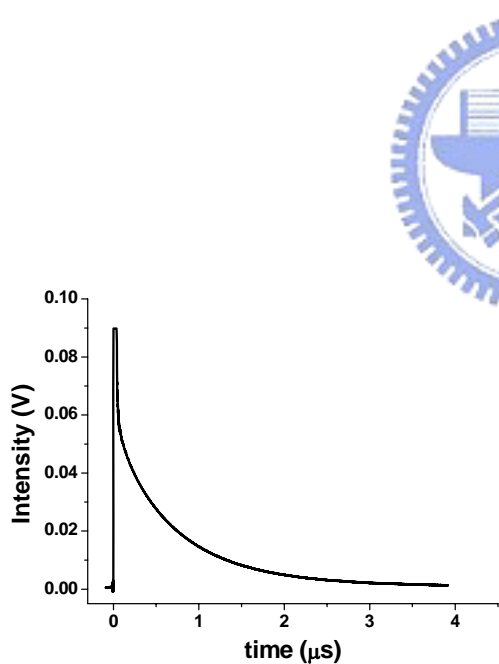


(a)

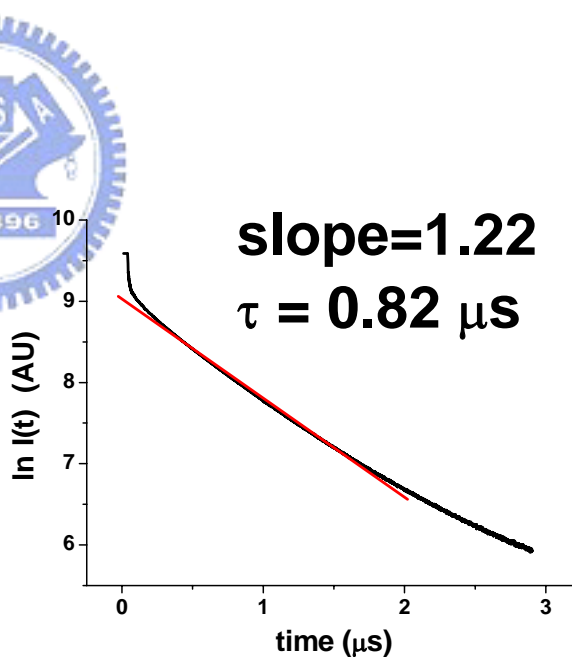


(b)

Figure A-1-3 For the PFam4-FIrpc system in the toluene solution, the photoluminescence decay curve of FIrpc at [PFam4]=2mM (a) photoluminescence intensity $I(t)$ versus t ; (b) $\ln I(t)$ versus t

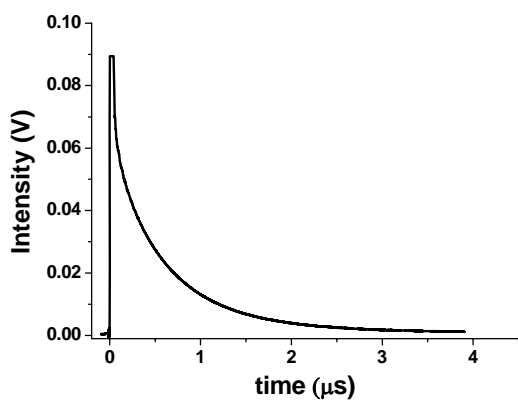


(a)

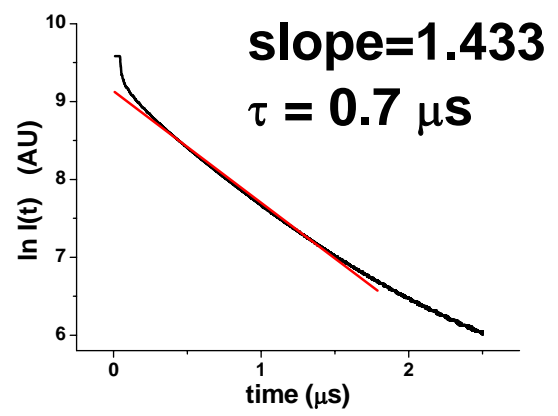


(b)

Figure A-1-4 For the PFam4-FIrpc system in the toluene solution, the photoluminescence decay curve of FIrpc at [PFam4]=3mM (a) photoluminescence intensity $I(t)$ versus t ; (b) $\ln I(t)$ versus t



(a)



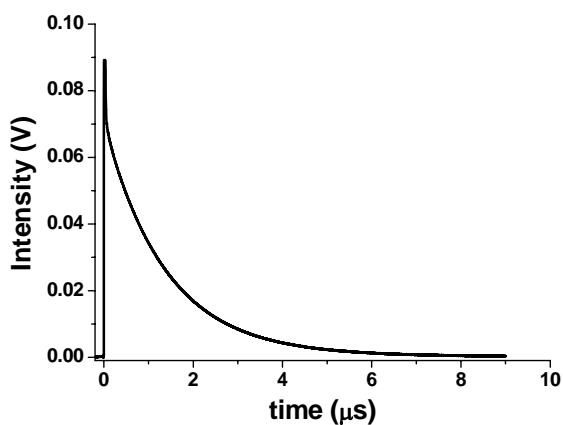
(b)

Figure A-1-5 For the PFam4-FIrpc system in the toluene solution, the photoluminescence decay curve of FIrpc at [PFam4]=4mM (a) photoluminescence intensity $I(t)$ versus t ; (b) $\ln I(t)$ versus t

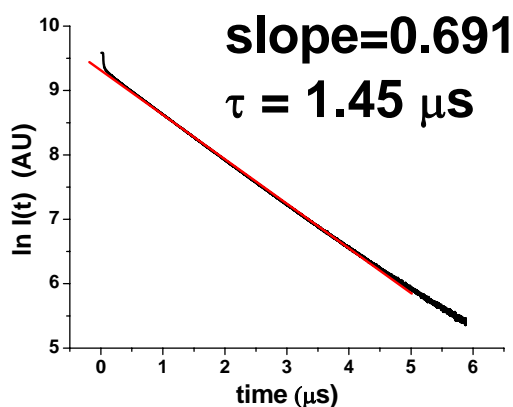


Appendix-2 The PFam4-FIrpc system in the DCB solution

Figure A-2-1, A-2-2, A-2-3, A-2-4 and A-2-5 show the processes to get the lifetimes of FIrpc at [PFam4]=0 M, 1mM, 2mM, 3mM and 4mM (in monomer unit) in the DCB solution, respectively.

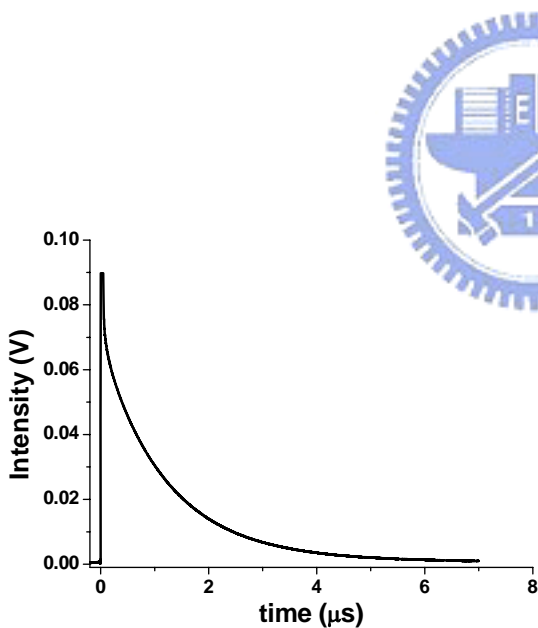


(a)

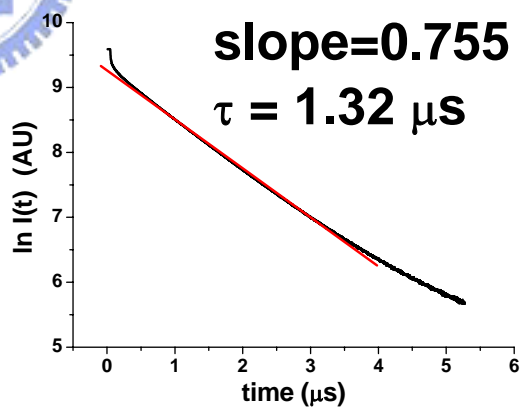


(b)

Figure A-2-1 For the PFam4-FIrpc system in the DCB solution, the photoluminescence decay curve of FIrpc at [PFam4]=0M (a) photoluminescence intensity $I(t)$ versus t ; (b) $\ln I(t)$ versus t



(a)



(b)

Figure A-2-2 For the PFam4-FIrpc system in the DCB solution, the photoluminescence decay curve of FIrpc at [PFam4]=1mM (a) photoluminescence intensity $I(t)$ versus t ; (b) $\ln I(t)$ versus t

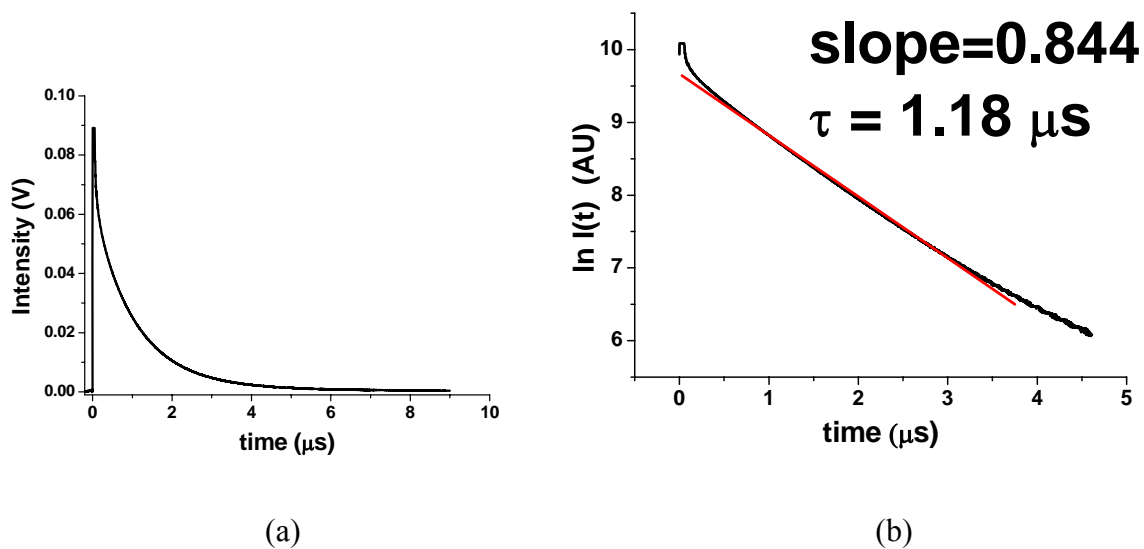


Figure A-2-3 For the PFam4-FIrpic system in the DCB solution, the photoluminescence decay curve of FIrpic at [PFam4]=2mM (a) photoluminescence intensity $I(t)$ versus t ; (b) $\ln I(t)$ versus t

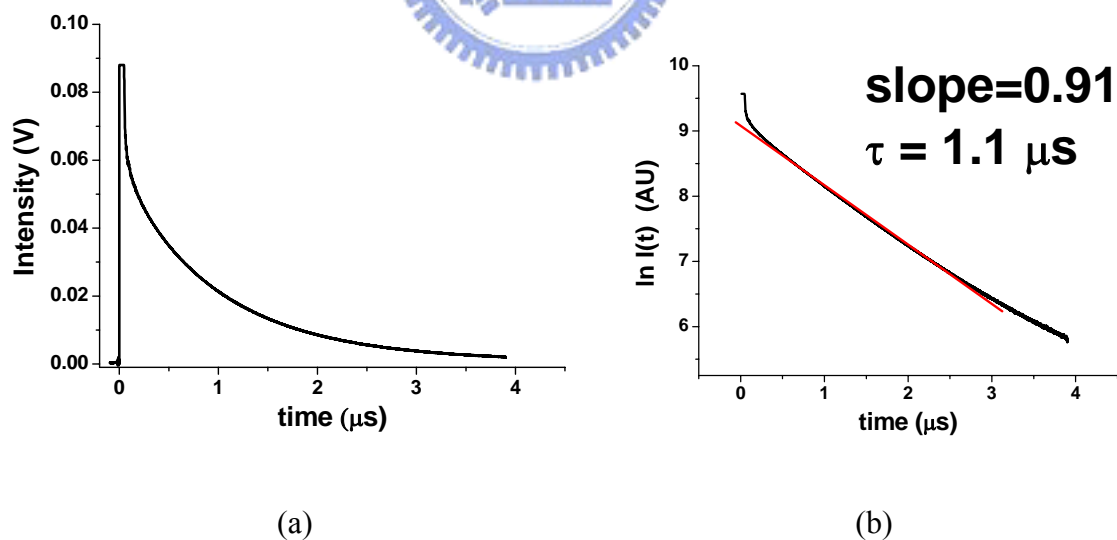
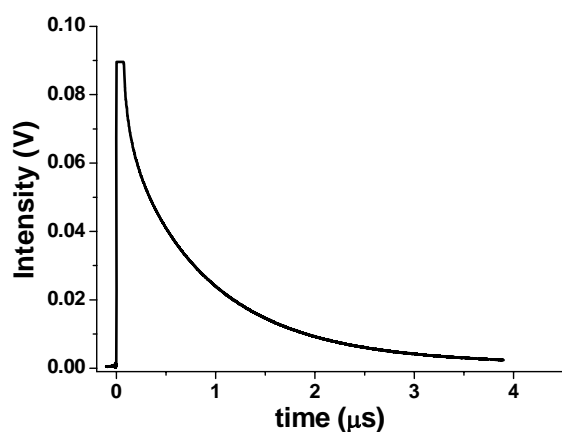
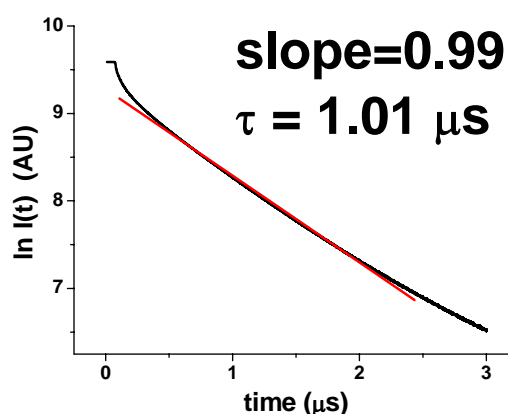


Figure A-2-4 For the PFam4-FIrpic system in the DCB solution, the photoluminescence decay curve of FIrpic at [PFam4]=3mM (a) photoluminescence intensity $I(t)$ versus t ; (b) $\ln I(t)$ versus t



(a)



(b)

Figure A-2-5 For the PFam4-FIrpic system in the DCB solution, the photoluminescence decay curve of FIrpic at [PFam4]=4mM (a) photoluminescence intensity $I(t)$ versus t ; (b) $\ln I(t)$ versus t



Appendix-3 The PFam4-FIrpic system in the cosolvent solution

Figure A-3-1, A-3-2, A-3-3, A-3-4 and A-3-5 show the processes to get the lifetimes of FIrpic at [PFam4]=0 M, 1mM, 2mM, 3mM and 4mM (in monomer unit) in the cosolvent solution, respectively.

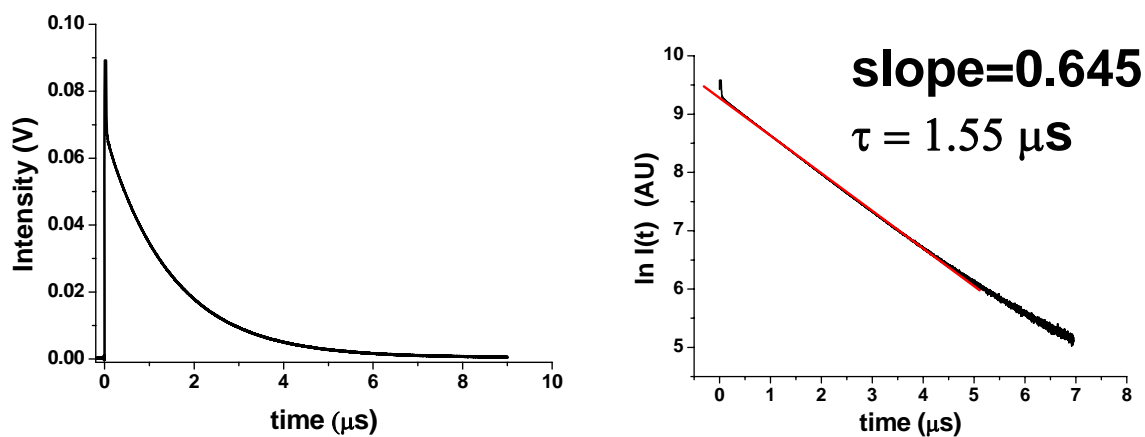


Figure A-3-1 For the PFam4-FIrpc system in the cosolvent solution, the photoluminescence decay curve of FIrpc at [PFam4]=0M (a) photoluminescence intensity $I(t)$ versus t ; (b) $\ln I(t)$ versus t

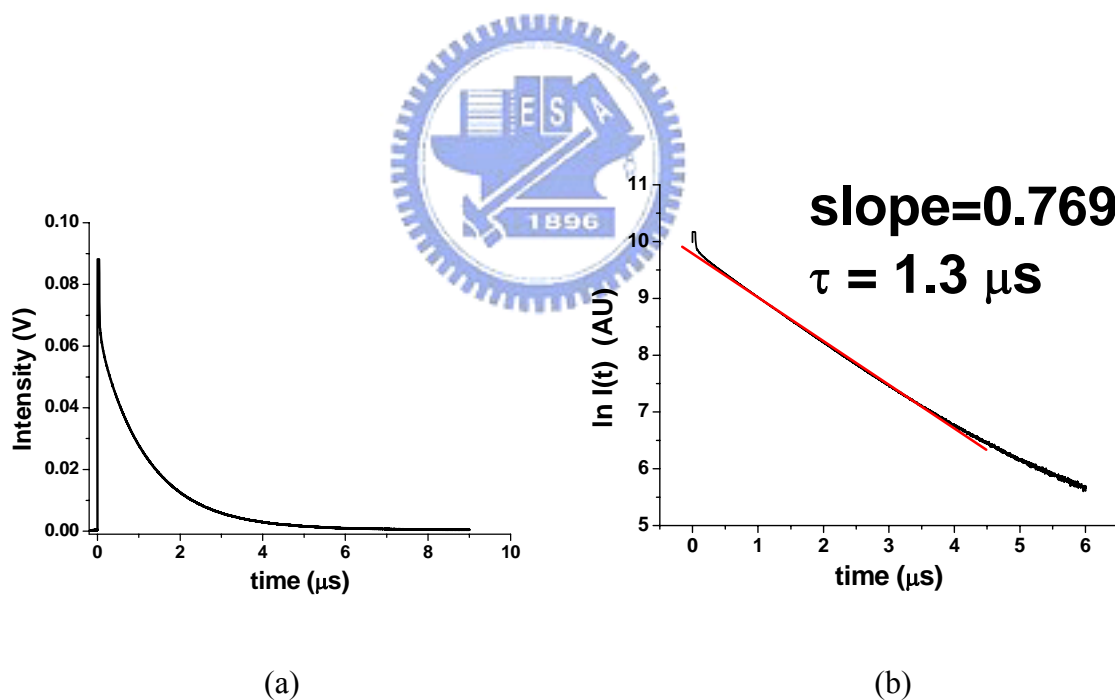
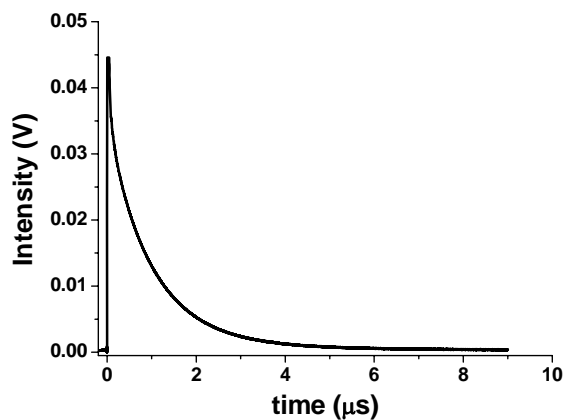
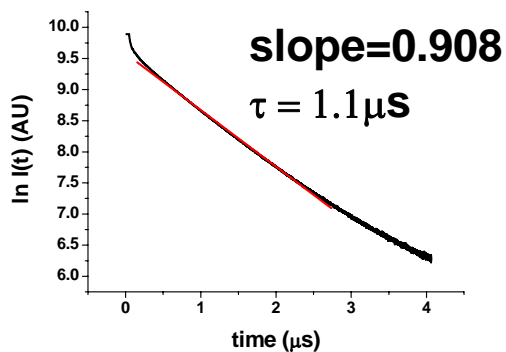


Figure A-3-2 For the PFam4-FIrpc system in the cosolvent solution, the photoluminescence decay curve of FIrpc at [PFam4]=1mM (a) photoluminescence intensity $I(t)$ versus t ; (b) $\ln I(t)$ versus t

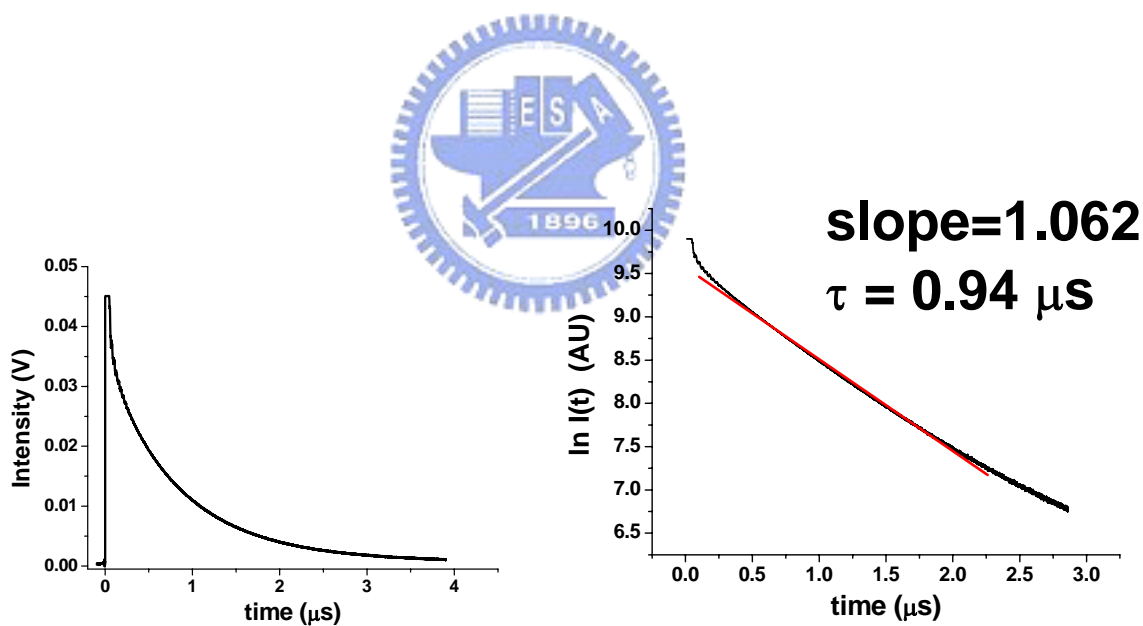


(a)



(b)

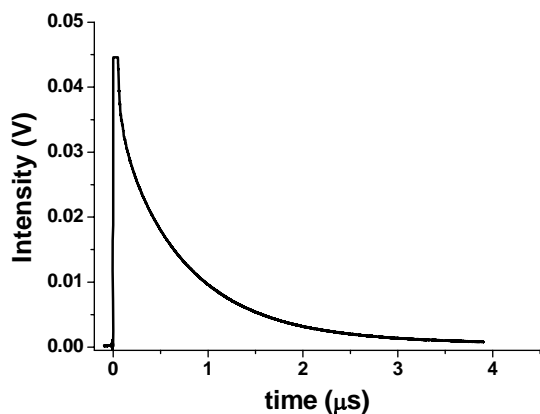
Figure A-3-3 For the PFam4-FIrpc system in the cosolvent solution, the photoluminescence decay curve of FIrpc at [PFam4]=2mM (a) photoluminescence intensity $I(t)$ versus t ; (b) $\ln I(t)$ versus t



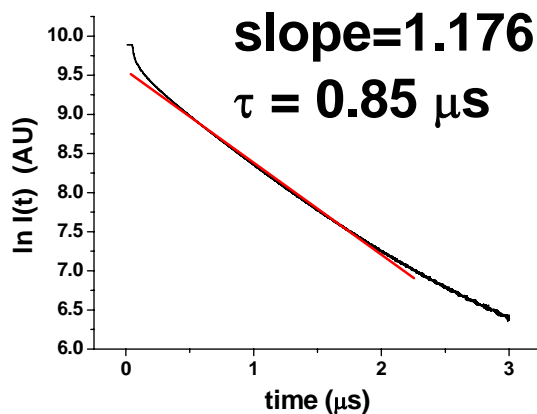
(a)

(b)

Figure A-3-4 For the PFam4-FIrpc system in the cosolvent solution, the photoluminescence decay curve of FIrpc at [PFam4]=3mM (a) photoluminescence intensity $I(t)$ versus t ; (b) $\ln I(t)$ versus t



(a)



(b)

Figure A-3-5 For the PFam4-FIrpic system in the cosolvent solution, the photoluminescence decay curve of FIrpic at [PFam4]=4mM (a) photoluminescence intensity $I(t)$ versus t ; (b) $\ln I(t)$ versus t



Appendix-4 The PFam4-Ir(mppy)₃ system in the toluene solution

Figure A-4-1, A-4-2, A-4-3, A-4-4 and A-4-5 show the processes to get the lifetimes of Ir(mppy)₃ at [PFam4]=0 M, 1mM, 2mM, 3mM and 4mM (in monomer unit) in the toluene solution, respectively.

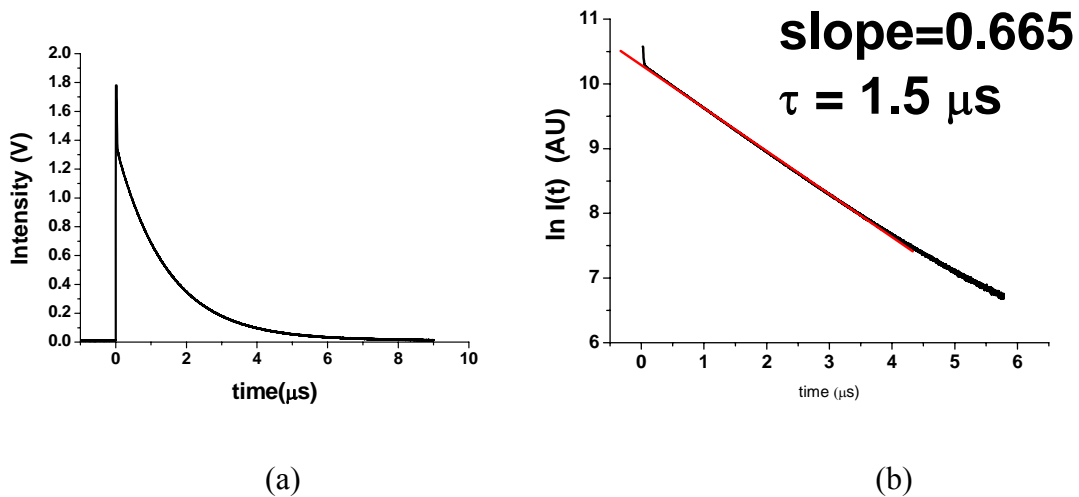


Figure A-4-1 For the PFam4-Ir(mppy)₃ system in the toluene solution, the photoluminescence decay curve of Ir(mppy)₃ at [PFam4]=0M (a) photoluminescence intensity I(t) versus t; (b) ln I(t) versus t

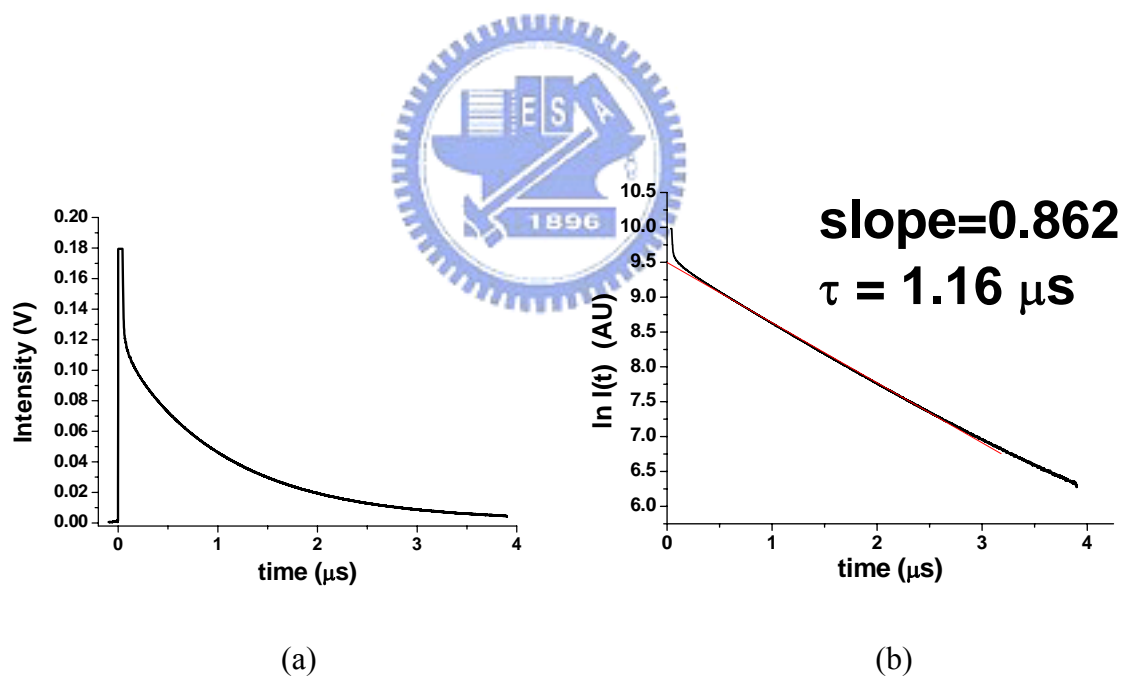


Figure A-4-2 For the PFam4-Ir(mppy)₃ system in the toluene solution, the photoluminescence decay curve of Ir(mppy)₃ at [PFam4]=1mM (a) photoluminescence intensity I(t) versus t; (b) ln I(t) versus t

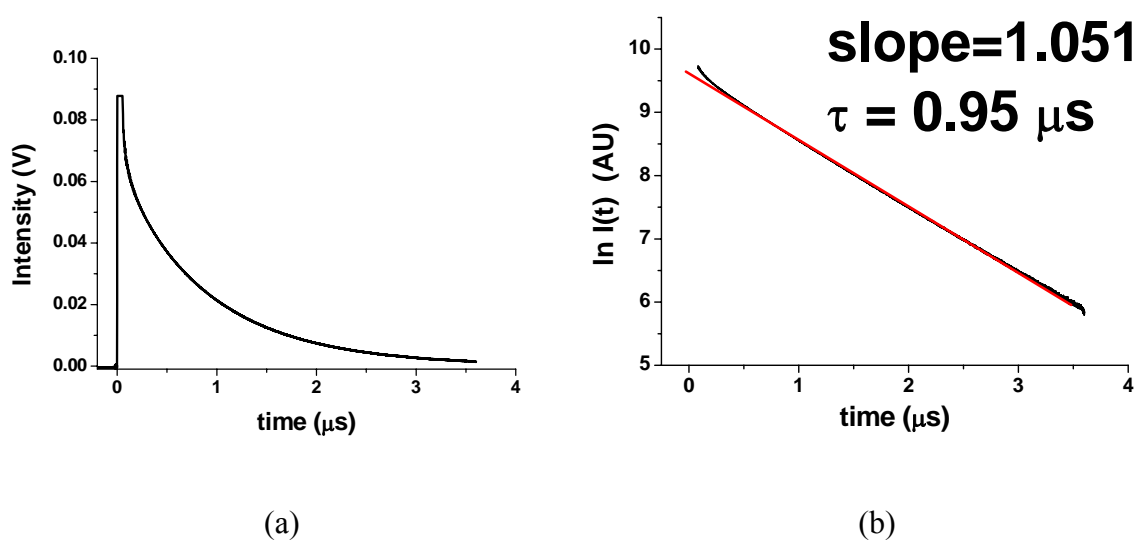


Figure A-4-3 For the PFam4-Ir(mppy)₃ system in the toluene solution, the photoluminescence decay curve of Ir(mppy)₃ at [PFam4]=2mM (a) photoluminescence intensity I(t) versus t; (b) ln I(t) versus t

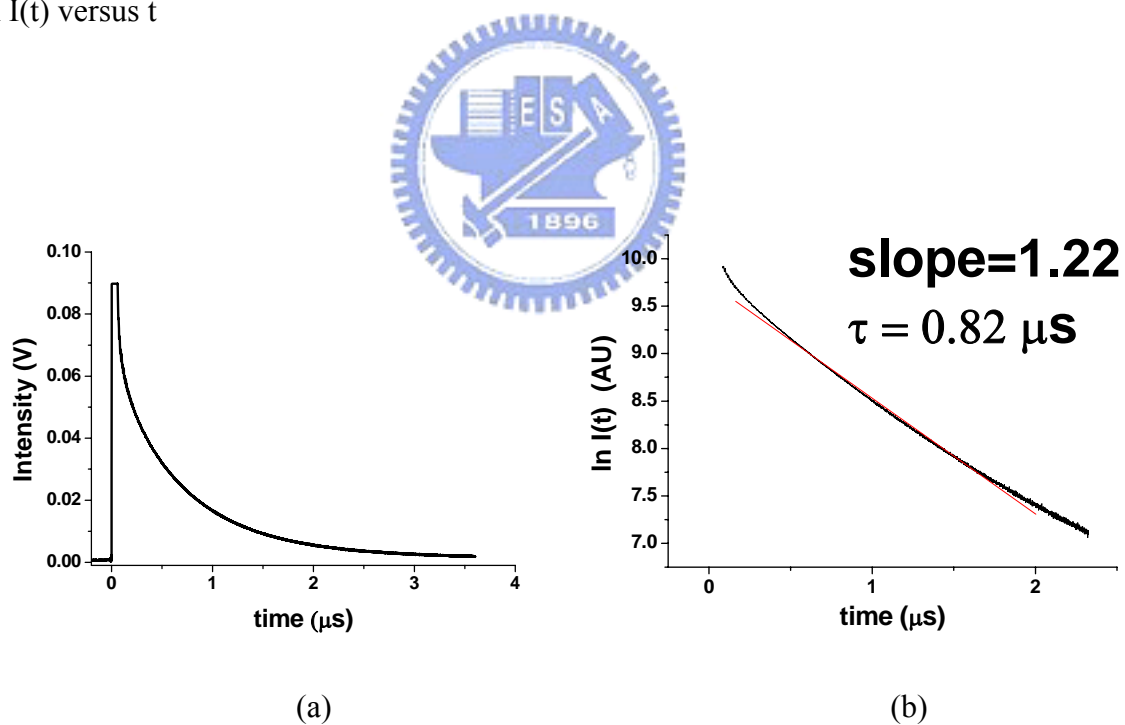
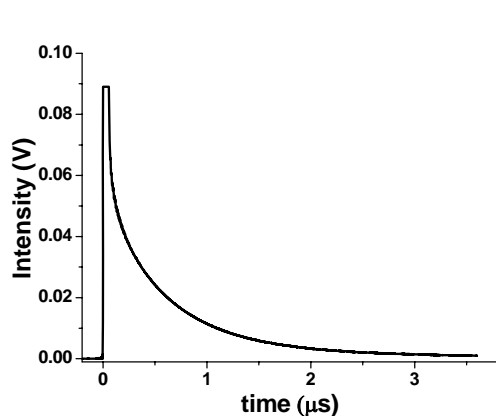
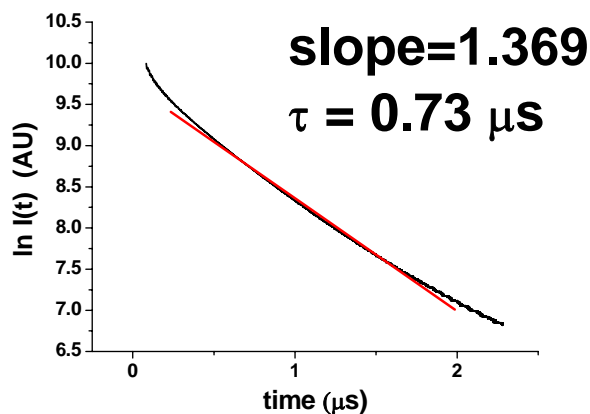


Figure A-4-4 For the PFam4-Ir(mppy)₃ system in the toluene solution, the photoluminescence decay curve of Ir(mppy)₃ at [PFam4]=3mM (a) photoluminescence intensity I(t) versus t; (b) ln I(t) versus t

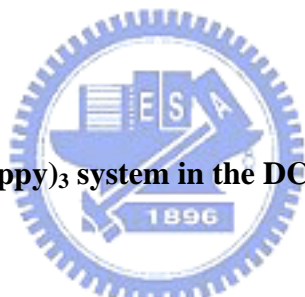


(a)



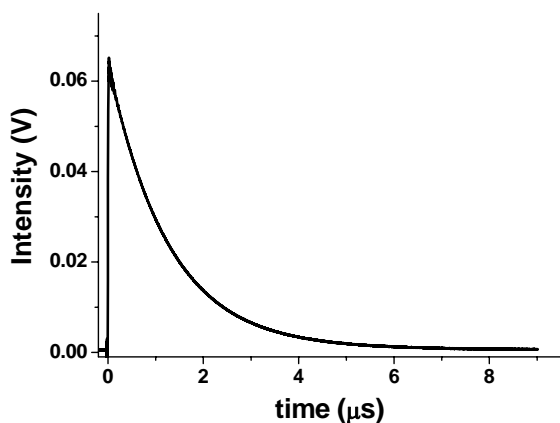
(b)

Figure A-4-5 For the PFam4-Ir(mppy)₃ system in the toluene solution, the photoluminescence decay curve of Ir(mppy)₃ at [PFam4]=4mM (a) photoluminescence intensity $I(t)$ versus t ; (b) $\ln I(t)$ versus t

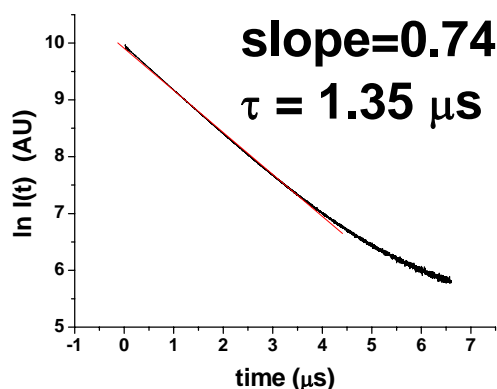


Appendix-5 The PFam4-Ir(mppy)₃ system in the DCB solution

Figure A-5-1, A-5-2, A-5-3, A-5-4 and A-5-5 show the processes to get the lifetimes of Ir(mppy)₃ at [PFam4]=0 M, 1mM, 2mM, 3mM and 4mM (in monomer unit) in the DCB solution, respectively.

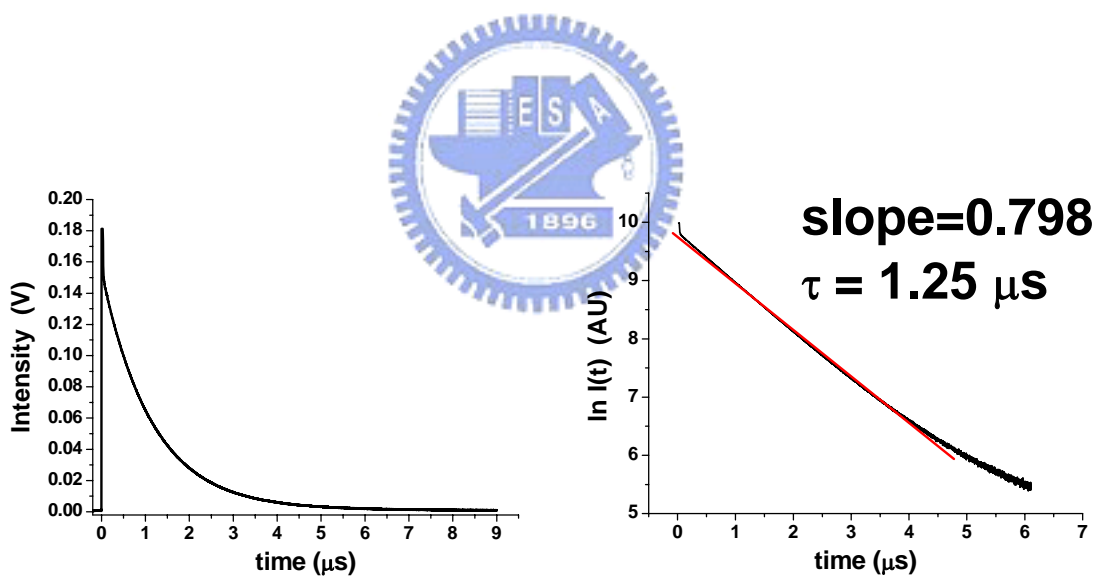


(a)



(b)

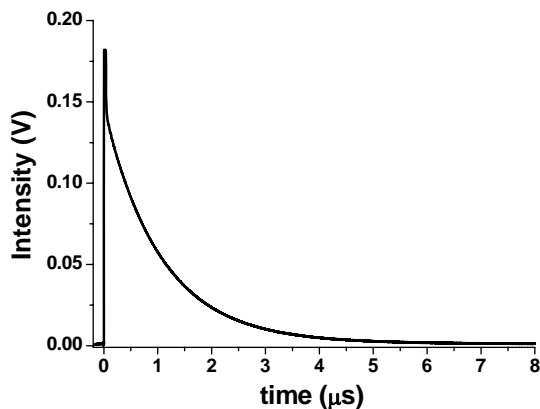
Figure A-5-1 For the PFam4-Ir(mppy)₃ system in the DCB solution, the photoluminescence decay curve of Ir(mppy)₃ at [PFam4]=0M (a) photoluminescence intensity I(t) versus t; (b) ln I(t) versus t



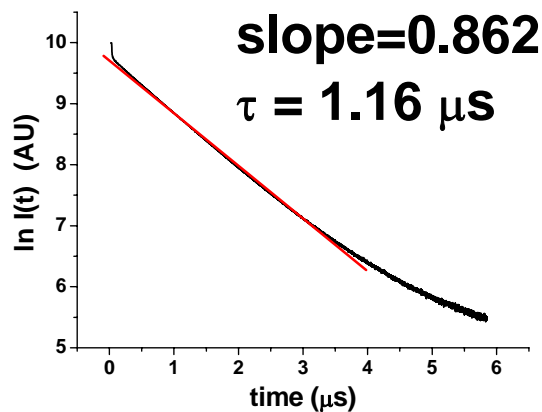
(a)

(b)

Figure A-5-2 For the PFam4-Ir(mppy)₃ system in the DCB solution, the photoluminescence decay curve of Ir(mppy)₃ at [PFam4]=1mM (a) photoluminescence intensity I(t) versus t; (b) ln I(t) versus t

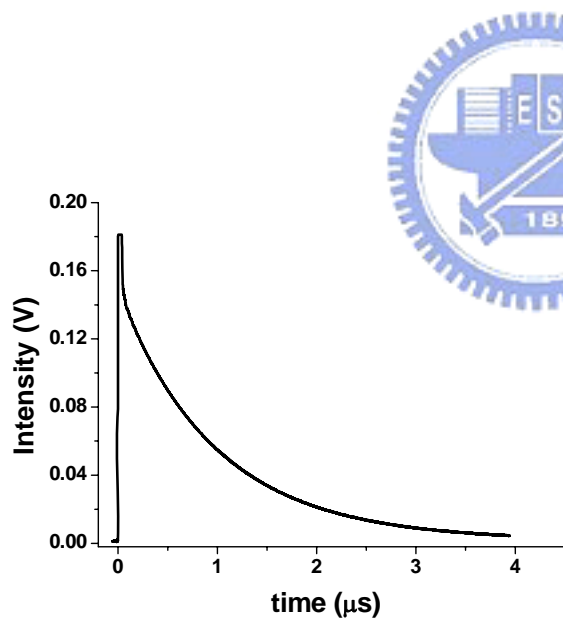


(a)

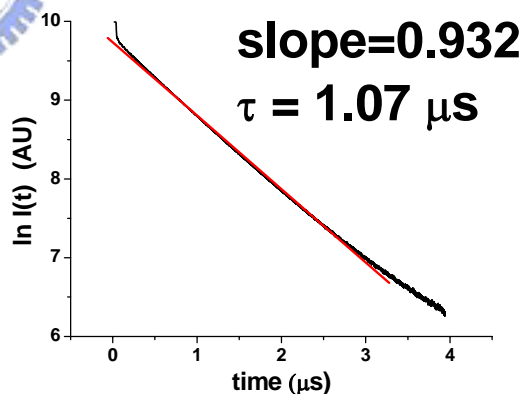


(b)

Figure A-5-3 For the PFam4-Ir(mppy)₃ system in the DCB solution, the photoluminescence decay curve of Ir(mppy)₃ at [PFam4]=2mM (a) photoluminescence intensity I(t) versus t; (b) ln I(t) versus t

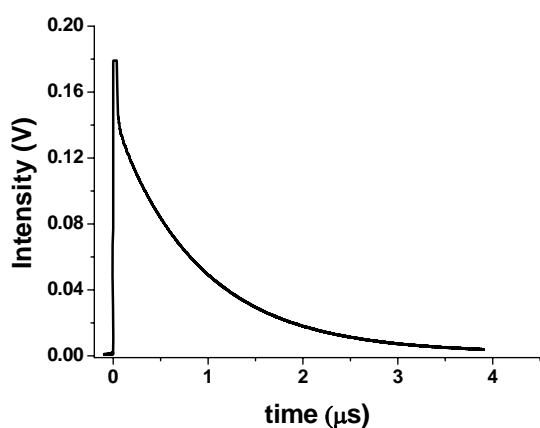


(a)

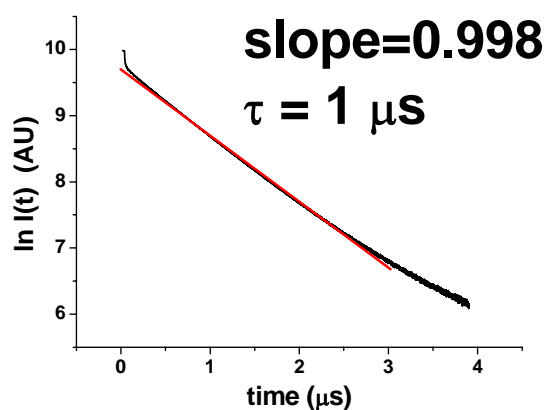


(b)

Figure A-5-4 For the PFam4-Ir(mppy)₃ system in the DCB solution, the photoluminescence decay curve of Ir(mppy)₃ at [PFam4]=3mM (a) photoluminescence intensity I(t) versus t; (b) ln I(t) versus t



(a)



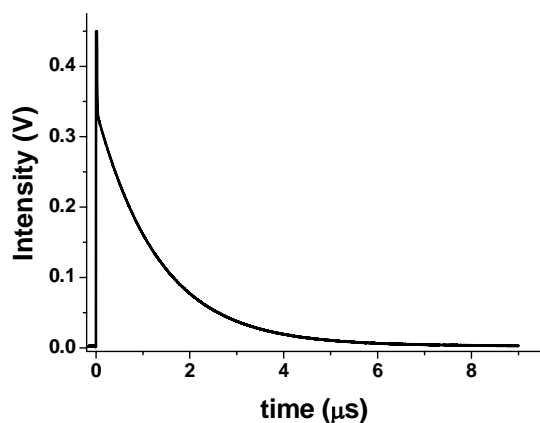
(b)

Figure A-5-5 For the PFam4-Ir(mppy)₃ system in the DCB solution, the photoluminescence decay curve of Ir(mppy)₃ at [PFam4]=4mM (a) photoluminescence intensity I(t) versus t; (b) ln I(t) versus t

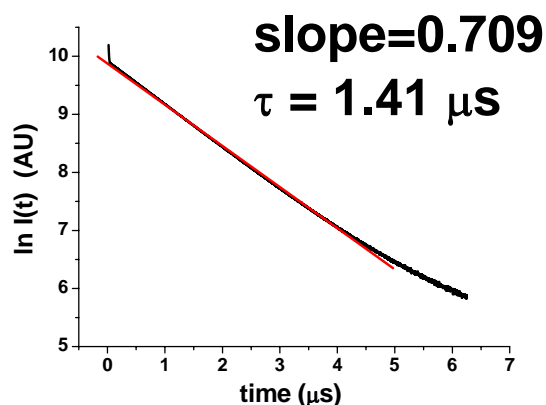


Appendix-6 The PFam4-Ir(mppy)₃ system in the cosolvent solution

Figure A-6-1, A-6-2, A-6-3, A-6-4 and A-6-5 show the processes to get the lifetimes of Ir(mppy)₃ at [PFam4]=0 M, 1mM, 2mM, 3mM and 4mM (in monomer unit) in the cosolvent solution, respectively

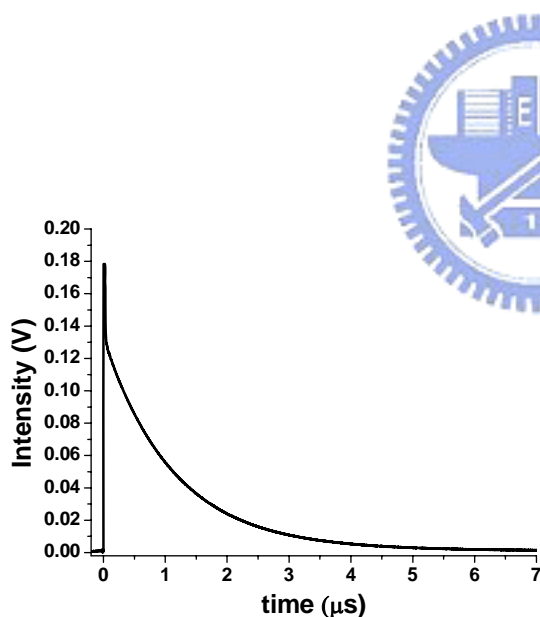


(a)

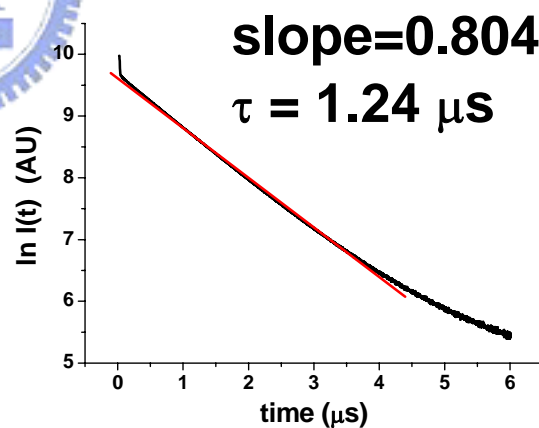


(b)

Figure A-6-1 For the PFam4-Ir(mppy)₃ system in the cosolvent solution, the photoluminescence decay curve of Ir(mppy)₃ at [PFam4]=0M (a) photoluminescence intensity I(t) versus t; (b) ln I(t) versus t

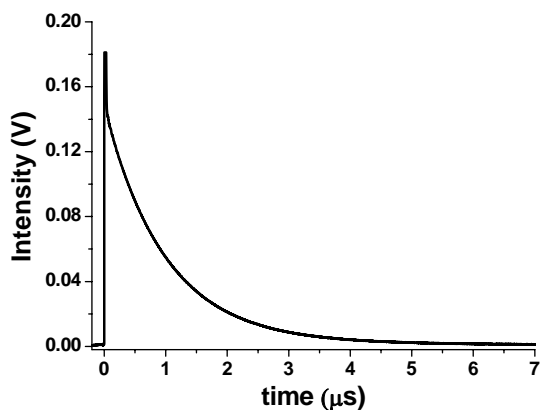


(a)

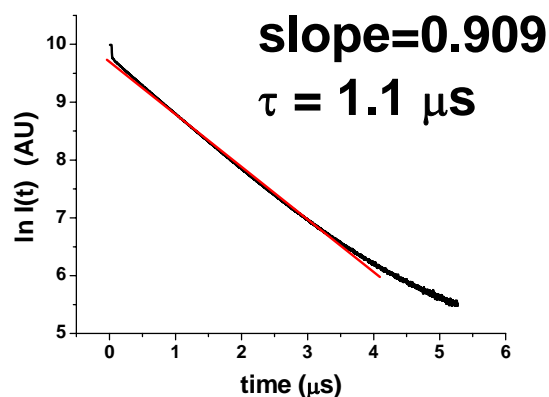


(b)

Figure A-6-2 For the PFam4-Ir(mppy)₃ system in the cosolvent solution, the photoluminescence decay curve of Ir(mppy)₃ at [PFam4]=1mM (a) photoluminescence intensity I(t) versus t; (b) ln I(t) versus t

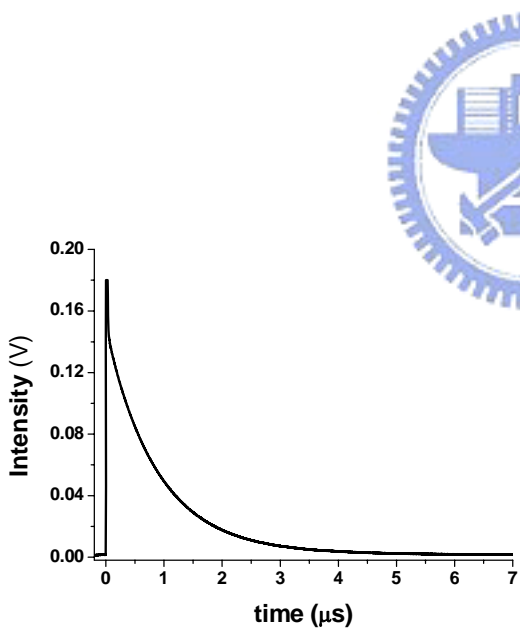


(a)

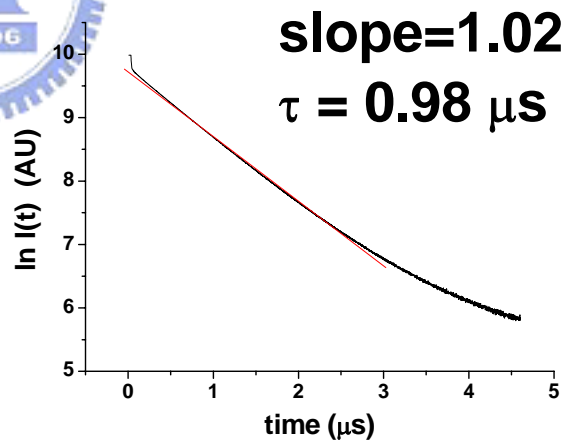


(b)

Figure A-6-3 For the PFam4-Ir(mppy)₃ system in the cosolvent solution, the photoluminescence decay curve of Ir(mppy)₃ at [PFam4]=2mM (a) photoluminescence intensity I(t) versus t; (b) ln I(t) versus t

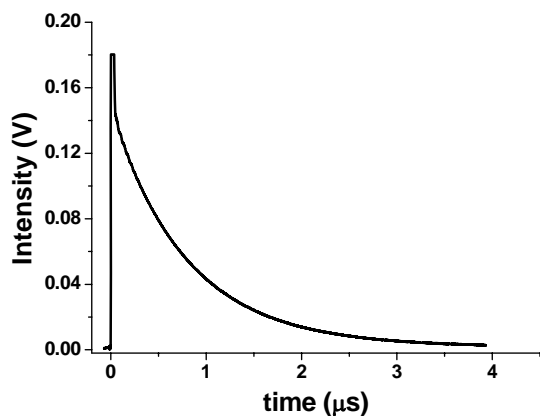


(a)

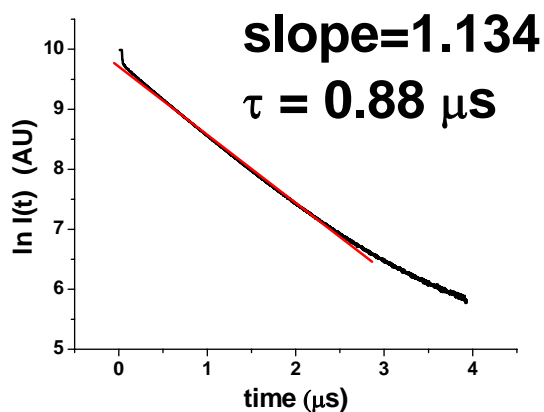


(b)

Figure A-6-4 For the PFam4-Ir(mppy)₃ system in the cosolvent solution, the photoluminescence decay curve of Ir(mppy)₃ at [PFam4]=3mM (a) photoluminescence intensity I(t) versus t; (b) ln I(t) versus t



(a)



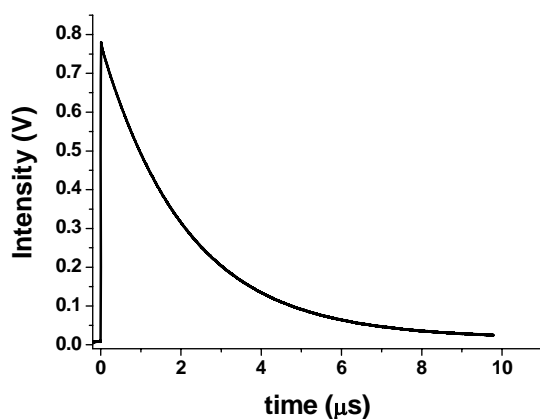
(b)

Figure A-6-5 For the PFam4-Ir(mppy)₃ system in the cosolvent solution, the photoluminescence decay curve of Ir(mppy)₃ at [PFam4]=4mM (a) photoluminescence intensity $I(t)$ versus t ; (b) $\ln I(t)$ versus t

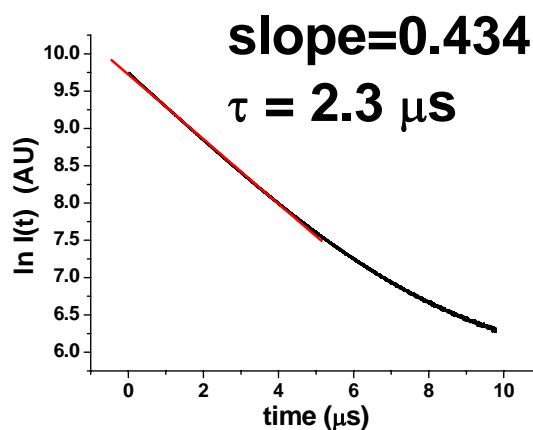


Appendix-7 The PFam4- Ir(FIPy)₂(acac) system in the toluene solution

Figure A-7-1, A-7-2, A-7-3, A-7-4 and A-7-5 show the processes to get the lifetimes of Ir(FIPy)₂(acac) at [PFam4]=0 M, 1mM, 2mM, 3mM and 4mM (in monomer unit) in the toluene solution, respectively

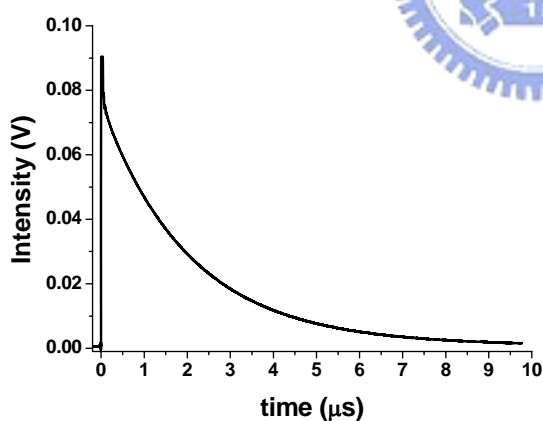


(a)

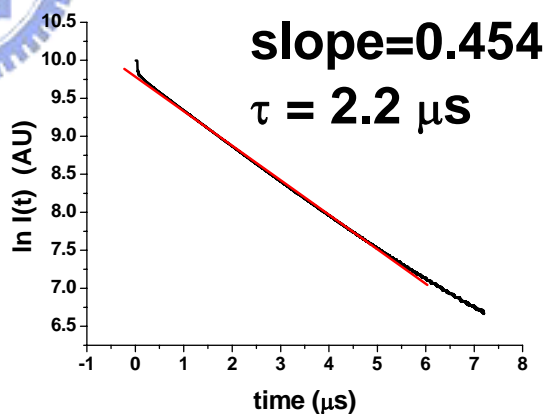


(b)

Figure A-7-1 For the PFam4-Ir(FIPy)₂(acac) system in the toluene solution, the photoluminescence decay curve of Ir(FIPy)₂(acac) at [PFam4]=0M (a) photoluminescence intensity $I(t)$ versus t ; (b) $\ln I(t)$ versus t

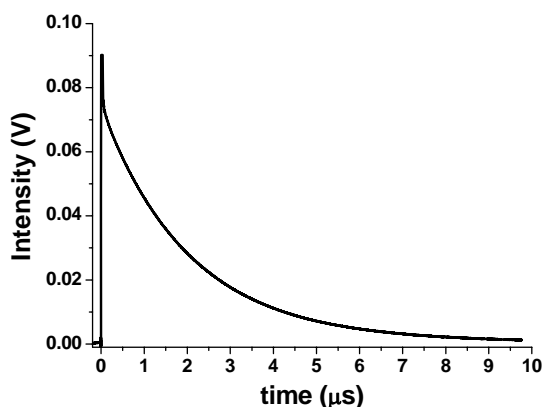


(a)

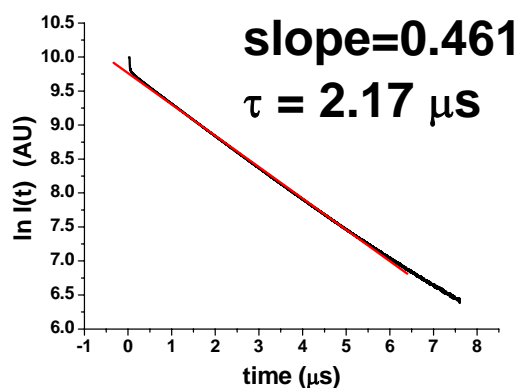


(b)

Figure A-7-2 For the PFam4-Ir(FIPy)₂(acac) system in the toluene solution, the photoluminescence decay curve of Ir(FIPy)₂(acac) at [PFam4]=1mM (a) photoluminescence intensity $I(t)$ versus t ; (b) $\ln I(t)$ versus t

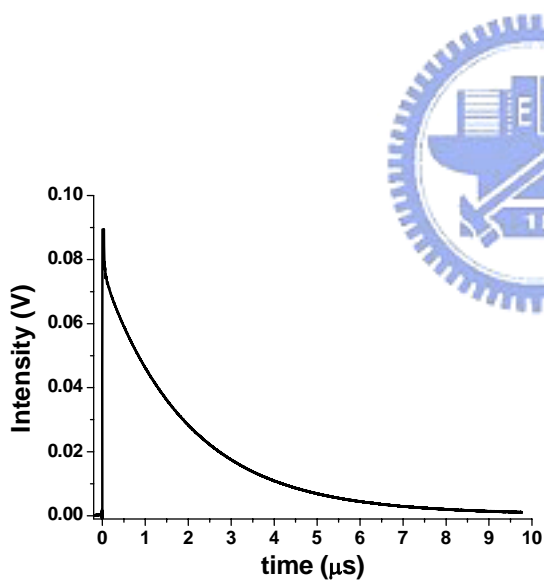


(a)

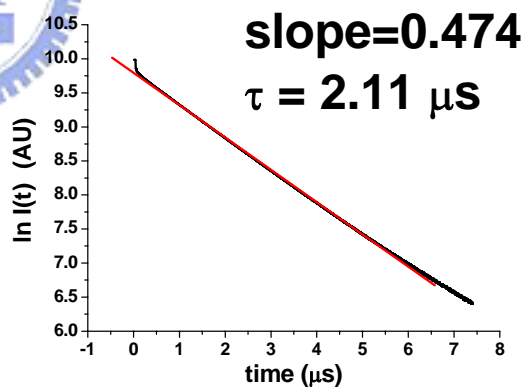


(b)

Figure A-7-3 For the PFam4-Ir(FIPy)₂(acac) system in the toluene solution, the photoluminescence decay curve of Ir(FIPy)₂(acac) at [PFam4]=2mM (a) photoluminescence intensity $I(t)$ versus t ; (b) $\ln I(t)$ versus t

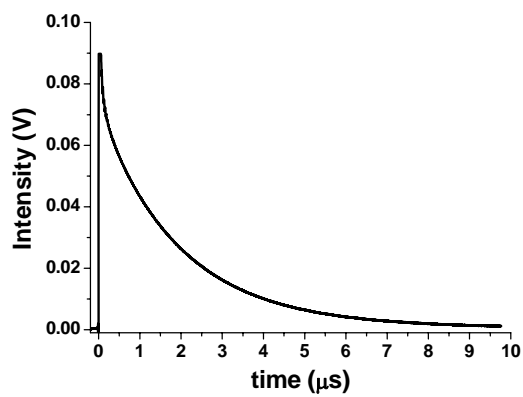


(a)

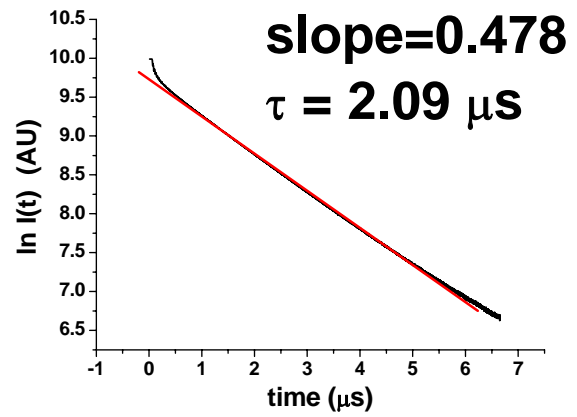


(b)

Figure A-7-4 For the PFam4-Ir(FIPy)₂(acac) system in the toluene solution, the photoluminescence decay curve of Ir(FIPy)₂(acac) at [PFam4]=3mM (a) photoluminescence intensity $I(t)$ versus t ; (b) $\ln I(t)$ versus t



(a)



(b)

Figure A-7-5 For the PFam4-Ir(FIPy)₂(acac) system in the toluene solution, the photoluminescence decay curve of Ir(FIPy)₂(acac) at [PFam4]=4mM (a) photoluminescence intensity I(t) versus t; (b) ln I(t) versus t

